University of Alberta

Performance Evaluation of High Bit Rate Cellular Packet Data Systems

by

Carlos Herman Rentel-Gómez ©

A thesis submitted to the Faculty of Graduate Studies and Research in partial
fulfillment of the requirements for the degree of Master of Science

Department of Electrical and Computer Engineering

Edmonton, Alberta

Fall 2002.

National Library
of Canada

Acquisitions and
Bibliographic Services

395 Wellington Street
Ottawa ON K1A 0N4
Canada

Bibliothèque nationale
du Canada

Acquisitions et
services bibliographiques

395, rue Wellington
Ottawa ON K1A 0N4
Canada

Your file Votre référence

Our file Notre référence

The author has granted a non-exclusive licence allowing the National Library of Canada to reproduce, loan, distribute or sell copies of this thesis in microform, paper or electronic formats.

The author retains ownership of the copyright in this thesis. Neither the thesis nor substantial extracts from it may be printed or otherwise reproduced without the author's permission.

L'auteur a accordé une licence non exclusive permettant à la Bibliothèque nationale du Canada de reproduire, prêter, distribuer ou vendre des copies de cette thèse sous la forme de microfiche/film, de reproduction sur papier ou sur format électronique.

L'auteur conserve la propriété du droit d'auteur qui protège cette thèse. Ni la thèse ni des extraits substantiels de celle-ci ne doivent être imprimés ou autrement reproduits sans son autorisation.

0-612-81468-8

Canada

University of Alberta

Library Release Form

Name of Author: Carlos Herman Rentel-Gómez

Title of the Thesis: Performance Evaluation of High Bit Rate Cellular Packet Data Systems

Degree: Master of Science

Year this Degree Granted: 2002

Permission is hereby granted to the University of Alberta Library to reproduce single copies of the thesis and to lend or sell such copies for private, scholarly or scientific research purposes only.

The author reserves all other publication and other rights in association with the copyright in the thesis, and except as herein before provided, neither the thesis nor any substantial portion thereof may be printed or otherwise reproduced in any material form whatever without the author's prior written permission.

Carlos H. Rentel-Gómez
9525 Genesee Ave. Apartment 232
San Diego, CA 92121 - 1714 USA

July 23rd, 2002

University of Alberta

Faculty of Graduate Studies and Research

The undersigned certify that they have read, and recommend to the Faculty of Graduate Studies and Research for acceptance, a thesis entitled *Performance Evaluation of High Bit Rate Cellular Packet Data Systems by Carlos Herman Rentel-Gómez* in partial fulfillment of the requirements for the degree of Master of Science.

Dr. Witold A. Krzymień

Dr. Ivan J. Fair

Dr. Xiaodai Dong

Dr. Janelle Harms

July 23rd, 2002

Abstract

This thesis presents performance evaluation of high bit rate cellular packet data systems employing adaptive transmission techniques. The performance evaluation is based on the IS-856 (HDR) and 1XTREME systems, both of which have been proposed as an evolution of the 1x cdma2000 cellular standard. Link performance has been estimated by symbol-level simulation of the forward data-traffic channel in the presence of additive white Gaussian noise (AWGN). Link level results are then used in a system level simulator of 19 three-sector cells. The system level simulator uses the standard channel models recommended by the International Telecommunications Union (ITU) in pedestrian and vehicular radio environments. The systems use modulation and code rate adaptation to achieve 1% packet error rate (PER). System performance is evaluated in terms of average sector throughput, packet delay, peak data rate, and fairness metrics. Performance advantages of HDR over 1XTREME are found and analyzed, including an approximate 20% higher average sector throughput in the low-speed pedestrian channel when using the proportionally fair scheduler. Results of this thesis provide useful guidelines for the deployment and better understanding of these new wireless packet data access systems.

Acknowledgements

I would like to thank my supervisor Dr. Witold A. Krzymień for its guidance and support throughout the development of this thesis. I would like to acknowledge the contributions of Miss Ge Li, (University of Alberta/ TR*Labs*) who generated the AWGN PER curves, and Dr. Bahman Darian who contributed with the system level simulation of 1XTREME. Also would like to acknowledge the contributions, and suggestions offered by Dr. Vieri Vanghi (Ericsson Wireless Communications), and Mr. Robert Elliot (University of Alberta/ TR*Labs*).

I am grateful for the financial assistance provided by TR*Labs*, and the University of Alberta, and for the support of the administrative staff in both institutions. Special thanks to my wife for all her sacrifices, and understanding.

To my father and my mother.

TABLE OF CONTENTS

Chapter 1. **Cellular radio communication** 1
1.1 Introduction 1
1.2 Review of present and future cellular radio standards 7
  1.2.1 Advanced mobile phone system (AMPS) 8
  1.2.2 Global system for mobile communication (GSM) 8
  1.2.3 CDMA digital cellular standard system 9
  1.2.4 Third generation standards 11
1.3 Thesis objectives and contributions 14
1.4 Related work 16
1.5 Outline of the thesis 17

Chapter 2. **High bit rate packet data systems** 18
2.1 Introduction 18
2.2 The HDR system 19
  2.2.1 HDR air interface overview 19
  2.2.2 Forward link physical layer description 26
  2.2.3 Reverse link physical layer description 30
2.2 The 1XTREME system 31
2.3 Summary 32

Chapter 3. **The cellular radio system environment** 33
3.1 Introduction 33
3.2 Cellular geometric structure 35
3.3 Path-loss and shadow fading model 36
3.4 Multi-path fading model 46
3.5 Summary 52

Chapter 4. **Simulation structure and link level simulations** 53

4.1 Introduction 53
4.2 General simulation structure 54
4.3 Link level simulations 56
  4.3 Structure and functionality of the HDR and 1XTREME Forward links 56
    4.3.1.1 HDR forward traffic channel transmission formats 56
    4.3.1.2 1XTREME forward shared channel transmission formats 58
    4.3.1.3 Turbo encoder and decoder 58
      4.3.1.3.1 Turbo encoder 59
        4.3.1.3.1.1 Turbo interleaver 61
      4.3.1.3.2 Turbo decoder 62
    4.3.1.4 Signal constellations and spectrum spreading 65
      4.3.1.4.1 HDR forward traffic channel spreading 67
      4.3.1.4.2 1XTREME forward shared channel spreading 68
    4.3.1.5 Slot and code channel structure 69
      4.3.1.5.1 HDR forward channel and slot structure 69
      4.3.1.5.2 1XTREME code channel structure 71
    4.3.1.6 Hybrid ARQ for HDR 71
    4.3.1.7 Soft packet combining and incremental redundancy 73
    4.3.1.8 AWGN performance evaluation and its relevance 74
  4.3.2 AWGN performance curves 75
    4.3.2.1 HDR forward traffic channel PER curves 75
    4.3.2.2 1XTREME forward shared channel PER curves 75
4.4 Summary 76

Chapter 5. **System level simulation** 77
5.1 Introduction 77
5.2 SIR lookup table generation in HDR 79

5.2.1 Power captured by the rake receiver 82
5.2.2 Evaluation of SIR values in the ITU pedestrian A radio channel 85
5.2.3 Evaluation of SIR values in the ITU vehicular B radio channel 87
5.3 MCS format determination 92
5.4 Scheduling of transmissions 93
5.4.1 Round robin scheduler 94
5.4.2 Proportionally fair (PF) scheduler 96
5.5 Packet erasure determination 97
5.6 HDR system level simulator 99
5.7 1XTREME system level simulator 99
5.8 Summary 101

Chapter 6. Performance results of HDR and 1XTREME 103
6.1 Introduction 103
6.2 Distribution of peak Bit Rates over the set of users 104
6.2.1 Pedestrian A channel 104
6.2.1.1 1XTREME 105
6.2.1.2 HDR 106
6.2.2 Vehicular B channel 107
6.2.2.1 1XTREME 107
6.2.2.2 HDR 108
6.3 Distribution of throughput over the set of users 109
6.3.1 Pedestrian A channel 110
6.3.1.1 1XTREME 110
6.3.1.2 HDR 111
6.3.2 Vehicular B channel 112
6.3.2.1 1XTREME 112
6.3.2.2 HDR 113
6.4 Average sector throughput 115

6.4.1 1XTREME 115
6.4.2 HDR 116
6.5 Distribution of delays per user 118
6.5.1 Pedestrian A channel 118
6.5.1.1 1XTREME 118
6.5.1.2 HDR 119
6.5.2 Vehicular B channel 120
6.5.2.1 1XTREME 120
6.5.2.2 HDR 121
6.6 Average delay per sector 122
6.6.1 1XTREME 123
6.6.2 HDR 124
6.7 Number of slots allocated per user 125
6.7.1 Pedestrian A channel 125
6.7.1.1 1XTREME 125
6.7.1.2 HDR 126
6.7.2 Vehicular B channel 127
6.7.2.1 1XTREME 127
6.7.2.2 HDR 128
6.8 Summary 130

Chapter 7 **Conclusion and future research** 131

Bibliography 135

Appendix. **Link level simulation results** 142

A.1 HDR forward link AWGN channel PER curves 142
A.2 1XTREME forward shared channel AWGN PER curves 153

LIST OF TABLES

Chapter 1. Cellular radio communication 1

1.1 IS-95 parameters 11

Chapter 2. High bit rate packet data systems 18

2.1 HDR forward link transmission formats 23

2.2 HDR parameters 30

2.3 1XTREME forward link transmission formats 31

Chapter 3. The cellular radio system environment 33

3.1 Link budget for the forward Link 39

3.2 Parameters used in cell size computation 39

Chapter 4. Simulation structure and link level simulations 53

4.1 Physical layer packets and rates supported by the HDR forward channel 57

4.2 Physical layer packets and rates supported by the 1XTREME Forward shared channel 58

4.3 Turbo code data bit puncturing pattern 60

4.4 Turbo code tail bit puncturing and repeating pattern 61

Chapter 5. System level simulation 77

5.1 Power and delay profile of the ITU pedestrian A channel 79

5.2 Power and delay profile of the ITU vehicular B channel 80

5.3 Parameters and assumptions of the system level simulation 81

5.4 SIR degradation due to imperfections 91

5.5 SIR require to achieved PER = 1% 94

Chapter 6. Performance results of HDR and 1XTREME 103

6.1 Fairness metric F for the number of slots allocated per user over 16 users per sector 129

Chapter 7 Conclusion and future research 131

7.1 Average throughput per sector for pedestrian A channel, 16 users for slow sector selection for round-robin and proportional fair schedulers 132

LIST OF FIGURES

Chapter 1. Cellular radio communication 1

1.1 Frequency reuse in a coverage area 2

1.2 The cellular network 3

1.3 Multiple access techniques 5

1.4 Hard (a), and soft (b) handoffs 6

1.5 Bandwidth of IS-95 and cdma2000 13

Chapter 2. High bit rate packet data systems 18

2.1 HDR forward link packet transmission 20

2.2.a HDR normal termination of a packet transmission on the forward link 24

2.2.b HDR early termination of a packet transmission on the forward link 24

2.3 Slot structure in HDR 27

2.4 HDR forward link traffic/control channel structure 28

2.5 Base-band 1XTREME forward link channel structure 32

Chapter 3. The cellular radio system environment 33

3.1 Cell layout 36

3.2 Antenna gain pattern 40

3.3 Ideal and simulated auto-correlation of Gaussian shadow numbers 45

3.4 Block diagram of the modified Smith channel model method 49

3.5 Pdf of theoretical and simulated correlated Rayleigh numbers 51

3.6 Auto-correlation comparison of theoretical and simulated Rayleigh numbers at 60km/h with fc = 1.9 GHz 51

3.7 Auto-correlation comparison of theoretical and simulated Rayleigh numbers at 3km/h with fc = 1.9 GHz 52

Chapter 4. **Simulation structure and link level simulations** 53

4.1 General simulation structure of HDR and 1XTREME 54
4.2 Turbo encoder used in HDR and 1XTREME 60
4.3 Interleaver structure 61
4.4 Turbo decoder 63
4.5 Signal constellation for QPSK modulation 65
4.6 Signal constellation for 8PSK modulation 65
4.7 Signal constellation for 16QAM modulation 66
4.8 Signal constellation for 64QAM modulation 66
4.9 HDR forward channel structure 69
4.10 HDR forward channel active slot structure (a) the first slot (b) the non-first slot for multi-slot transmission 70
4.11 HDR forward channel idle slot structure 70
4.12 1XTREME forward shared channel structure 71
4.13 Example of slot interlacing for multi-slot packet transmission in HDR forward channel 72
4.14 HDR forward traffic channel structure in simulation 74
4.15 1XTREME forward shared channel structure in simulation 74

Chapter 5. System level simulation 77

5.1 System-level simulation structure 78
5.2 cdf's of SIR values in ITU ped. A radio environment with slow best sector selection at 3km/h 87
5.3 cdf of SIR values in ITU veh. B radio environment with slow best sector selection at 60km/h 90
5.4 cdf's of estimated SIRs in pedestrian A channel with imperfections 91
5.5 cdf's of estimated SIRs in vehicular B channel with imperfections 92

Chapter 6. Performance results of HDR and 1XTREME 103

6.1 1XTREME distribution of peak bit rates in an embedded sector for 100 drops of 16 users each for the ITU pedestrian A channel with RR scheduler 105

6.2 1XTREME distribution of peak bit rates in an embedded sector for 100 drops of 16 users each for the ITU pedestrian A channel with PF scheduler 105

6.3 HDR distribution of peak bit rates in an embedded sector for 100 drops of 16 users each for the ITU pedestrian A channel with RR scheduler 106

6.4 HDR distribution of peak bit rates in an embedded sector for 100 drops of 16 users each for the ITU pedestrian A channel with PF scheduler 106

6.5 1XTREME distribution of peak bit rates in an embedded sector for 100 drops of 16 users each for the ITU vehicular B channel with RR scheduler 107

6.6 1XTREME distribution of peak bit rates in an embedded sector for 100 drops of 16 users each for the ITU vehicular B channel with PF scheduler 107

6.7 HDR distribution of peak bit rates in an embedded sector for 100 drops of 16 users each for the ITU vehicular B channel with RR scheduler 108

6.8 HDR distribution of peak bit rates in an embedded sector for 100 drops of 16 users each for the ITU vehicular B channel with PF scheduler 108

6.9 1XTREME distribution of throughput per user over the set of users (100 drops of 16 users each) in an embedded sector for ITU pedestrian A channel with RR scheduler 110

6.10 1XTREME distribution of throughput per user over the set of users (100 drops of 16 users each) in an embedded sector for ITU pedestrian A channel with PF scheduler 110

6.11 HDR distribution of throughput per user over the set of users (100 drops of 16 users each) in an embedded sector for ITU pedestrian A channel with RR scheduler 111

6.12 HDR distribution of throughput per user over the set of users (100 drops of 16 users each) in an embedded sector for ITU pedestrian A channel with PF scheduler 111

6.13 1XTREME distribution of throughput per user over the set of users (100 drops of 16 users each) in an embedded sector for ITU vehicular B channel with RR scheduler 112

6.14 1XTREME distribution of throughput per user over the set of users (100 drops of 16 users each) in an embedded sector for ITU vehicular B channel with PF scheduler 112

6.15 HDR distribution of throughput per user over the set of users (100 drops of 16 users each) in an embedded sector for ITU vehicular B channel with RR scheduler 113

6.16 HDR distribution of throughput per user over the set of users (100 drops of 16 users each) in an embedded sector for ITU vehicular B channel with PF scheduler 113

6.17 1XTREME total average throughput per embedded sector as a function of the number of users per drop for 100 drops, RR scheduler 115

6.18 1XTREME total average throughput per embedded sector as a function of the number of users per drop for 100 drops, PF scheduler 116

6.19 HDR total average throughput per embedded sector as a function of the number of users per drop for 100 drops, RR scheduler 116

6.20 HDR total average throughput per embedded sector as a function of the number of users per drop for 100 drops, PF scheduler 117

6.21 1XTREME distribution of delays per delivered packet over the set of users (100 drops of 16 users each) in an embedded sector for ITU pedestrian A channel with RR scheduler 118

6.22 1XTREME distribution of delays per delivered packet over the set of users (100 drops of 16 users each) in an embedded sector for ITU pedestrian A channel with PF scheduler 119

6.23 HDR distribution of delays per delivered packet over the set of users (100 drops of 16 users each) in an embedded sector for ITU pedestrian A channel with RR scheduler 119

6.24 HDR distribution of delays per delivered packet over the set of users (100 drops of 16 users each) in an embedded sector for ITU pedestrian A channel with PF scheduler 120

6.25 1XTREME distribution of delays per delivered packet over the set of users (100 drops of 16 users each) in an embedded sector for ITU vehicular B channel with RR scheduler 120

6.26 1XTREME distribution of delays per delivered packet over the set of users (100 drops of 16 users each) in an embedded sector for ITU vehicular B channel with PF scheduler 121

6.27 HDR distribution of delays per delivered packet over the set of users (100 drops of 16 users each) in an embedded sector for ITU vehicular B channel with RR scheduler 121

6.28 HDR distribution of delays per delivered packet over the set of users (100 drops of 16 users each) in an embedded sector for ITU vehicular B channel with PF scheduler 122

6.29 1XTREME average delay per delivered packet in an embedded sector as a function of the number of users per drop for 100 drops, RR scheduler 123

6.30 1XTREME average delay per delivered packet in an embedded sector as a function of the number of users per drop for 100 drops, PF scheduler 123

6.31 HDR average delay per delivered packet in an embedded sector as a function of the number of users per drop for 100 drops, RR scheduler 124
6.32 HDR average delay per delivered packet in an embedded sector as a function of the number of users per drop for 100 drops, PF scheduler 124
6.33 1XTREME distribution of the number of slots allocated per user over the set of users (100 drops of 16 users each) in an embedded sector for ITU pedestrian A channel with RR scheduler 125
6.34 1XTREME distribution of the number of slots allocated per user over the set of users (100 drops of 16 users each) in an embedded sector for ITU pedestrian A channel with PF scheduler 126
6.35 HDR distribution of the number of slots allocated per user over the set of users (100 drops of 16 users each) in an embedded sector for ITU pedestrian A channel with RR scheduler 126
6.36 HDR distribution of the number of slots allocated per user over the set of users (100 drops of 16 users each) in an embedded sector for ITU pedestrian A channel with PF scheduler 127
6.37 1XTREME distribution of the number of slots allocated per user over the set of users (100 drops of 16 users each) in an embedded sector for ITU vehicular B channel with RR scheduler 127
6.38 1XTREME distribution of the number of slots allocated per user over the set of users (100 drops of 16 users each) in an embedded sector for ITU vehicular B channel with PF scheduler 128
6.39 HDR distribution of the number of slots allocated per user over the set of users (100 drops of 16 users each) in an embedded sector for ITU vehicular B channel with RR scheduler 128
6.40 HDR distribution of the number of slots allocated per user over the set of users (100 drops of 16 users each) in an embedded sector for ITU vehicular B channel with PF scheduler 129

Appendix. Link level simulation results 142

A.1 HDR PER vs. Es/No curves in AWGN for transmission formats 1-8 142

A.2 HDR PER vs. Es/No curves in AWGN for transmission formats 9-16 143

A.3 HDR PER vs. Es/No curves in AWGN for transmission formats 17-24 144

A.4 HDR PER vs. Es/No curves in AWGN for transmission formats 25-31 145

A.5 HDR PER vs. Es/No curves in AWGN for transmission formats 32-37 146

A.6 HDR PER vs. Es/No curves in AWGN for transmission formats 38-41 147

A.7 HDR PER vs Es/No curves in AWGN for rates 76.8kb/s to 122.88 kb/s with maximum number of slots = 8, and 16 148

A.8 HDR PER vs Es/No curves in AWGN for rates 153.6 And 204.8 with maximum number of slots = 4, 8, and 16 149

A.9 HDR PER vs. Es/No curves in AWGN for rate 307.2 kb/s with maximum number of slots = 2, 4, 8, 16, and packet sizes 1,024 and 2,048 150

A.10 HDR PER vs. Es/No curves in AWGN for rate 614.4 kb/s with maximum number of slots = 1, 2, 4, 8, 16, and packet sizes 1,024 and 2,048 151

A.11 HDR PER vs. Es/No curves in AWGN for rate 1,228.8 kb/s with maximum number of slots = 1, 2, 4, and packet sizes 2,048 and 4,096 152

A.12 1XTREME PER vs. Es/No curves in AWGN for the Forward Shared channel 153

ABBREVIATIONS

1XEV-DO	1x Evolution Data-Only
1XEV-DV	1xEvolution Data-Voice
2G	Second Generation Cellular Systems
3G	Third Generation Cellular Systems
ACK	Acknowledgement
AMC	Adaptive Modulation and Coding
AWGN	Additive White Gaussian Noise
cdf	Cumulative Distribution Function
CDMA	Code Division MultipleAccess
DRC	Data Request Channel
DSL	Digital Subscriber Line
FDD	Frequency Division Duplex
H-ARQ	Hybrid Automatic Repeat Request
HDR	High Data Rate system
IDFT	Inverse Discrete Fourier Transform
IP	Internet Protocol
IS-2000	Interim Standard 2000 (cdma2000)
ISI	Inter-symbol Interference
ITU	International Telecommunications Union
MAC	Medium Access Control
MCS	Modulation and Coding Scheme
N-ACK	Negative-Acknowledgment
OQPSK	Off-set Quadrature Phase-Shift Keying
pdf	Probability Density Function
PER	Packet Error Rate
PF	Proportionally Fair
PN	Pseudo Noise
PPP	Point-to-Point Protocol
QAM	Quadrature Amplitude Modulation
QPSK	Quadrature Phase-Shift Keying
RR	Round Robin
RRM	Radio Resource Management
SBSS	Slow Best Sector Selection
SIR	Signal to Interference Ratio
TDD	Time Division Duplex
TDM	TimeDivision Multiplexing
W-CDMA	Wide-Band CDMA

LIST OF SYMBOLS

$\Phi(n)$	Auto-correlation function
σ	Standard deviation
Es / No	Symbol energy-to-noise power spectral density ratio
$f_{D\max}$	Maximum Doppler frequency
d_{dec}	De-correlation distance
Ω_p	Total average received signal power
L_{rs}	Roof-top-to street diffraction loss
L_{msd}	Multi-screen diffraction loss
L_{bf}	Free space path-loss
L	Path loss
G_b	Antenna gain
P_t	Transmission power per sector
h_b	Base station antenna height
h_m	Mobile terminal antenna height
b	Building separation
w	Street width
H	Average roof-top height
$\overline{P}_i$	Small-scale average power received by i^{th} mobile
R_i	Random variable with Rayleigh distribution
I_i	Interference received by i^{th} mobile
ξ	First order recursive filter coefficient
v	Gaussian random variable with auto-correlation different than zero

Chapter 1

Cellular radio communication

1.1 Introduction

Initially, radio communications were carried out utilizing high powered, high mounted base stations and big portable radios to provide voice communication services. The idea was to offer a maximum coverage and a good quality of the radio signal; the allocated frequency spectrum was used only by a few channels, and therefore, the radio spectrum was not efficiently used in terms of users served per frequency allocation. The advent of more efficient and smaller semiconductors and integrated circuits reduced the size and cost of portable radios, expanding the corporate based market of radio communications to the general public. The original radio communication system needed an improvement in terms of capacity and spectrum efficiency in order to take advantage of a potentially large market.

The initial solution to this capacity and spectrum efficiency problem is known as the cellular concept [1]. The cellular concept is the basis of all present cellular systems and it represents a major achievement in the radio communications field.

The main idea behind the cellular concept is that of frequency reuse depicted in Figure 1.1; here the total coverage area is divided into imaginary regions in space

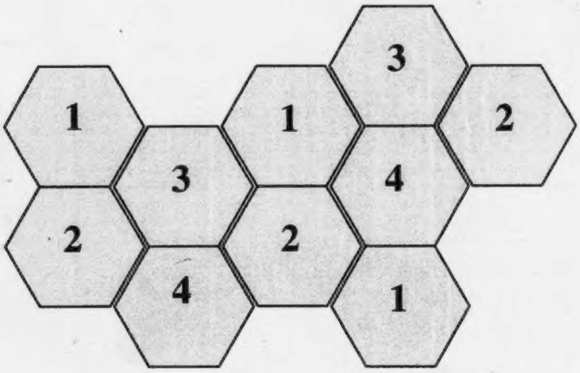

Figure 1.1. Frequency reuse in a coverage area.

called cells (which are drawn as hexagons in Figure 1.1 for the purpose of illustration, but in reality have different shapes due to radio propagation considerations). The first cellular systems comprised cells which serve a region in space with a low powered base station utilizing part of the allocated frequency spectrum; neighboring cells used different portions of the allocated spectrum, and cells separated by a considerable distance reuse the same set of frequencies. The reuse of the frequencies is possible if the separation of both regions in space is large enough to cause the mutual interfering signals to be at a tolerable level. The development of the cellular concept provided the necessary steps toward the materialization of the first generation of cellular systems which are still in use mainly in South and North America.

The classical cellular network architecture (Figure 1.2) is based on the cellular concept. Each cell is served by a base transceiver station (BTS) and the BTSs are connected to a base station controller (BSC) which in turn is connected to other BSCs and the central unit called the mobile switching center (MSC). The MSC handles the interconnection of the mobile stations with each other and with the Public Switched Telephone Network (PSTN), and it is also responsible along with the BSCs for ensuring uninterrupted communication throughout the entire region covered . The region between the base station and the mobile station is called the air-interface, and the network that supports over the air-interface connections is called the core network. Mobile terminals are also part of the cellular network (not shown in Figure 1.2)

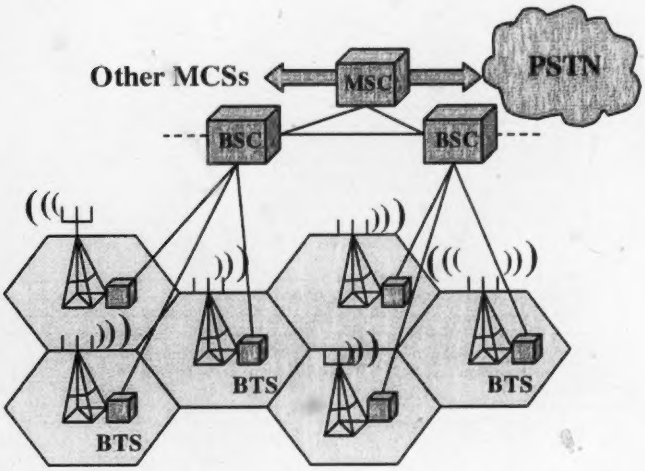

Figure 1.2. The cellular network.

The base station's main function is to serve the mobile stations as a point of interface between the air-interface and the core network. It is the point where users access different services provided by the cellular network.

Multiple access techniques are used to divide the radio resource among the users. Three multiple access techniques are commonly employed in cellular systems: frequency-division multiple access (FDMA), time-division multiple access (TDMA), and code- division multiple access (CDMA). In FDMA the allocated frequency band is sub-divided into smaller sub-bands (Figure 1.3-a); each sub-band is permanently assigned to a particular user that accesses the system for the total duration of the connection. More efficient variations to this technique are employed, in which the sub-bands are temporarily assigned to low priority services (low bit rate packet data transmissions) and hopped to a different sub-band when higher priority services try to access the system. This former technique is employed in the Cellular Digital Packet Data (CDPD) system [2]. In TDMA (Figure 1.3-b) several users share a common sub-band at different ordered time slots, and in CDMA (Figure 1.3-c), all users utilize the same allocated spectrum at the same time; the different transmissions are separated by different orthogonal and/or semi-orthogonal codes embedded to the transmitted signals [3]. Hybrids of these multiple access techniques are usually used in real systems such as FDMA/CDMA, TDMA/CDMA or FDMA/TDMA, the later used in most so-called TDMA systems (i.e., GSM, IS-136, PDC etc). Another multiple access technique that has gained some attention recently is space-division multiple access (SDMA), where the transmissions to multiple users are separated in space by controlling the radiation of the base station antennas.

It is necessary to ensure uninterrupted communication when the user is moving from one access point into a neighboring one. The process of handing over a user from one access point to another is known as handoff.

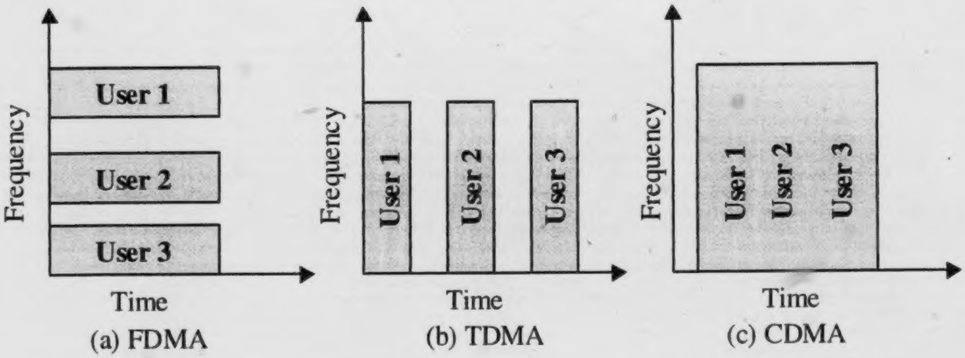
Frequency
User 1
User 2
User 3
Time
Frequency
User 1
User 2
User 3
Time
Frequency
User 1
User 2
User 3
Time

(a) FDMA

(b) TDMA

(c) CDMA

Figure 1.3. Multiple access techniques.

There are different types of handoffs depending on the mode of operation and the system where they are employed [4].

The two most representative types of handoffs are hard handoff, and soft handoff.

Hard handoff (Figure 1.4-a) occurs when the mobile station is transferred to a new access point by first breaking the connection with the old access point. It is a break before make connection over the air-interface.

Soft handoff (Figure 1.4-b) is a make before break transfer of a mobile station over the air-interface. During the execution of this handoff, the mobile station is connected to at least two access points at the same time before breaking with the old access point.

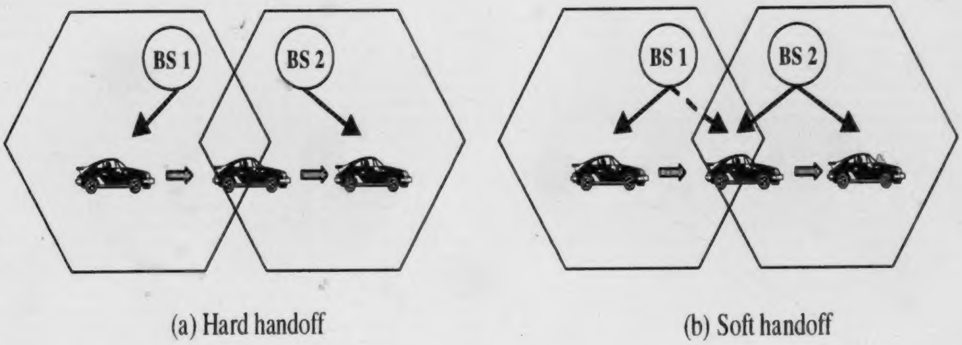

(a) Hard handoff (b) Soft handoff

Figure 1.4. Hard (a), and Soft (b) Handoffs.

In order to achieve an efficient operation of the cellular network, it is also necessary to control the power emitted by the mobile and base station transmitters. The primary reason for this is to ensure a minimum acceptable signal to interference ratio (SIR) of the received signal by off-setting the attenuation caused by the variable distance separation between the transmitter and the receiver. Power control helps to increase battery life and the capacity (users/cell) of the system.

Power control is particularly important in CDMA systems, where all users are transmitting in the same frequency band, and hence all interfere with one another. In CDMA systems, power control is also used to keep the mean powers of all received signals at the base station at the same level; this not only increases capacity, but also reduces the *near-far* problem. The *near-far* problem in CDMA occurs when two users are simultaneously transmitting with the same power to a base station receiver; the user closer to the base station can effectively capture the receiver leaving the other user without service. In order to solve the *near-far* problem, the system has to control the transmitted powers of the mobiles, so that they reach the base station with equal mean powers.

Radio resource management (RRM) is another important system level concept in cellular radio systems. Once a band of frequencies is allocated for the use of radio communications in a cell or a particular region, it is desirable to make efficient use of it among the multiple users trying to access the common service access point (i.e., base station). RRM primary objectives are to guarantee a desired quality of service and provide continuous support of the multiple radio connections throughout the entire coverage region. RRM primary functions are to allocate and if necessary re-allocate channels for the connections, selection of the best service access point for the connections, and congestion control. RRM relies on multiple access techniques, handoff, and power control.

1.2 Review of present and future cellular radio standards

Presently deployed cellular systems constitute what is called the first and second generation of cellular systems; from these groups the most representative standards are, the Advanced Mobile Phone System (AMPS), Global System for Mobile Communications (GSM), and the CDMA digital cellular standard IS-95. Future cellular radio standards known as third generation (3G) systems are now fully specified. The initial deployment of the 1x (1.25 MHz) version of the IS-2000 system began already in 2001in the U.S and Korea. Similarly, the initial deployment of the 5 MHz W-CDMA system began in 2001 in Japan. This section provides a brief overview of these systems with emphasis on the IS-95 and IS-2000 systems.

1.2.1 Advanced mobile phone system (AMPS)

The AMPS system belongs to the first-generation (1G) of cellular systems, it was developed in AT&T Bell laboratories with the idea to provide voice services only. It was first deployed in Chicago in 1983 by Ameritech [5]. AMPS is an analog system using frequency modulation (FM), and FDMA as the multiple access technique. Each channel occupies a 30 kHz bandwidth of a total of 832 possible channels, and frequency division duplex (FDD) is used to separate the transmission and reception paths of every full-duplex channel. AMPS is still used in South and North America, but its use has started to decline mainly due to the competition from second-generation systems that provide more services with better quality, more capacity, and lower cost of deployment and of mobile terminals.

1.2.2 Global system for mobile communications (GSM)

GSM is the second-generation cellular system (2G) standard with more subscribers worldwide. It was first introduced in Europe in 1991 in order to serve as a Pan-Eropean cellular system. GSM uses digital modulation with hybrid

TDMA/FDMA, and each channel bandwidth is 200 kHz. The services provided are divided in three groups [6].

- Telephone service;
- Bearer service for the provision of data services up to 9.6 kb/s; it includes the support of packet switching protocols, and automatic request for retransmission (ARQ) for error detection;
- Supplementary services include number identification services, call forwarding, multiparty services, call restriction services etc.

GSM represents an evolution of 1G systems due mainly to the digital services provided, and its network architecture.

1.2.3 CDMA digital cellular standard IS-95

CDMA IS-95 was adopted as a U.S digital cellular standard in 1993 by the Telecommunications Industry Association (TIA). IS-95 is a dual mode system that provides a digital cellular service through spread-spectrum techniques [7]; it also provides first generation analog service to ease the transition from first to second generation cellular systems.

The network structure of the IS-95 system is the same as the classical network previously depicted in Figure 1.2, with an MSC that controls and handles the radio connections, interface with the PSTN, and base stations that serve as points of access for the mobile stations to the cellular services. The path from the mobile station to the base station is called the *reverse link*, and the path from the base station to the mobile is called the *forward link*. A number of different radio channels are specified per link. In the forward link they include, the pilot, synchronization, paging, and traffic channel. In the reverse link they include, the access, and traffic channels. Traffic channels are used to convey voice or data to or from an individual mobile station. The pilot channel is used as a reference for coherent detection at the mobile station receiver, paging channels are used to signal a mobile station of an incoming call, and the sync channel is used by the mobile station to acquire system time synchronization. Table 1.1 shows the most important parameters of the IS-95 air interface standard.

IS-95 forward link

The forward link of the IS-95 system consists of up to 61 traffic channels, up to 7 paging channels, 1 sync channel, and 1 pilot channel. All channels are orthogonally multiplexed to a common RF carrier using Walsh functions [8]. The different base station transmissions are separated by different offsets of the same short pseudo noise (PN) sequence. Hence, channelization in the forward link is achieved by a combination of orthogonal Walsh functions and short PN sequences. The Walsh covered symbols quadrature-modulate a short PN sequence before transmission in a form of QPSK modulation of the RF carrier.

IS-95 reverse link

The reverse link of IS-95 consists of traffic channels, and access channels. Channelization on the reverse link is achieved by different phase shifts of a long PN code sequence, the different phase shifts are obtained by masking of a 0 offset PN sequence, the mask is partially derived from the electronic serial number

(ESN) of the mobile terminal. Therefore separation of different transmissions on the reverse link is achieved by means code multiplexing. Modulation on the reverse link is by means of an 64-ary orthogonal modulation in base-band, and OQPSK modulation of the RF carrier.

Bandwidth	1.25 MHz
Chip rate	1.2288 Mchips/s
Frequency band reverse link	869-894 MHz 1930-1980 MHz
Frequency band forward link	824-849 MHz 1850-1910 MHz
Bit rates for data services	Rate set 1: 9.6 kb/s Rate set 2: 14.4 kb/s IS-95B: 115.2 kb/s
Soft handoff	Yes
Power control	Reverse link: open loop + closed loop (fast) Forward link: closed loop (slow)
Modulation	Forward link: QPSK Reverse link: OQPSK
Speech code	8, 13 kb/s
Frame length	20 ms
Error control coding	Convolutional codes (constraint length = 9, forward link code rate = 1/2 or 3/4, reverse link code rate = 1/3 or 1/2)

Table 1.1 IS-95 parameters [9].

1.2.4 Third generation standards

First and second generation cellular systems were primarily designed for voice and low data rate services. 3G systems are designed to improve 2G voice services, and include multimedia services and wireless Internet access. In the International Telecommunications Union (ITU), the 3G cellular systems are called International Mobile Telecommunications-2000 (IMT-2000). The objectives of the IMT-2000 systems are

- Flexibility to include new services;
- Provide data rates up to 384 kb/s for high mobility environments;
- Provide data rates up to 2 Mb/s for low mobility environments;
- High spectrum efficiency in comparison to 2G systems.

It has been recognized that a unified approach to a ubiquitous global 3G system is not possible at this time [9], and that some future 3G systems will evolve from the different 2G systems in existence. 2G systems based on GSM will evolve through the Enhanced Data for GSM Evolution (EDGE) system, and the General Packet Radio Service (GPRS) core network for packet switched services [10,11]. EDGE and GPRS use the GSM network infrastructure.

2G systems based on the IS-95 cellular standard will evolve through cdma2000 for the circuit switched and medium data rate services. For packet switching services at high data rates (up to 2Mb/s), several systems have been proposed including High Data Rate (HDR) system by Qualcomm Inc. [12, 13] and 1XTREME by Motorola and Nokia [14]. These systems are called 1x Evolution Data-Only (1xEV-DO) and 1x Evolution Data-Voice (1xEV-DV) respectively. These systems are aimed to provide higher data rates than 3G solutions designed around circuit switched technology. The specifics of the data optimization techniques utilized by these systems will be explained in later chapters. 1xEV-DO is a separate standard called IS-856.

Cdma2000 is a solution that utilizes a multi-carrier forward link with in principle up to 12 parallel CDMA carriers of 1.25 MHz each, and the same chip rate as that of IS-95 (see Table 1.1). Direct-spread with chip rate of 3.6864

Mchips/s is used on the reverse link. The first release will be deployed with one carrier (a 1X mode), see Figure 1.5 for 3x mode version of this system.

A new system standard has also been developed for future new service providers called WCDMA [15]. WCDMA uses 5 MHz bandwidth on both the forward and reverse links; two versions of channel duplexing are specified, time division duplex (TDD), and frequency division duplex (FDD) [16].

The major technical improvements of 3G systems with respect to 2G systems are

- Fast forward link power control;
- Improved error correction techniques for data transmission (Turbo coding);
- Pilot channel on the reverse link for coherent demodulation;
- Wider bandwidth;
- Optimized packet switched network for high bit data rate transmission;
- Capacity enhancement enabling techniques such as smart-antennas [17].

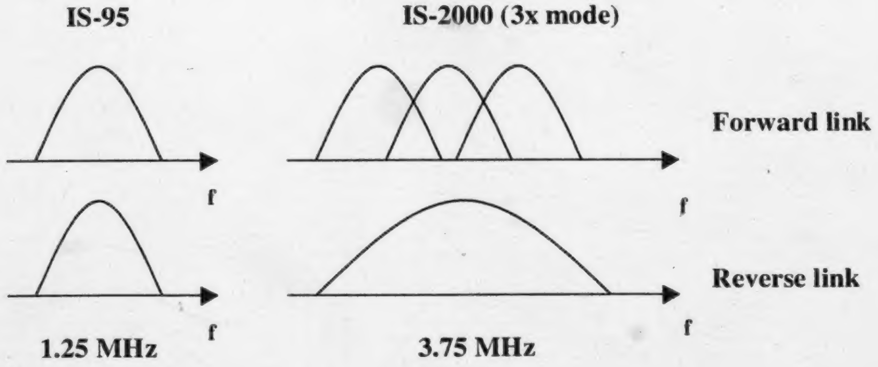

Figure 1.5. Bandwidths of IS-95 and cdma2000 (a possible configuration).

Beyond 3G cellular systems, a seamless Internet Protocol (IP) core network is envisioned, providing services between different wireless and wired applications. A user may have access to different systems adapted to a particular need and environment through a common packet switched platform [18, 19]. Future cellular radio systems will provide even higher capacities and higher data rates for future services.

1.3 Thesis objectives and contributions

The primary objective of this research work is to analyze the forward link performance of high bit-rate packet data systems designed as an evolution of the IS-2000 system through the development of a system level simulator, with emphasis on the 1xEV-DO system or HDR. The entire system will be modeled under different radio environments and system level assumptions to compute performance metrics that will help to understand its capabilities and limitations. The system level simulator will be useful for the future study of RRM algorithms, scheduling algorithms, and network optimization techniques.

The specific contributions of this research work are

- A complete modeling of the radio environment of a cluster of 19 tri-sectored cells is carried out; vehicular and pedestrian environments are considered following the recommendations of the International Telecommunications Union (ITU) for the evaluation of radio transmission technologies for IMT-2000 [20]. Measured antenna data are used to model the antenna gain-pattern in the simulation.

- Link level simulation results are presented for all HDR and 1XTREME transmission formats in order to use them in the system level simulator. The link level simulation results are obtained in an additive white Gaussian noise (AWGN) channel due to the very small slot size in the system (1.67ms and 5ms) that causes the channel to be practically time-invariant during a single-slot packet transmission.
- Scheduling of the transmissions is important to ensure optimum utilization of the radio resources, and fairness among the users accessing a system; two scheduling mechanisms are evaluated; a modified round robin scheduler, and a proportionally fair (PF) scheduler.

The following metrics are used for the comparative performance evaluation:

- Distribution of bit rates over the set of users
- Distribution of average throughput over the set of users
- Average throughput per sector
- Distribution of delays over the set of users
- Distribution of average delay over the set of users
- Average delay per sector
- Distribution of the number of allocated transmission slots per user.

1.4 Related work

System level simulators have been developed before for the performance analysis of 3G cellular radio systems. In [21] an advanced WCDMA system level simulator has been developed, in which traffic and mobility of the users are simulated using statistical models specified in [22]. Another WCDMA system level simulator has been described in [10], where the authors model the mobility of the users by adding the speed-dependant time-correlation to the fading signals generated, calling this procedure a semi-static approach.

In [23], the authors provided simulation results for the average throughput in one sector of the central cell of a cluster of 19 cells for the HDR system. The results are shown for 6, 3, and Omni-sector deployments, and for 1 and 2 access terminal (mobile station) antennas. The advantage of multi-user diversity is identified with the use of the proportionally fair scheduler over the round robin scheduler. No effects on the throughput due to speed, or specific radio environment are presented, and additional important metrics such as fairness, delays or data rates achieved are not discussed.

In [24], 1XTREME forward link level simulation results are presented and the average sector throughput is calculated for vehicle speeds of 0 and 3 km/hr. Two schedulers are presented. The *equal average power* scheduler equalizes the number of frames assigned to each user for transmission, and the *equal average data* scheduler equalizes the amount of data delivered to all users. The former scheduler is used to avoid the unfair situation occurring in the latter in which one user close to the serving base station can get higher data rates than another user farther away.

1.5 Outline of the thesis

A system level simulator for the IS-2000 compatible high bit-rate packet data systems has been developed and performance results have been obtained and presented with different system level assumptions.

Chapter 2 presents a description of the air-interface, physical layer, and design principles behind the high bit-rate packet data systems for IS-2000, with especial emphasis on the HDR system.

Chapter 3 addresses the cellular radio environment assumptions used in this research work; path-loss model, large and small scale fading models are presented and justified.

Chapter 4 describes the link level simulation procedure and presents the results.

Chapter 5, The structure of the system level simulator is presented along with the channel predictor, the schedulers, and the best sector selection methods.

Chapter 6, The performance results are discussed; throughput, delay, and fairness metrics are obtained and analyzed under different radio environments and system level assumptions.

Chapter 7 Presents the conclusions of this research work and future research directions are suggested.

Chapter 2

High bit-rate packet data systems

2.1 Introduction

HDR and 1XTREME have been proposed for standardization as evolution of the existing 3G IS-2000 standard [25], [12]. These systems are known as the 1xEvolution of IS-2000 and are expected to provide high packet data rate services for nomadic users [26]. The nomadic user expects to be able to access the same *Home* data services while he/she is traveling or has reached his/her final destination. It would be desirable to access the data services independently of location or motion, and the performance of the services provided should at least equal those of the present cable or DSL wire-line systems. 1xEvolution systems try to fill the present gap of an efficient high data rate wireless system through the use of data optimization techniques such as: packet switching and data rate adaptation.

The 1xEvolution systems take advantage of the radio frequency equipment and base stations already deployed of the IS-95 cellular digital network to provide the adequate coverage; 1xEvolution terminals will differ only in their base-band processing portion. The network architecture is expected to follow an Internet-Protocol structure, with the ultimate intention of implementing Mobile IP.

This chapter offers a description of the 1xEvolution systems with special emphasis on HDR. Section 2.2 addresses the air-interface, physical layer, and network architecture descriptions of HDR. Section 2.3 presents a brief description of the 1XTREME system.

2.2 The HDR system

Most of our description will be focused on the forward link since it is expected that most of the data services provided will have a highly asymmetrical behavior [9] (i.e., most of the data traffic will flow from the network to the mobile terminal).

2.2.1 HDR air-interface overview

Recognizing that the requirements of data and voice are very different in terms of delay constrain, bandwidth utilization, and traffic characteristics, the HDR system's first fundamental design principle is to separate voice from data services by using non-overlapping frequency spectrum allocations. The 1.25 MHz IS-95 or 1x cdma2000 RF carrier can provide voice and low/medium rate data services, and a separate carrier with the same RF components as the IS-95 system is used exclusively for the high bit-rate data services provided by HDR. The separation of the services is a natural choice since optimization of radio resource utilization is less effective when very different services are sharing a common frequency band at the same time. A high bit-rate data user can take much more bandwidth and power resources from a network than a voice user, therefore, its requirements in terms of coverage and quality of service are quite different, making it difficult to optimize a single network for both services.

The forward link packet transmissions of the different users are time-multiplexed as shown in Figure 2.1; and the base station transmits at the maximum power at all times. The pilot signal is not continuously beaming on the forward link, since it is also time division multiplexed with the data; this allows for the reduction of the interference when packets of a given user are not being transmitted in a different sector.

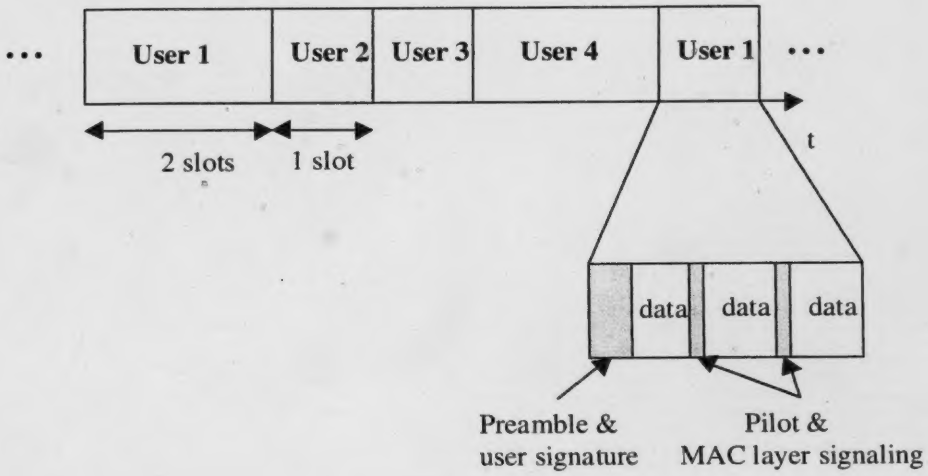
...
User 1
User 2
User 3
User 4
User 1
...
2 slots
1 slot
t
data
data
data
Preamble &
user signature
Pilot &
MAC layer signaling

Figure 2.1. Forward link packet transmission.

The preamble is sent at the beginning of every packet transmission attempt in order to assist the mobile terminal with synchronization and identification of the data packet. (The preamble in HDR is covered by a specific Walsh cover or MAC index)

The wireless channel is characterized by rapid variations of signal power caused by multi-path fading and Doppler frequency shifts [26]. These features make the wireless channel a very unfriendly environment for the transmission of information. Techniques to combat fading are necessary in order to be able to successfully transmit information through a wireless channel.

Transmission on the forward link of HDR is enhanced through the use of adaptive modulation and coding (AMC) and hybrid-automatic repeat request (H-ARQ) techniques, [27], [28], [29], [30]. AMC takes advantage of the time-varying nature of the fading channel to change the modulation and coding rate of the transmitted signal. More bandwidth efficient modulations (e.g., larger constellation sizes) and higher code rates are used when the signal experiences a boost in power, and more robust modulation (e.g., smaller constellation size) and lower code rates are used during fades of the signal. Since the fading signal experiences actually wider peaks than deep fades, the adaptive technique provides higher efficiency and higher data rates.

The modulation and coding rate formats used in HDR are presented in Table 2.1. The information of the transmission format to be used, and the *best* sector that should transmit the data is sent from the mobile to the base station through the Data Rate Control (DRC) channel. The DRC indicates through a 4 bit symbol, which one of the 12 possible transmission formats the selected sector is going to use to transmit the packets to the particular user. The DRC symbols are covered with a specific Walsh function; each Walsh function represents a particular sector of the active set that is chosen as the transmitting sector [31].

A Type II Hybrid-Automatic Repeat Request (H-ARQ) scheme is used on the forward link to further decrease the error rate of the air-interface and maximize throughput [32]. A packet is transmitted in one slot of 1.67 ms of duration on the data traffic channel. The mobile terminal sends an acknowledgement message on the ACK channel of the reverse link if the packet is decoded successfully, otherwise it sends a negative acknowledgement message and the packet is re-transmitted. The Type II H-ARQ is a technique that adapts to the changing conditions of the radio channel by utilizing incremental redundancy and packet combining. In the simplest form of incremental redundancy the transmitter responds to re-transmission requests by sending additional parity bits to the receiver. The receiver appends these additional parity bits to the original packet received, effectively increasing the decoding power of the decoder. The combining of the re-transmitted packets; the noisy packets (i.e., packets not-successfully decoded) in one transmission are not discarded but *soft* combined with future noisy packets to effectively decode the packet.

Code combining is a technique that is more effective in high-interference environments where the classical ARQ scheme of repeating the transmission of a packet until a good one is received, fails. Soft combining implies that soft samples of corresponding bits of packets transmitted in different slots are combined, using e.g. maximal ratio combining. In HDR both incremental redundancy and soft packet combining are used. Soft combining is performed whenever an encoded bit of a packet is received again (the same bit has been received already at least once in earlier packet transmissions).

Format	Data rate (kb/s)	Max. no. of slots	Modulation	Code rate	Packet size (bits)
1	38.4	16	QPSK	1/5	1,024
2	76.8	8	QPSK	1/5	1,024
3	153.6	4	QPSK	1/5	1,024
4	307.2	2	QPSK	1/5	1,024
5	614.4	1	QPSK	1/5	1,024
6	307.2	4	QPSK	1/3	2,048
7	614.4	2	QPSK	1/3	2,048
8	1,228	1	QPSK	1/3	2,048
9	921.6	2	8PSK	1/3	3,072
10	1,843	1	8PSK	1/3	3,072
11	1,228.8	2	16QAM	1/3	4,096
12	2,476.6	1	16QAM	1/3	4,096

Table 2.1. HDR forward link transmission formats [31].

The SIR values computed in the mobile terminal are subject to errors of prediction and measurement, therefore the mapping of predicted SIR values to formats in Table 2.1 has to be conservative in many cases in order to achieve a desired packet error rate performance. The conservative nature of the mapping can affect the maximum throughput achievable by the connections due to excess SIR values (i.e., higher than expected SIR values) [33]. The H-ARQ scheme takes advantage of excess SIR values by acknowledging the packets transmitted before the maximum number of slots is reached. The H-ARQ technique can effectively increase the data rate and maximize throughput. The specific mapping table from SIR values to formats is presented in chapter 6.

The transmission of a packet in one of the formats can take a maximum number of slots for re-transmission as specified in the third column of Table 2.1. Figure 2.2-a shows the case where the transmitted packet is acknowledged before the maximum number of slots for re-transmission are used, in this case the packet has been effectively sent in fewer slots than expected, and hence higher data rate has been achieved.

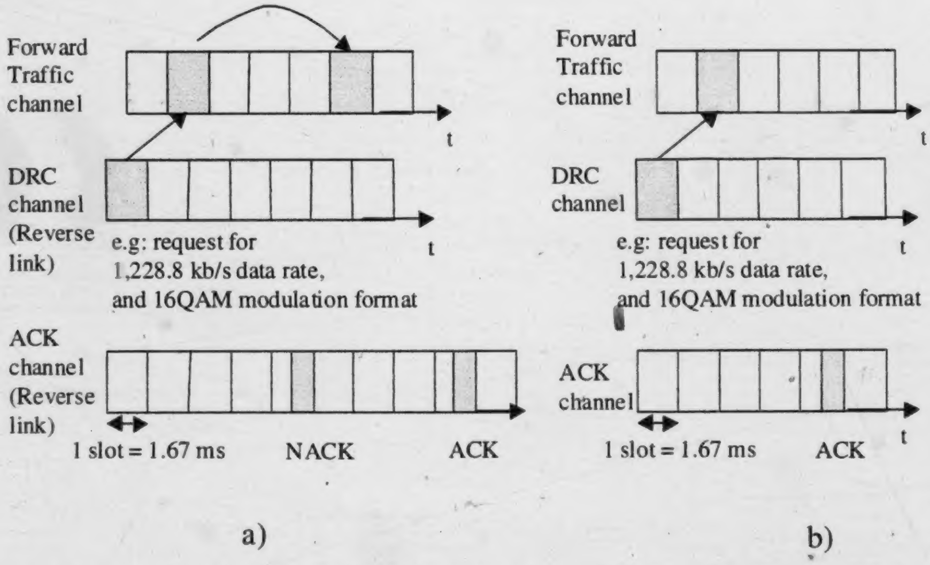
Forward Traffic channel
t
DRC channel (Reverse link)
e.g: request for 1,228.8 kb/s data rate, and 16QAM modulation format
t
ACK channel (Reverse link)
1 slot = 1.67 ms
NACK
ACK
a)
Forward Traffic channel
t
DRC channel
e.g: request for 1,228.8 kb/s data rate, and 16QAM modulation format
t
ACK channel
1 slot = 1.67 ms
ACK
t
b)

Figure 2.2. a) *Normal* termination of a packet transmission on the forward link (data rate achieved = 1,228.8 kb/s); b) Early termination of a packet transmission on the forward link (data rate achieved = 2,457.6 kb/s)

Figure 2.2-b depicts the case where the packet uses the maximum number of re-transmission slots; in this case the rate of transmission of the packet is the one specified in the second column of Table 2.1 for any specific format used. In all cases the re-transmission of a packet occurs at every fourth slot to allow for time-diversity and give time to decode a packet and transmit the acknowledgment to the corresponding sector.

In order for Type II H-ARQ schemes and the format of transmission adaptation technique to work properly, it is necessary to estimate the channel-state at the receiver for channel prediction and format of transmission determination. In HDR the mobile terminal estimates the channel condition by measuring the received signal to interference ratio (SIR) from the pilot signal. The value of SIR is then mapped to a transmission format that the forward link connection can support with adequate error performance. The mapping from a channel estimation metric to a particular format implies the use of channel-prediction methods because the times of estimation and actual transmission are different. Channel prediction is particularly difficult in multi-path fading channels with mobiles traveling at high speeds. High speed translates into small channel coherence-time or rapid variations in channel conditions. Many researchers have addressed the prediction of channel conditions in fading channels, [34], [35], [36]. The prediction method used in this research work is presented in Chapter 6.

On the reverse link of HDR, packets of different users are transmitted at the same time in the same frequency band using code division multiple access (CDMA). The packets of the different users are separated by distinct long code sequences, therefore the reverse link of HDR is a standard direct-sequence CDMA system that also uses soft handoff and power control to adapt to the varying conditions of the wireless fading channel.

On the forward link of HDR the sectors are transmitting at all times and at the maximum allowable power. No soft handoff or power control is in operation. Adaptive Modulation and Coding and Type II H-ARQ are used instead as mechanisms for channel adaptation. In the forward link of HDR the traffic channel is transmitted by only one sector, estimated to be the best of the sectors in the active set. The selection of this sector depends on the application, but it is usually the strongest sector as perceived by the mobile terminal.

The network layer protocol that will support the transmission of packets will likely be based on the Internet-protocol due to its widespread use. The chosen protocol for the transmission of packets is the Point-to-point protocol (PPP) [37], [38], this is a protocol used to communicate between two entities (i.e., a laptop and a host) and it is functionally below TCP/IP. PPP is the most common protocol used for modem connections today. PPP uses low overhead, methods to support differing quality of service requirements, and support of different authentication methods such as the challenge handshake authentication protocol (CHAP).

2.2.2 Forward link physical layer description

The HDR forward channel consists of the pilot channel, medium access control (MAC) channel, forward traffic channels, and control channels [31]. All the channels on the forward link are time-multiplexed in one slot, see Figure 2.3.

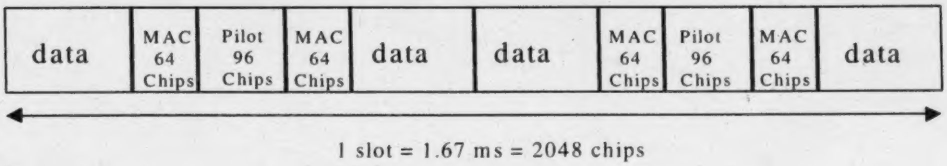

Figure 2.3. Slot structure in HDR.

The pilot channel is used for SIR estimation, selection of the best sector from the set of available sectors, and coherent demodulation. The MAC channel is subdivided into two channels, the reverse power control channel and the reverse activity channel. The reverse power control channel transmits the power control commands to the mobile terminals, and the reverse activity channel is used to transmit MAC layer information in order to control the mobile terminals reverse channel transmissions. The forward traffic and control channels are used to convey dedicated data or control information to a mobile terminal. The forward traffic channel is a packet-based channel that provides variable data rates from 38.4kb/s to 2.4Mb/s as specified previously in Table 2.1. A simplified block diagram of the forward channel structure is depicted in Figure 2.4. The data on the traffic or control channels is first encoded using turbo codes with rates 1/3 or 1/5 [39]. The output of the encoder is scrambled and interleaved before modulation. Modulation in the forward channel can be QPSK, 8-PSK or 16-QAM [40] depending on the format chosen by the mobile terminal (see Table 2.1). The modulation symbols at the output of the modulators are de-multiplexed into 32 streams of symbols; 16 streams take the in-phase branch, and the other 16 take the quadrature-phase branch.

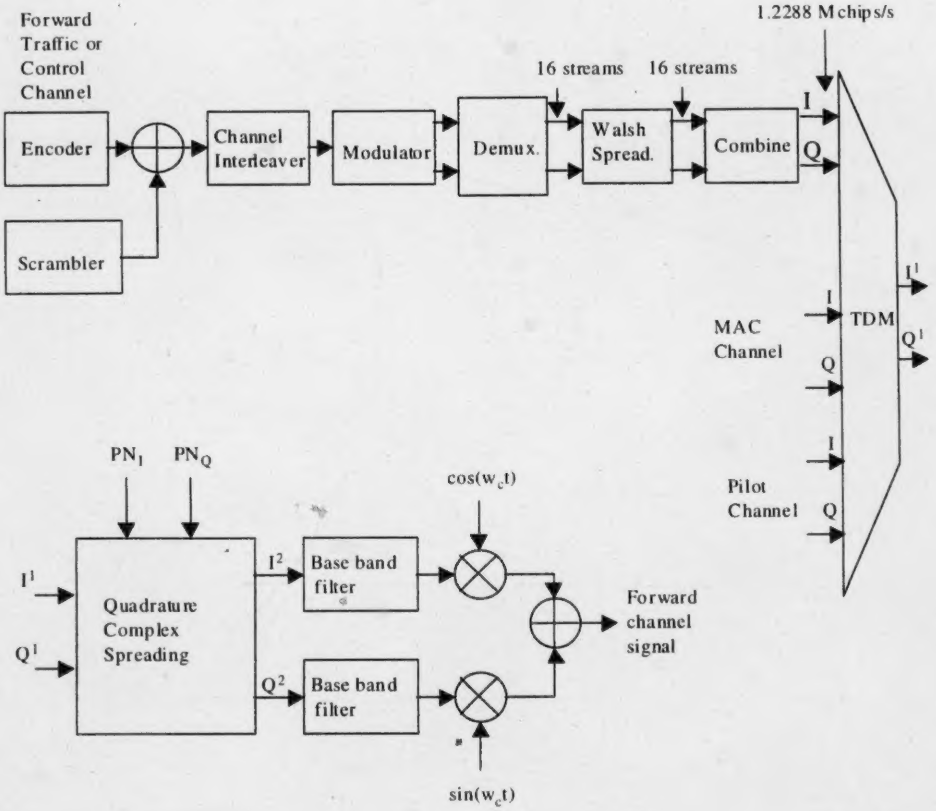
Forward Traffic or Control Channel
1.2288 Mchips/s
16 streams
16 streams
Encoder
Channel Interleaver
Modulator
Demux.
Walsh Spread.
Combine
I
Q
Scrambler
MAC Channel
I
Q
TDM
I¹
Q¹
Pilot Channel
I
Q
PN_I
PN_Q
cos(w_c t)
I¹
Q¹
Quadrature Complex Spreading
I²
Q²
Base band filter
Base band filter
Forward channel signal
sin(w_c t)

Figure 2.4. HDR forward link traffic/control channel structure.

Each stream is spread with a 16-ary Walsh function to achieve 76.8ksymbol/s, and at the next stage the 16 streams of each branch are combined to form the main stream at 1.2288 Mchips/s that is time-multiplexed with the rest of the forward channels. Symbol repetition and puncturing is performed between the modulator and de-multiplexer.

The in-phase and quadrature-phase branches at the output of the time-division multiplexer are fed into a complex spreader. The complex spreader combines the short PN sequences PN_I and PN_Q with the data in the I^1 and Q^1-phase branches according to equation (2.1).

$$\begin{aligned} I^2 &= I^1 PN_I - Q^1 PN_Q \\ Q^2 &= I^1 PN_Q + Q^1 PN_I \end{aligned} \tag{2.1}$$

The complex spreader is performing complex multiplication. Complex spreading after Walsh spreading helps to ensure a low cross-correlation between the different channels separated by Walsh sequences. Walsh sequences have to be synchronized to be orthogonal. Due to multi-path, the synchronization of the Walsh functions is not ensured and complex spreading on top of the Walsh sequences helps to keep a low cross-correlation even in the presence a multi-path environment. The instantaneous relative powers of the in-phase and q-phase channels can differ, causing an imbalance of the transmitted signal and inefficiency of the power transmitter amplifier. Complex spreading further improves this situation by balancing the in-phase and q-phase channels. Base-band filters are used to meet bandwidth constraint requirements and minimize inter-symbol interference (ISI) [41]. In HDR the signals from sectors of different cells are identified by a particular time-shifted version of a short PN code, this can effectively reduce inter-cell interference since the cross-correlation between codes generated in this way is low.

2.2.3 Reverse link physical layer description

The reverse channel in HDR is sub-divided into the access channel and the reverse traffic channel. The access channel is further sub-divided into a pilot channel and a data channel. The traffic channel consists of the pilot channel, reverse rate indicator (RRI) channel, the data rate control (DRC) channel, the acknowledgement (ACK) channel, and the traffic channel.

The access channel is used to initiate communication with the active sector, and transmit short packets. The traffic channel is used to send user data; the rate on the reverse link varies between 9.6 kb/s to 153.6 kb/s. The RRI channel is used to indicate the rate used on the reverse traffic channel. Table 2.2 summarizes the most important parameters of the HDR system.

Bandwidth	1.25 Mhz
Chi rate	1.2288 Mchips/s
Frequency band reverse link	Cellular and PCS
Frequency band forward link	Cellular and PCS
Bit rates for data services	Forward link: 38.4 kb/s to 2.5 Mb/s Reverse link: 9.6 to 153.6 kb/s
Soft handoff	Forward link: No Reverse link: Yes
Power control	Reverse link: open loop + closed loop Forward link: Sector always transmits at maximum power.
Adaptive Modulation & Coding (AMC)	Forward link: Yes Reverse link: No
Hybrid-ARQ	Yes
Modulation	Forward link: QPSK, 8PSK, 16QAM Reverse link: BPSK
Slot length	1.67ms or 2048 chips
Error control coding	Forward link: 1/3 and 1/5 rate turbo encoder Reverse link: 1/4 and 1/2 rate turbo encoder

Table 2.2. HDR parameters.

2.2 The 1XTREME system

1XTREME represents a proposed evolution of IS-2000 that provides packet data services, and *real-time* services simultaneously in the same 1.25 MHz bandwidth. Best-effort packet data services are characterized by tolerance to delays, and low error rate requirement; examples of these services are email, and Web browsing. Real-time services are characterized by intolerance to delays, and higher tolerance to error rates than best-effort packet data services; examples of these services are voice and live video services. As in HDR, the 1XTREME system utilizes adaptive modulation and coding, hybrid ARQ, and turbo codes. Table 2.2 shows the forward link transmission formats used in 1XTREME.

Format	Modulation	Code rate
1	QPSK	½
2	QPSK	¾
3	8-PSK	½
4	8-PSK	¾
5	16-QAM	½
6	16-QAM	¾
7	64-QAM	½
8	64-QAM	¾

Table 2.3. 1XTREME forward link transmission formats [42]

The base-band 1XTREME forward traffic channel structure is depicted in Figure 2.5 [19]. Data is transmitted in frames of 5ms of time duration. The data is transmitted in N parallel streams ($N \leq 14$), and each stream is covered with a different 16-ary Walsh function (Code Division Multiple Access). As in HDR the active sector selects the transmission format on the forward link based on SIR measurements at the mobile terminal, and the results of this measurement are sent to the active sector by the *Reverse link Quality Indicator* Channel (R-QICH) [23].

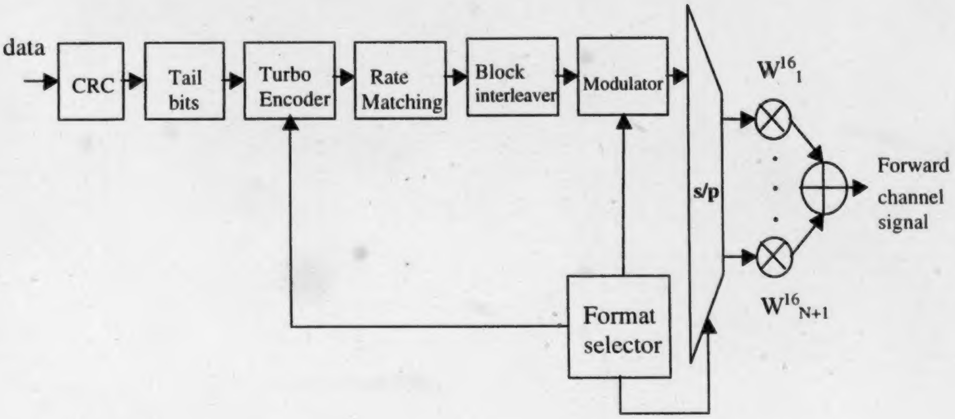
data
CRC
Tail bits
Turbo Encoder
Rate Matching
Block interleaver
Modulator
s/p
W^{16}_{1}
W^{16}_{N+1}
Forward channel signal
Format selector

Figure 2.5. Baseband 1XTREME forward link channel structure.

2.3 Summary

The primary design fundamentals behind HDR and 1XTREME were discussed, including the Adaptive Modulation and Coding (AMC), and H-ARQ channel adaptation techniques. A brief description of the structure of the forward and reverse link channels was also presented. A more detailed description of the HDR and 1XTREME physical layers will be presented in chapter 4 under the scope of the link-level simulator description.

Chapter 3

The cellular radio system environment

3.1 Introduction

The cellular radio system environment can be characterized by its geometric structure in space and the propagation details of the wireless channel.

It is necessary to define the layout of the cells across the coverage area in order to make possible the analysis and design of cellular radio systems. In the most common geometrical model, all the cells in the coverage area are represented by non-overlapping hexagons, and the serving base station of each cell is located in the center of the hexagon. Sectors of a cell are modeled by equally dividing the area of the hexagon according to the number of sectors used. This type of cell-layout model neglects the fact that cells actually overlap causing changes in the performance of the system. In systems that utilize hard-handoff the overlapping region can cause undesired frequent switching of the mobile terminal between different base stations, and in soft-handoff systems the overlapping region will represent the most likely region for soft-handoff to occur.

The cellular radio environment modeling is also influenced by the propagation characteristics of the wireless channel. The information-bearing signals transmitted over a wireless channel are affected by a number of adverse random propagation phenomena. These adverse phenomena represent a major limitation when high bit rate with low bit error rate transmission is desired. The cause of the wireless channel behavior is frequently attributed to path-loss, reflection, diffraction, and scattering.

Path-loss causes the attenuation of the signal as a consequence of the space separation between the transmitter and receiver antennas. The ratio of power transmitted to power received is proportional to the distance of separation. Several models have been proposed for the estimation of path-loss such as the Okumura model [43] commonly used in urban areas, the Hata model [44], and the Walfish-Ikegami model proposed by the committee 231 of the European co-operative for scientific and technical research (COST) [45].

Reflection, diffraction and scattering are related electromagnetic propagation phenomena encountered when an electromagnetic wave travels through a region with physical obstacles. All these phenomena are present in the wireless channel, and their effect is to cause multi-path fading of the transmitted signals [2].

Shadow fading is another phenomena observed in the wireless channel, it is the mean signal variation over large areas due to large obstacles such as buildings and hills; it has been characterized by a Gaussian random variable. Shadow fading takes into account the fact that different locations with the same transmitter-receiver distance have different path-loss.

Multi-path fading is the rapid fluctuation of the signal transmitted over a wireless channel. The rapid fluctuations are due to the self-interference caused by delayed replicas of the transmitted signal that combine in the receiver antenna. When the channel bandwidth is smaller than the transmitted signal bandwidth, the delayed replicas arrive at the receiver with large differences in time, causing inter-symbol interference (ISI) and frequency selective fading. When the signal bandwidth is smaller than the channel bandwidth the signal undergoes what is called flat fading [2], [46]. In a CDMA system the RAKE receiver helps to resolve the different paths when the multi-path fading is frequency-selective. Other types of multi-path fading are fast and slow multi-path fading. In fast fading the channel-variation times are faster than the symbol period, in this type of channel there is a high frequency spread caused by the high Doppler shift of the frequencies. High Doppler shift is caused by high mobile speed. Slow fading is characterized by channel-variation times larger than the symbol period.

This chapter presents the cellular radio environment models and assumptions taken in this research work. Section 3.2 describes the cellular layout used. Section 3.3 presents the path-loss Walfish-Ikegami model, the cell size computation, and the shadow-fading model used, and finally section 3.4 addresses the multi-path fading model.

3.2 Cellular geometric structure

The cell layout is depicted in Figure 3.1, as given in [22]. There are 19 cells consisting of two rings of 3 sectors each. There are 57 sectors altogether.

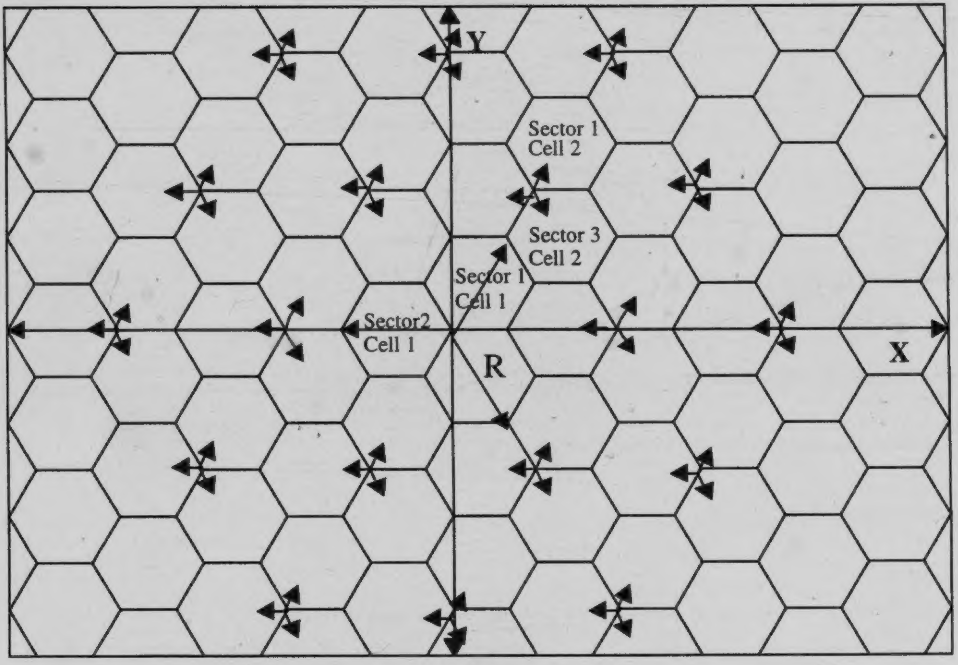
Y
Sector 1
Cell 2
Sector 3
Cell 2
Sector 1
Cell 1
Sector2
Cell 1
R
X

Figure 3.1. Cell layout as recommended in [6]. Bore-sight of antennas is shown with small arrows at the center of 3 sectored cells.

3.3 Path-loss and shadow fading models

The path-loss in free-space, assuming an isotropic antenna is given by Equation 3.1 [2]

$$L_{fs} = \left(\frac{4\pi d f_c}{c} \right)^2 \tag{3.1}$$

d = distance separation between the transmitter and receiver antennas;

c = speed of light; f_c = frequency of the transmitted sinusoid waveform in Hz.

The free-space path-loss formula is used in the design of line-of-sight (LOS) communication systems where there is an unobstructed path between the transmitter and receiver antennas; an example of such a system is the microwave-radio-link communication system. The cellular radio system environment rarely presents LOS radio links. More accurate models have to be used to estimate the path-loss attenuation in cellular radio environments. A commonly used path-loss estimation formula is given by Equation 3.2 [2]

$$L = \overline{L}_r(d_0)\left(\frac{d}{d_0}\right)^n \tag{3.2}$$

In equation 3.2, d_0 represents a reference distance taken close to the transmitter antenna, $\overline{L}_r(d_0)$ is the average measured path-loss at reference-distance d_0, and n is a exponent that indicates the degree of attenuation suffered by a signal depending on distance separation; n ranges between 3.0 to 5.0 [10]. The exponent n depends on the structure of the physical surroundings. The model in equation (3.2) is known as the general empirical model for the estimation of path-loss.

In this research work the COST231-Walfish Ikegami model is used [45], [47]. The Walfish-Ikegami model is applicable for transmitter-receiver distances greater than or equal to 20 meters, and base-station antennas above or below the roof tops. For non-line-of-sight (NLOS) propagation the Walfish-Ikegami model is given by

$$L = L_{bf} + L_{rts} + L_{msd} \tag{3.3}$$

where

$$L_{bf} = 32.4 + 20\log(d) + 20\log(f_C); \tag{3.4}$$

$$L_{rts} = -16.9 - 10\log(w) + 10\log(f_C) + 20\log(H - h_m) + L_{ori,}); \tag{3.5}$$

$$L_{msd} = 54 - 18\log(1 + h_b - H) + 18\log(d) + \left[-4 + 0.7\left(\frac{f_C}{925} - 1\right)\right]\log(f_C) - 9\log(b). \tag{3.6}$$

are free space, roof-top-to-street diffraction, and multi-screen diffraction losses respectively; The path-loss in equations (3.3)-(3.6) is expressed as a function of the separation distance between transmitter and receiver antennas (d), the carrier frequency in MHz (fc), the street width (w), building separation (b), base-station and mobile station antenna heights (h_b, h_m), average rooftop height (H). L_{ori} is the orientation loss. We have assumed $L_{\text{ori}} = 0\,\text{dB}$, which is a usual default value.

Cell size calculation is performed using the Walfish-Ikegami model and values presented in Table 3.1. The path loss is computed along the bore sight line of the antenna. After inserting the parameters given by Table 3.2 in equations (3-3)-(3-6), and given $L_{b(\max)} = 130.87\,\text{dB}$; the cell radius is computed to be 473 meters, which implies site-to-site separation of 709 m.

The directivity loss (horizontal pattern) of the antenna (EMS, RR65-18-00DP) used is available as a data file. The directivity loss vs. relative orientation with respect to the antenna bore sight can be seen in Figure 3.2, The 3dB bandwidth is

$\theta_{3dB} \cong 66^0$,and the front-to-back ratio for this antenna is about 35 dB. This ratio affects the maximum available SIR in each sector.

Parameter	Value	Comments
(a) Transmission Power per sector $Pt_{\max}$.	42.3 dBm (17 W)	-
(b) BS Bore-sight antenna gain, G_b.	17.54 dBi	Antenna EMS WIRELESS RR 65-18-00DP
(c) Antenna cable Loss, L_c.	3 dB	-
(d) Effective data transmission power	80% of $Pt_{\max}$	-
(e) Total transmitted power on the traffic channel at the bore sight of the antenna.	a+b-c+d=55.87 dBm	-
(f) Penetration loss, L_p.	10.0 dB	-
(g) Minimum required received data channel power on BS antenna bore sight line, P_{rec}.	-85 dBm	Includes large scale fading margin
(h) PSD of thermal noise	-174 dBm/Hz	Ignored
(j) Maximum allowable over-the-air loss, $L_{b(\max)}$.	e-f-g=130.87 dB	-

Table 3.1. Link budget values for the forward Link

Parameter	Range	Values Used in Simulation
Carrier frequency	$800 \le f \le 2000\,\text{MHz}$	1960 MHz
Distance to BS antenna	$0.02 \le d \le 5\,\text{km}$	Variable
BS antenna height	$4 \le h_b \le 50\,\text{m}$	3 m above average roof top
MS antenna height	$1 \le h_m \le 3\,\text{m}$	1.5 m
Building separation *b*	-	40 m
Street width *w*	-	20 m
Average roof top height H	-	18 m

Table 3.2. Values of parameters used in cell size computation.

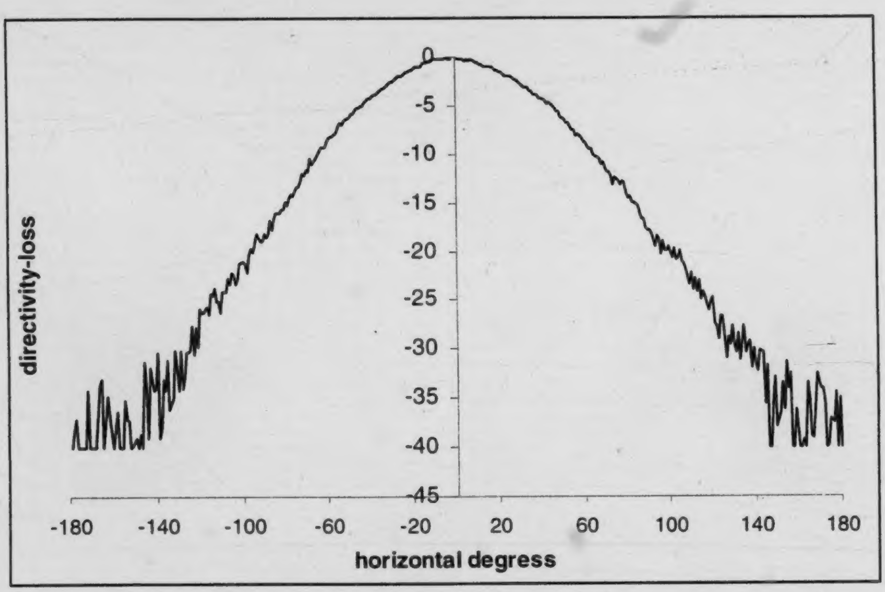

Figure 3.2. The directivity loss pattern for the EMS RR65-18-00DP antenna.

The log-normal shadowing effect is modeled by a zero mean Gaussian random process added to the path-loss in dB [47]. Therefore, the signal power averaged over small scale is given by

$$P^{i}_{\text{rec}} = P_{\text{t}} + G_{\text{b}} + G^{i}_{\text{d}}(\theta) - L_{\text{p}} - L^{i}_{\text{b(dB)}} - \mathrm{X}^{i}, \qquad i = 1,\Lambda\ ,57. \tag{3.7}$$

where, P^{i}_{rec} is the received power by a mobile terminal from sector i, P_t is the transmitted power, G_b is the base station antenna gain, $G^{i}_{\text{d}}(\theta)$ is the directivity loss, L_{P} is penetration loss, L^{i}_{b} is given by (3.3), L^{i} is the path-loss between a mobile terminal and sector i, and X^{i} is the shadowing variable.

On the dB scale, X^i is a zero mean Gaussian random variable with standard deviation σ_X. A typical range of values for σ_X in macro-cellular environments is 5-12 dB. In micro-cellular environments, a typical value of σ_X is 4-13 dB [47]. We use 6.5 dB in our simulations.

The cross-correlation of the log-normal shadowing term for signals arriving from base stations *i* and *j* is denoted by α.

$$\frac{E[X^i X^j]}{\sqrt{Var(X^i)}\sqrt{Var(X^j)}} \equiv \alpha, \qquad i \neq j,\ i = 1,\Lambda\ ,19,\ \ j = 1,\Lambda\ ,19. \tag{3.8}$$

In this work we assume a constant value of $\alpha = 0.5$ for shadowing cross-correlation of signals received from different cell sites. The cross-correlation of shadowing variables between signals from different sectors of the same base station is one [47]. To ensure proper cross-correlation of the log-normal shadowing variable, X^i is generated as a linear combination of a component representing the base-station dependent shadowing Z^i such that $E[Z^i Z^j] = 0$ for $i \neq j$, and a component *Z* common to all base stations. In order to generate cross-correlated Gaussian sequences, the shadowing variable can be written as

$$X^i = aZ + bZ^i,\ i = 1,2,\ldots,19;\ a \geq 0, \quad b \geq 0. \tag{3.9}$$

where Z, Z^i are i.i.d Gaussian random variables with zero mean and standard deviation $\sigma_Z = \sigma_X$.

Note that

$$\sigma_X{}^2 = E[X^{i^2}] = a^2 E[Z^2] + b^2 E[Z^{i^2}] = (a^2 + b^2)\sigma_Z{}^2,$$

Therefore, $(a^2 + b^2) = 1$ (3.10)

From (3.8) - (3.10)

$$E[X^i X^j] = \alpha \sigma_X{}^2 = a^2 E[Z^2],$$

Therefore, $a^2 = \alpha, \ b^2 = 1 - \alpha.$ (3.11)

By taking $a = b = \sqrt{1/2}$ in Equation (3.9) we can generate Gaussian random sequences with 50% cross-correlation and standard deviation σ_X.

Shadow fading is spatially auto-correlated (i.e., values of shadow fading terms are correlated in different points in space). Spatial auto-correlation of shadow fading has to be taken into account when the mobile is moving. In this research work the spatial auto-correlation is modeled as an exponential function as proposed by Gudmundson in [48].

$$\Phi(k) = E[X^i{}_d X^i{}_{d+k\Delta d}] = (\sigma_X)^2 \quad e^{-\frac{|k|\Delta d \ln 2}{d_{dec}}} = (\sigma_X)^2 \quad e^{-\frac{|k|\Delta t v \ln 2}{d_{dec}}} \qquad (3.12)$$

where d_{dec} is the decorrelation distance, and v is the mobile speed. In [20], and [22] $d_{dec} = 20\,\text{m}$ is suggested for vehicular test environments, and $d_{dec} = 5\,\text{m}$ for outdoor to indoor and pedestrian environments. In our simulations, we use these two values for vehicular B and pedestrian A environments, respectively. The vehicular B and pedestrian A radio environment specifications and definitions are given in [20]. A vehicular B environment is characterized by larger cells, higher transmit powers and higher mobile speeds; the pedestrian A environment main characteristics are small cell size and low mobility.

The update rate of the shadowing factor should in principle depend on the mobile velocity and the relative contribution of shadowing to $L^i_{b(\mathrm{dB})} + \mathrm{X}^i$. We have decided to update the shadowing variable at $\Delta d = d_{\mathrm{dec}}/10$ intervals.

The exponential auto-correlation function given by (3-12) can be generated with a first order discrete time recursive filter [47];

$$X^i{}_{k+1} = \xi X^i{}_k + (1-\xi)\upsilon_k\,; \tag{3.13}$$

where X_{k+1} is the updated shadow term at position $k+1$ that is correlated with the previous value X_k at position k. ξ is a parameter used to control the spatial auto-correlation of shadowing, and υ_k is a zero-mean Gaussian random variable with standard deviation σ_υ. The auto-correlation of (3.13) is given by

$$\Phi(n) = E[\mathrm{X}^i{}_k \mathrm{X}^i{}_{k+n}] = \frac{1-\xi}{1+\xi}\sigma_\upsilon{}^2 \xi^{|n|}\,. \tag{3.14}$$

Comparing equation (3.12) and (3.14), it is possible to find a value of ξ and σ_υ to make the auto-correlation of the recursion in (3.13) equal to that in (3.12). Choosing

$$\xi = e^{-\frac{\Delta d \ln 2}{d_{dec}}} \text{ ; and } \sigma_\upsilon{}^2 = \frac{1+\xi}{1-\xi}\sigma_X{}^2 . \tag{3.15}$$

The auto-correlation of the discrete recursion in equation (3.13) becomes

$$\Phi(n) = (\sigma_X{}^2)e^{-\frac{|n|\Delta d \ln 2}{d_{dec}}} . \tag{3.16}$$

Therefore the recursion in (3.13) can be used with the values in (3.15) to generate a sequence of correlated Gaussian random numbers; each number $X_k{}^i$ is associated with the position $k\Delta d$.

In order to model shadow fading for our simulation we are interested in 19 sequences of Gaussian random numbers with fix cross-correlation of 50%, auto-correlation given by equation (3.16), and with standard deviation σ_X . In order to achieve the above constrains the following procedure is applied.

We first generate 19 sequences with cross-correlation of 50% as follows

$$v^i = \sqrt{\frac{1}{2}}Z + \sqrt{\frac{1}{2}}Z^i \quad i = 1,2,\ldots,19; \tag{3.17}$$

where

$$Z = Gaussian\left(0 \text{ mean}, {\sigma_Z}^2\right)$$
$$Z^i = Gaussian\left(0 \text{ mean}, {\sigma_Z}^2\right)$$
$${\sigma_Z}^2 = {\sigma_\upsilon}^2 = \frac{1+\xi}{1-\xi}\left({\sigma_X}^2\right)$$
$$\xi = e^{-\frac{\Delta d \ln 2}{d_{dec}}}$$

The sequences in (3.17) are used next to generate the 19 sequences with desired auto-correlation and fixed cross-correlation of 50% as follows

$$X^i{}_{k+1} = \xi X^i{}_k + (1-\xi)\upsilon_k{}^i \quad i = 1,2,\ldots,19; \quad 0 \le k < N; \qquad (3.18)$$

where N is the desired length of the sequences. Figure 3.3 shows the comparison between an ideal auto-correlation function and the auto-correlation of 200,000 shadow numbers generated using equations (3.17) and (3.18). $\sigma_X = 6.5\,\text{dB}$ and $d_{dec} = 5$ m ($\Delta d = 0.5\,\text{m}$) are assumed.

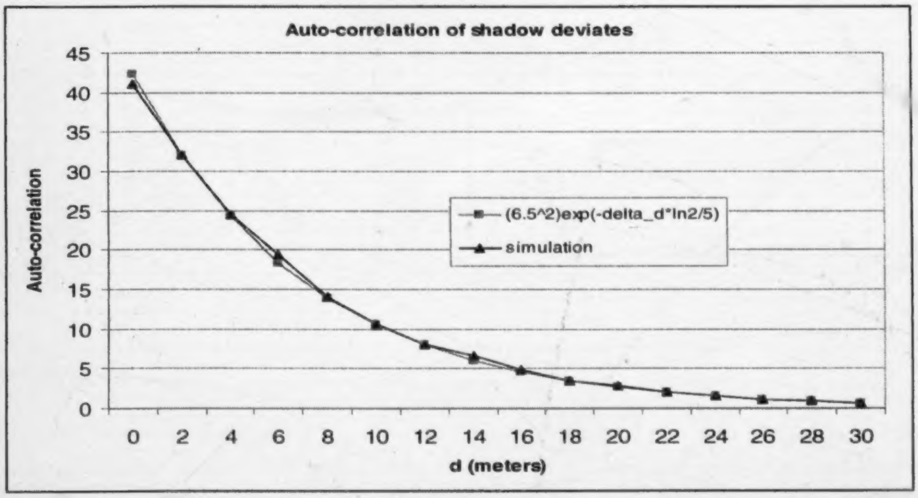

Figure 3.3. Ideal and simulated auto-correlation of 200,000 log-normal shadow fading variables.

3.4 Multi-path fading model

To take into account the impact of fast fading of the signal on the performance of the systems, Rayleigh fading is modeled. In a Rayleigh fading channel, the probability density function (pdf) of the received signal power γ is given by the exponential distribution

$$p_{\gamma}(\gamma) = \frac{1}{\bar{\gamma}} e^{-\gamma/(\bar{\gamma})} \tag{3.19}$$

where $\bar{\gamma} = 10^{P_{\text{rec}}/10}$ is the small scale averaged signal power. P_{rec} (dBm) is given by (3.7). In the simulation, an exponential random variable with mean P_{rec} is obtained by multiplying P_{rec} by the normalized exponential random variable γ with $\bar{\gamma} = 1$. Alternatively, (3.7) is replaced by

$$P^{i}{}_{\text{rec}} = P_{\text{t}} + G_{\text{b}} + G^{i}{}_{\text{d}}(\theta) - L_{\text{p}} - L^{i}{}_{\text{b(dB)}} - X^{i} + \gamma_{(\text{dB})}, \qquad i = 1, \Lambda, 57, \tag{3.20}$$

where $p_{\gamma}(\gamma) = e^{-\gamma}$.

The Rayleigh fading process exhibits an auto-correlation that can be described using Clark's model [49]. In Clark's model, the field incident on the mobile antenna is assumed to be comprised of *N* azimuthal plane waves with arbitrary carrier phases, arbitrary azimuthal angles of arrival, and equal average amplitudes. The equal average amplitude assumption is based on the fact that in the absence of a direct line of sight path, the scattered components arriving at a receiver from all directions will experience similar attenuation over small distances. In this model, the auto-correlation function of the real and imaginary parts $x_R(t)$ and $x_I(t)$ of the complex envelope is given by [47]

$$\phi_{x_R x_R}(\tau) = \phi_{x_I x_I}(\tau) = \Omega_P J_0(2\pi f_{D\max}\tau), \tag{3.21}$$

where J_0 is the zero-order Bessel function of the first kind, Ω_P is the total average received power from all multi-path components, and $f_{D\max}$ is the maximum Doppler frequency. The power spectral density (psd) of $x_R(t)$ and $x_I(t)$ is given by [47]

If $\Omega_p = E[r^2(t)]/2$, then

$$S_{x_R x_R}(f) = S_{x_I x_I}(f) = \begin{cases} \dfrac{\Omega_P}{2\pi f_{D\max}} \dfrac{1}{\sqrt{1-(f/f_{D\max})^2}} & |f| \le f_{D\max}, \\ 0 & \text{otherwise.} \end{cases} \tag{3.22}$$

Where *r(t)* is the received band-pass signal. It should be noted that the psd of the real and imaginary parts of the amplitude of the base band signal is singular at $f = \pm f_{D\max}$. A modified Smith method [50] is used to generate a Rayleigh random process with the auto-correlation that approximates (3.22). In this method, first, *N* samples of a complex Gaussian white noise in frequency domain are filtered to obtain psd given by (3-22). Then IDFFT is used to obtain a sequence of *N* correlated complex Gaussian random variables in the time domain.

A block diagram of the modified Smith method is given in Figure 3.4. Since psd of a discrete time process is periodic with period equal to f_{sampling}, instead of sampling a Gaussian white noise in frequency domain in $|f| \le f_{D\max}$ as (3-22) suggests, one can sample the Gaussian noise in $0 \le f \le f_{D\max}$ and $f_{\text{sampling}} - f_{D\max} \le f \le f_{\text{sampling}}$ intervals. More specifically, in this method, a white Gaussian noise in frequency domain is passed through a low-pass filter with filter coefficients given in (3-23).

$$F_M[k] = \begin{cases} 0 \quad k = 0, \\ \sqrt{\dfrac{1}{2\sqrt{1-\left(\dfrac{k}{Nf_m}\right)^2}}} & k = 1,2,\ldots,k_m - 1, \\ \sqrt{k_m\left[\dfrac{\pi}{2} - \arctan\left(\dfrac{k_m - 1}{\sqrt{2k_m - 1}}\right)\right]} & k = k_m, \\ 0 \quad k = k_m + 1,\ldots,N - k_m - 1, \\ \sqrt{k_m\left[\dfrac{\pi}{2} - \arctan\left(\dfrac{k_m - 1}{\sqrt{2k_m - 1}}\right)\right]} & k = N - k_m, \\ \sqrt{\dfrac{1}{2\sqrt{1-\left(\dfrac{N-k}{Nf_m}\right)^2}}} & k = N - k_m + 1,\ldots,N - 1 \end{cases} \tag{3.23}$$

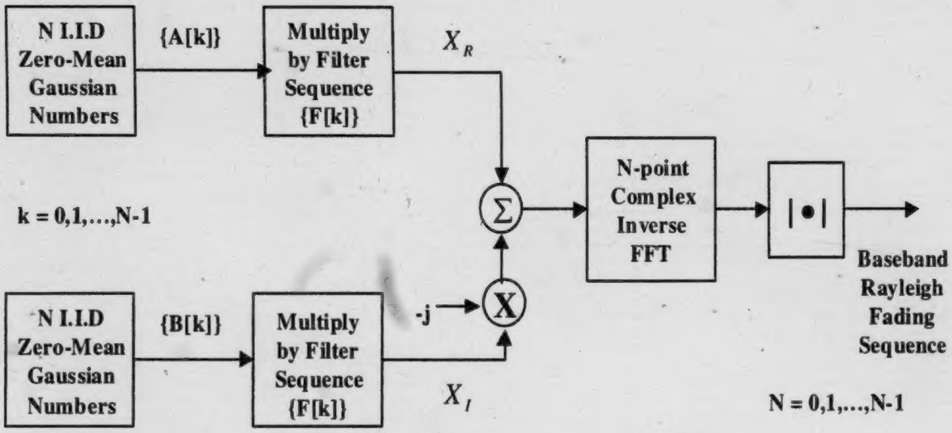
N I.I.D
Zero-Mean
Gaussian
Numbers
{A[k]}
Multiply
by Filter
Sequence
{F[k]}
X_R
k = 0,1,…,N-1
Σ
N-point
Complex
Inverse
FFT
|•|
Baseband
Rayleigh
Fading
Sequence
N I.I.D
Zero-Mean
Gaussian
Numbers
{B[k]}
Multiply
by Filter
Sequence
{F[k]}
-j
X
X_I
N = 0,1,…,N-1

Figure 3.4. Block diagram of the modified Smith method.

In (3-23), $f_m = f_{D\max} / f_{\text{sampling}}$ is the ratio of the maximum Doppler frequency to sampling frequency and $k_m = \lfloor f_m N \rfloor$, where N is the number of sampling points in the frequency domain and the corresponding number of points per period of the auto-correlation function. After filtering the sampled white Gaussian noise in frequency domain, the inverse discrete Fourier transform (IDFT) is used to obtain the complex fading random process in the time domain. The filter coefficients are chosen in such a way that the real and imaginary parts of the output variables are statistically independent. The modified Smith model presented has the advantage of less computational complexity in comparison with the standard Smith model. In the standard Smith model [2] two branches similar to the one in Figure 3.4 are used to produce the desired result due to the independence requirement of the real and imaginary parts of the Gaussian sequences after IDFT operation.

The normalized real and imaginary parts of the output of the IDFT are

$$x_c(n) = x_R(n) + jx_I(n) \tag{3.24}$$

where n refers to sampling time t_n. The auto-correlation is given by

$$\phi_{x_R x_R}(\tau) = \phi_{x_I x_I}(\tau) = J_0(2\pi f_{D\max}\tau). \tag{3.25}$$

where τ can take discrete values only.

Simulated and theoretical pdf's of Rayleigh variables generated using the modified-Smith method presented above are shown in Figure 3.5. In this figure the comparison is made with the normalized pdf function for which $2\sigma^2 = \Omega_p = 1$. Figures 3.6 and 3.7 show a comparison of the theoretical and simulated auto-correlation of x_R for user speeds of 3 and 60km/h. At these speeds the Doppler frequency is 5.3 and 105.6Hz respectively. As can be seen by the auto-correlation functions, when higher speeds are involved, the correlation of Rayleigh fading numbers decreases faster in time

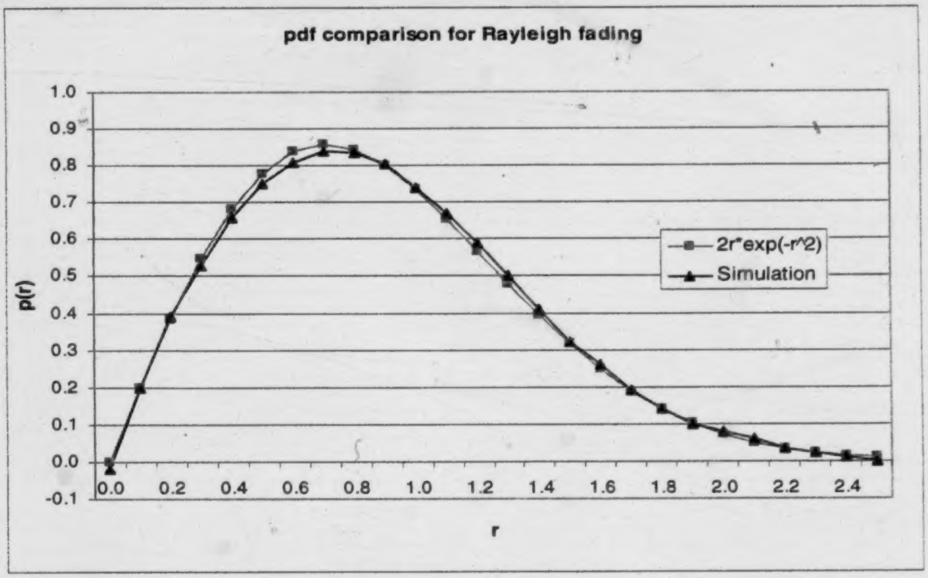

Figure 3.5. pdf comparison of theoretical and simulated correlated Rayleigh process.

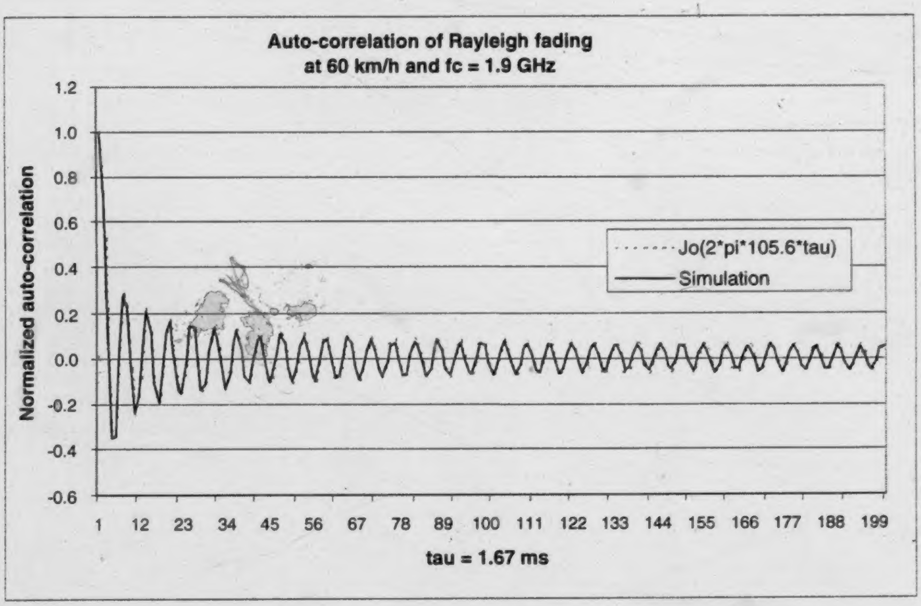

Figure 3.6. Auto-correlation comparison of theoretical and simulated Rayleigh process at 60km/h with f_c = 1.9GHz.

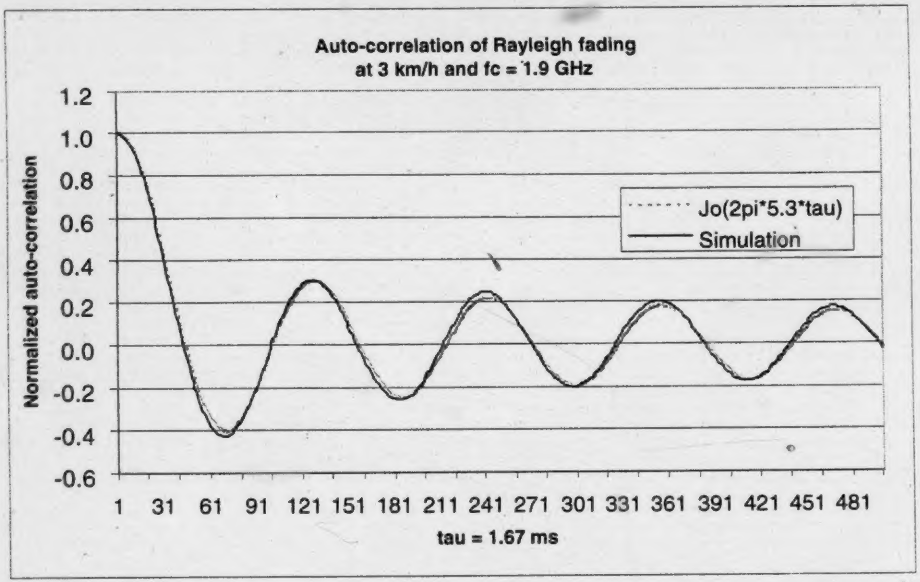

Figure 3.7. Auto-correlation comparison of theoretical and simulated Rayleigh process at 3km/h with $f_c = 1.9$GHz.

3.5 Summary

We have presented the algorithms and equations to model the cellular radio environment for this research work. The cell layout defined in [22] is going to be used for vehicular B and pedestrian A radio environments as defined in [20]. The COST-231 Walfish-Ikegami model will be implemented for path-loss estimation. Shadow fading will be modeled as a log-normal process with fix cross-correlation to model shadow fading coming from different cell-sites and exponential auto-correlation as proposed in [48] to model spatial correlation. The method proposed in [50] will be used to model multi-path fading at different speeds.

Chapter 4

Simulation structure and link level simulations

4.1 Introduction

There are two possible approaches for the simulation of a cellular radio system. In one approach the system is simulated entirely from the transmitter-receiver modeling of a single radio link to the modeling of radio-links and operations for a multitude of mobiles and base stations present in the network. This approach is the most accurate one, but its complexity is extremely high considering the number of waveforms to generate and the simulation run-time. A preferred two-stage method is to separate the simulation of the transmitter-receiver pair from the simulation of the operations and signals of the entire system.

In the two-stage approach, the simulation of the transmitter-receiver pair is called the link-level simulation, and the entire-network simulation is called the system-level simulation. The link and system level simulations have to be properly interfaced to obtain the desired network performance results.

Section 4.2 describes the general simulation structure applied in this research work and the interface between the link-level and system-level simulations.

Section 4.3 presents the link-level simulation structure and results for HDR and 1XTREME; in this section a more detailed description of the physical layer of HDR and 1XTREME will be presented. System-level simulation will be described in Chapter 5.

4.2 General simulation structure

The combined link-level and system-level simulations represent the modeling of the entire cellular system. First the link-level simulations are performed independently and the results are fed into the system-level simulator. A block diagram description of this operation is shown in Figure 4.1. The link-level simulation section comprises a link level simulator that models the transmitter-receiver structure with a time resolution of a modulation symbol; the encoder/decoder, modulator/demodulator and signal processing associated with

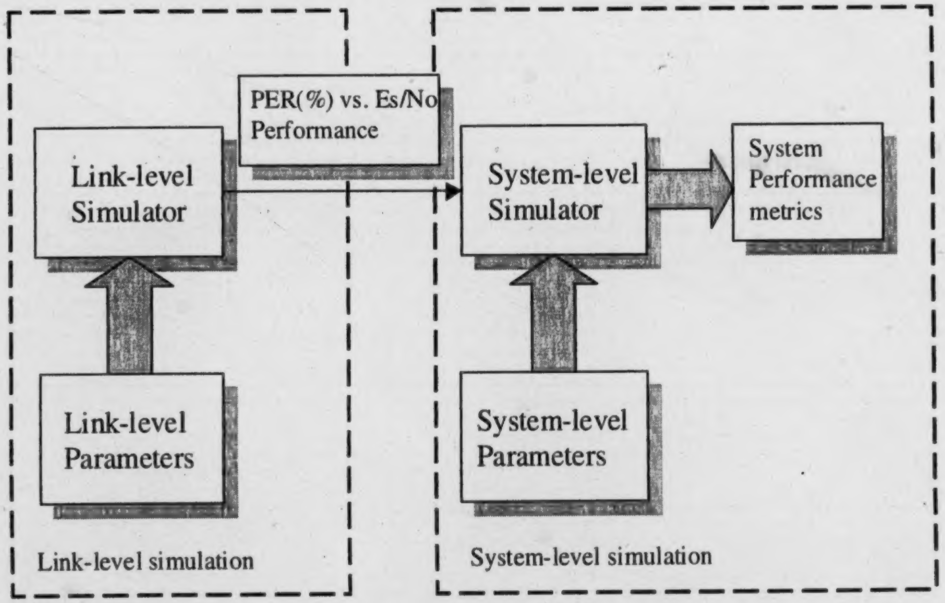
PER(%) vs. Es/No
Performance
Link-level
Simulator
Link-level
Parameters
Link-level simulation
System-level
Simulator
System
Performance
metrics
System-level
Parameters
System-level simulation

Figure 4.1. General simulation structure of HDR and 1XTREME.

the operations of a single transmitter-receiver pair are modeled. The link-level simulator also includes the model and assumptions of the channel between the transmitter and receiver. For this research work the channel used in the link level simulator is an Additive White Gaussian Noise (AWGN) channel. The reason for this choice is that HDR and 1XTREME are systems designed for bursty packet transmission within short-time slots (1.67ms for HDR, and 5ms for 1XTREME) during which the fading radio channel is practically time-invariant, even for highly mobile user terminals (up to 60km/h). Hence, the SIR seen by the mobile receiver over one slot is practically constant and AWGN results are applicable. At 60km/h and carrier frequency of 2GHz the coherence time of the radio channel [2] is on the order of 5ms. Hence, the radio channel will display some variability over one 1XTREME slot. This variability is accounted for in system level simulations. It also needs to be mentioned that HDR and 1XTREME systems are primarily designed for nomadic users as pointed out in Chapter 1. Nomadic users can be stationary for the duration of a given transmission session.

The parameters of the link-level simulator are the different formats of transmission, the modulations used, the packet sizes, the code rates, interleaver method etc. The desired output of the link-level simulator is the packet error rate (PER) for every format of transmission in the AWGN channel for different fixed values of energy-symbol over noise ratio (E_s / N_o). The AWGN curves of PER (%) vs. E_s / N_o out of the link-level simulator are fed into the system-level simulator for its operation. The system level simulation will be described in Chapter 5.

4.3 Link level simulations

4.3.1 Structure and functionality of the HDR and 1XTREME forward links.

4.3.1.1 HDR forward traffic channel transmission formats

The HDR Forward Traffic Channel is a packet-based, variable-rate channel. The user data for an access terminal is transmitted at a data rate that varies from 38.4kbp/s to 2.4576Mbp/s. The data is encoded in blocks called physical layer packets. The physical layer packets and rates supported by the HDR Forward Traffic Channel are specified in Table 4.1, along with the corresponding modulation/coding schemes (MCS) and maximum allowed number of re-transmissions. Table 4.1 includes also bit rates resulting from early termination of retransmissions, occurring when a positive acknowledgement is sent by a mobile before the maximum allowed number of retransmissions is reached. Link-level simulations have generated AWGN PER vs. E_s / N_o curves for all rates listed in this table.

Transmission Format Number	Max. Allowed Slots	Transmitted Slots	Packet Size (bits)	Preamble Size (chips)	Data Rate (kbp/s)	Turbo Code Rate	Modul.
1	16	16	1,024	1,024	38.4	1/5	QPSK
2	16	15	1,024	1,024	40.96	1/5	QPSK
3	16	14	1,024	1,024	43.89	1/5	QPSK
4	16	13	1,024	1,024	47.26	1/5	QPSK
5	16	12	1,024	1,024	51.2	1/5	QPSK
6	16	11	1,024	1,024	55.85	1/5	QPSK
7	16	10	1,024	1,024	61.44	1/5	QPSK
8	16	9	1,024	1,024	68.27	1/5	QPSK
9	16	8	1,024	1,024	76.8	1/5	QPSK
10	16	7	1,024	1,024	87.77	1/5	QPSK
11	16	6	1,024	1,024	102.4	1/5	QPSK
12	16	5	1,024	1,024	122.88	1/5	QPSK
13	16	4	1,024	1,024	153.6	1/5	QPSK
14	16	3	1,024	1,024	204.8	1/5	QPSK
15	16	2	1,024	1,024	307.2	1/5	QPSK
16	16	1	1,024	1,024	614.4	1/5	QPSK
17	8	8	1,024	512	76.8	1/5	QPSK
18	8	7	1,024	512	87.77	1/5	QPSK
19	8	6	1,024	512	102.4	1/5	QPSK
20	8	5	1,024	512	122.88	1/5	QPSK
21	8	4	1,024	512	153.6	1/5	QPSK
22	8	3	1,024	512	204.8	1/5	QPSK
23	8	2	1,024	512	307.2	1/5	QPSK
24	8	1	1,024	512	614.4	1/5	QPSK
25	4	4	1,024	256	153.6	1/5	QPSK
26	4	3	1,024	256	204.8	1/5	QPSK
27	4	2	1,024	256	307.2	1/5	QPSK
28	4	1	1,024	256	614.4	1/5	QPSK
29	2	2	1,024	128	307.2	1/5	QPSK
30	2	1	1,024	128	614.4	1/5	QPSK
31	1	1	1,024	64	614.4	1/5	QPSK
32	4	4	2,048	128	307.2	1/3	QPSK
33	4	3	2,048	128	409.6	1/3	QPSK
34	4	2	2,048	128	614.4	1/3	QPSK
35	4	1	2,048	128	1,228.8	1/3	QPSK
36	2	2	2,048	64	614.4	1/3	QPSK
37	1	1	2,048	64	1,228.8	1/3	QPSK
38	2	2	3,072	64	921.6	1/3	8PSK
39	1	1	3,072	64	1,843.2	1/3	8PSK
40	2	2	4,096	64	1,228.8	1/3	16QAM
41	1	1	4,096	64	2,457.6	1/3	16QAM

Table 4.1. Physical layer packet sizes and rates supported by the HDR Forward Channel.

4.3.1.2 1XTREME forward shared channel transmission formats

The Forward Shared Channel (F-SHCH) is one of the two new channels on the forward link of cdma2000 introduced in the 1XTREME system. The 1XTREME Forward Shared Channel uses an adaptive modulation and coding scheme (MCS) with four possible types of modulation: QPSK, 8PSK, 16QAM and 64QAM. The packet lengths and rates supported by the Forward Shared Channel are specified in Table 4.2. The Forward Shared Channel can be mapped to multiple (*N* up to a maximum of 14 codes) parallel code channels of Walsh length 16.

Transmission Format Number	**Packet Size (Bits)**	**Data Rate (kbps)**	**Turbo Code Rate**	**Modulation Scheme**
1	384 x *N*	76.8 x *N*	½	QPSK
2	576 x *N*	115.4 x *N*	¾	QPSK
3	768 x *N*	153.6 x *N*	½	16QAM
4	864 x *N*	172.8 x *N*	¾	8PSK
5	1152 x *N*	230.4 x *N*	¾	16QAM
6	1728 x *N*	345.6 x *N*	¾	64QAM

Table 4.2. Physical layer packet sizes and rates supported by the 1XTREME Forward Shared Channel (N is the number of orthogonal codes allocated to the Forward Shared Channel)

4.3.1.3 Turbo encoder and decoder

The HDR Forward Traffic Channel physical layer packets (excluding the 6-bit TAIL field) and 1XTREME Forward Shared Channel packets (including two reserved bits) are encoded with a turbo encoder of code rate *R* (see Tables 4.1 and 4.2). The turbo encoder will add an internally generated tail of 6/*R* output code symbols, so that if the number of input bits to the turbo encoder is N_{turbo}, the turbo encoder generates N_{turbo}/R encoded data output symbols followed by $6/R$ tail output symbols.

4.3.1.3.1 Turbo encoder

The HDR Forward Traffic Channel and the 1XTREME Forward Shared Channel use the same turbo encoder, as shown in Figure 4.2. It employs two systematic recursive convolutional (RSC) encoders [51], [39], connected in parallel, with a turbo interleaver preceding the second convolutional encoder. The recursive convolutional codes are the constituent codes of the turbo code. They have the same transfer function given by

$$G(D) = \begin{bmatrix} 1 & \frac{n_0(D)}{d(D)} & \frac{n_1(D)}{d(D)} \end{bmatrix} \qquad (4.1)$$

where $d(D)=1+D^2+D^3$, $n_0(D)=1+D+D^3$, and $n_1(D)=1+D+D^2+D^3$.

Initially, the states of the constituent encoder registers in Figure 4.2 are set to zero. Then, the constituent encoders are clocked with the two switches in the upper positions. The encoded data output symbols are generated by clocking the constituent encoder N_{turbo} times with the switches in the upper positions.

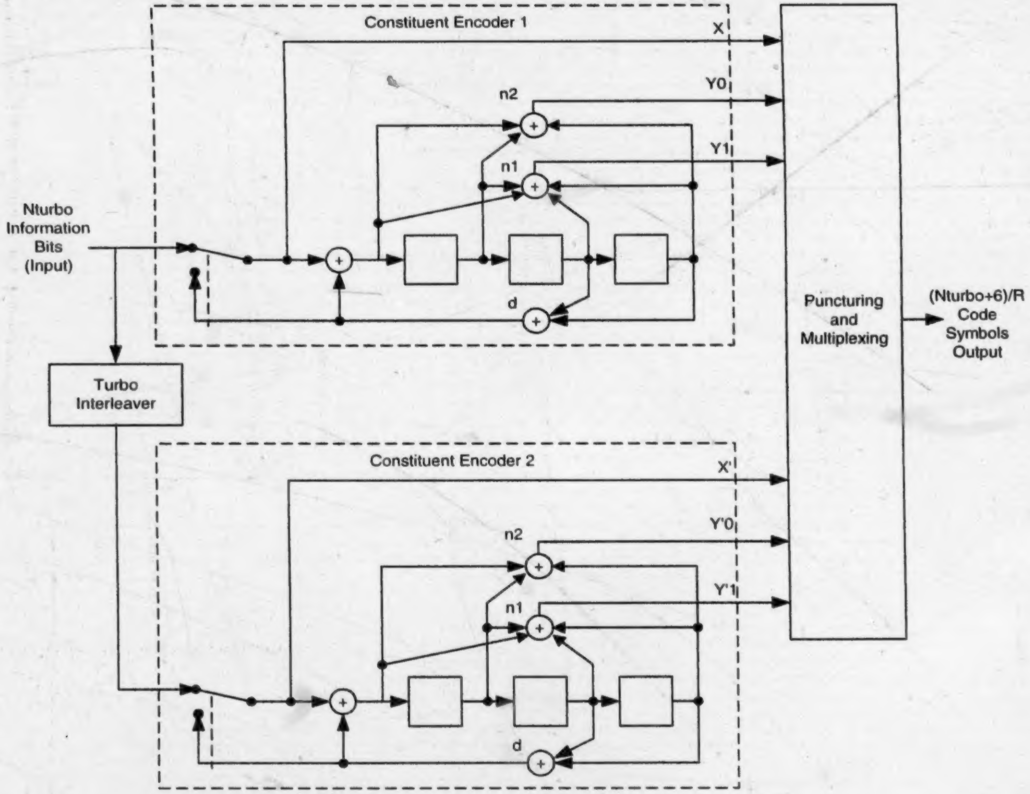
Constituent Encoder 1
X
Y0
n2
Y1
n1
Nturbo Information Bits (Input)
d
Puncturing and Multiplexing
(Nturbo+6)/R Code Symbols Output
Turbo Interleaver
Constituent Encoder 2
X'
Y'0
n2
Y'1
n1
d

Figure 4.2. Turbo encoder used in HDR and 1XTREME.

The resulting constituent encoder output sequences are then punctured as specified in Table 4.3. Within a puncturing pattern, a '0' means that the symbol shall be deleted and a '1' means that the symbol shall be passed.

	Code Rate *R*			
Output	¾	1/2	1/3	1/5
X	111111	11	1	1
Y_0	100000	10	1	1
Y_1	000000	00	0	1
X'	000000	00	0	0
Y'_0	000100	01	1	1
Y'_1	000000	00	0	1

Table 4.3. Puncturing pattern for the data bit periods. The table is read first from top to bottom and then from left to right. (e.g., for code rate ¾, 8 coded symbols are passed out of 6 data symbols)

The turbo encoder shall generate $6/R$ tail output symbols following the encoded data output symbols. The tail output symbols are generated by clocking each constituent encoder separately three times with the switch in the lower position. The resulting constituent encoder output symbols are then punctured and repeated as specified in Table 4.4.

	Code Rate *R*			
Output	¾	½	1/3	1/5
X	111000	111000	111000	111000
Y_0	100000	111000	111000	111000
Y_1	000000	000000	000000	111000
X'	000111	000111	000111	000111
Y'_0	000100	000111	000111	000111
Y'_1	000000	000000	000000	000111

Table 4.4. Puncturing and repeating pattern for the tail bit periods. For rate 1/3, the puncturing table is read first from top to bottom repeating X and X', and then from left to right. For rate 1/5, the repeated coded symbols are X, X', Y_1, and Y'_1.

4.3.1.3.1.1 Turbo interleaver

The turbo interleaver, which is part of the turbo encoder, interleaves the N_{turbo} bits input to the turbo encoder. It is functionally equivalent to an approach (see Figure 4.3) in which the N_{turbo} input bits are written sequentially into an array at a sequence of addresses from 0 to N_{turbo}-1, and then the entire

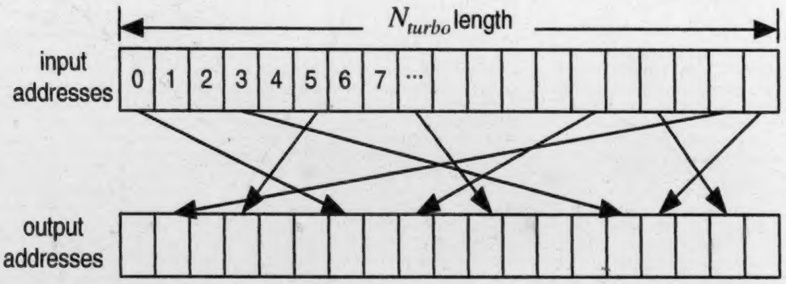

Figure 4.3. Interleaver structure.

sequence is read out from a sequence of addresses that are defined by the procedure described below:

1. Counter values (0 to 2^{n+5}-1) are written by rows into an array of 2^5 rows by 2^n columns, where $n = \lceil \log_2 N_{turbo} \rceil - 5$.

2. The elements within each row are permuted to $C(i)*(j+1)$, where indices i, j are the original row and column indices of the element, and $C(i)$ is a row-specific value from a table lookup (defined in Table 9.3.1.3.2.3.2.2-2 in [31]).

3. The rows are shuffled according to a bit-reversal rule. For example, for i=12 (01100), the bit reversed value of i is 5 (00110).

4. The elements in the array with values less than N_{turbo} are finally read out by columns. The new sequence consists of the interleaver output addresses.

4.3.1.3.2 Turbo decoder

Turbo decoder is based on an iterative application of maximum a posteriori (MAP) decoding to each constituent code.

A MAP decoder accepts as soft inputs the *a-priori log-likelihood ratio* (LLR) $L_a(X)$ and *soft channel input* { $L_c(X)$, $L_c(Y_0)$, $L_c(Y_1)$ } and delivers as soft output *a-posteriori LLR* of information bit which can be split into three terms: $L_a(X)$, $L_c(X)$ and *extrinsic information* $L_e(X)$. It makes possible the information exchange between decoders: each constituent decoder performs MAP decoding, and its outputs are used as the soft inputs for the next constituent decoder. Figure 4.4 demonstrates how soft information is forwarded/feed-backed inside the turbo decoder and how the turbo decoding works with the tail bits appending/removing.

Superscripts ^{1} and ^{2} are used in this figure to differentiate the *a-priori* and *extrinsic information* for MAP1 and MAP2, which correspond to the Constituent Encoder 1 and 2 in Figure 4.2, respectively.

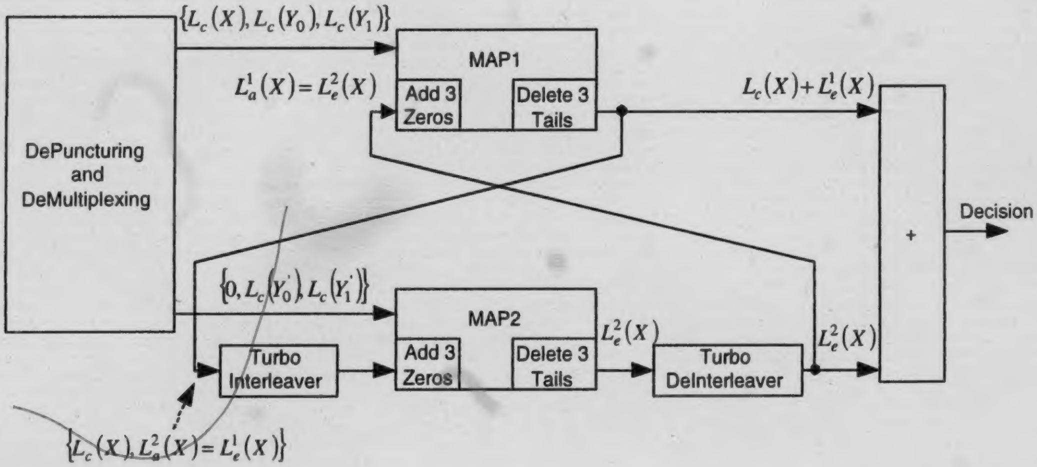
$\{L_c(X), L_c(Y_0), L_c(Y_1)\}$
MAP1
$L_a^1(X) = L_e^2(X)$
Add 3 Zeros
Delete 3 Tails
$L_c(X)+L_e^1(X)$
DePuncturing and DeMultiplexing
Decision
+
$\{0, L_c(Y_0'), L_c(Y_1')\}$
MAP2
$L_e^2(X)$
Turbo Interleaver
Add 3 Zeros
Delete 3 Tails
Turbo DeInterleaver
$L_e^2(X)$
$\{L_c(X), L_a^2(X) = L_e^1(X)\}$

Figure 4.4. Turbo decoder.

The turbo decoder operates in serial mode (i.e., the MAP1 decoder processes before the MAP2 decoder starts operation). The turbo decoder operates as described below:

1. In the first step, the *a-priori probability* is unavailable. An equally likely assumption is made by setting $L_a{}^1(X) = 0$.

2. The MAP1 decoder takes in the *channel soft input* { $L_C(X)$, $L_C(Y_0)$, $L_C(Y_1)$ } from the upper branch of the DeMUX, and the zero *a-priori*. It updates the *a-posterior probability* of the information bit based on its code constraint and then delivers both the *channel soft input* and the extrinsic information, $L_C(X)+L_e{}^1(X)$, as soft input to MAP2.

3. The systematic bit X of the constituent Encoder 2 was punctured in the Puncturing and Multiplexing block at the transmit side. Hence, zero is inserted as $L_c(X)$ in the lower branch of DeMUX outputs, which is then sent as input to MAP2. Although DeMUX delivers zero $L_c(X)$ to the MAP2 decoder, MAP2 will learn its *channel soft input* of the systematic bit $L_c(X)$ from MAP1, along with the *a-priori LLR* $L_a^2(X)$ by taking $L_a^2(X)=L_e^1(X)$.

4. The *extrinsic* output $L_e^2(u)$ from MAP2 is interleaved and fed back to MAP1.

5. Subsequently, MAP1 has available an estimation of the *a-posteriori LLR*. It may consider this as *a-priori LLR* of its information bit X, i.e. $L_a^1(X)=L_e^2(X)$, and update it as the new log-likelihood ratio.

6. This process continues until a desired performance is achieved, at which point a final decision is made by comparing the final log-likelihood ratio $L_c(X)+L_e^1(X)+L_e^2(X)$ to zero.

It should be noted that each constituent MAP decoder works on both encoded data symbols and tail symbols. As the two don't share the 6-bit tail, the *a-priori LLR* values for the 6 tail bits will remain at zero during iterations. Thus, the output from each constituent MAP decoder shall be deleted the 3 tail bits, whereas at the input to each constituent MAP decoder, three zeros shall be appended (see Figure 4.4).

4.3.1.4 Signal constellations and spreading

The modulator generates in-phase and quadrature streams of QPSK, 8PSK, 16QAM or 64QAM modulation symbols, depending on the data rate. The signal constellations for the four modulation schemes are shown in Figures 4.5 – 4.8.

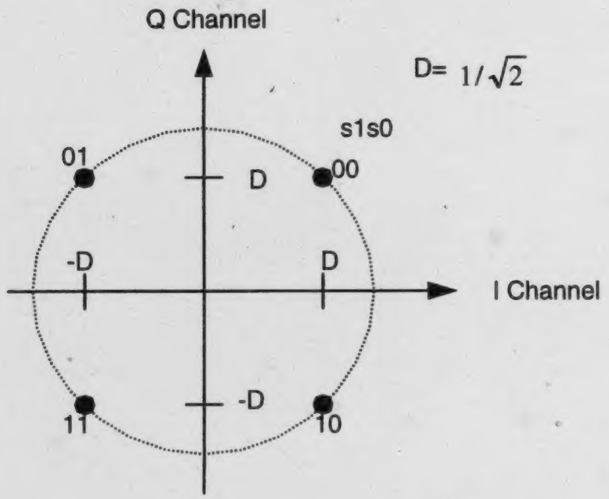
Q Channel
D= $1/\sqrt{2}$
s1s0
01
00
D
-D
D
I Channel
-D
11
10

Figure 4.5. Signal constellation for QPSK modulation.

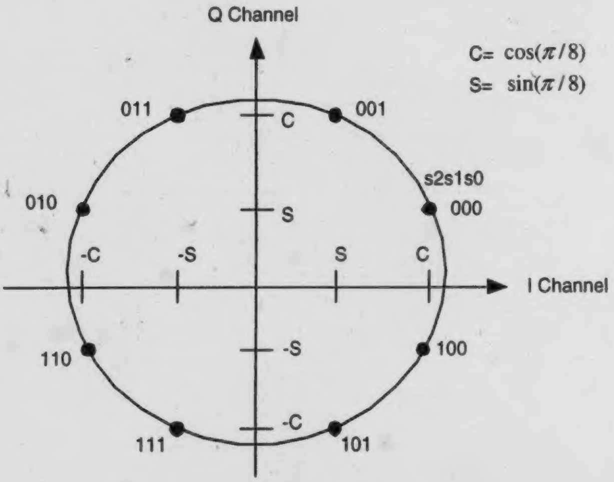
Q Channel
C= $\cos(\pi/8)$
S= $\sin(\pi/8)$
011
C
001
s2s1s0
010
S
000
-C
-S
S
C
I Channel
110
-S
100
111
-C
101

Figure 4.6. Signal constellation for 8PSK modulation.

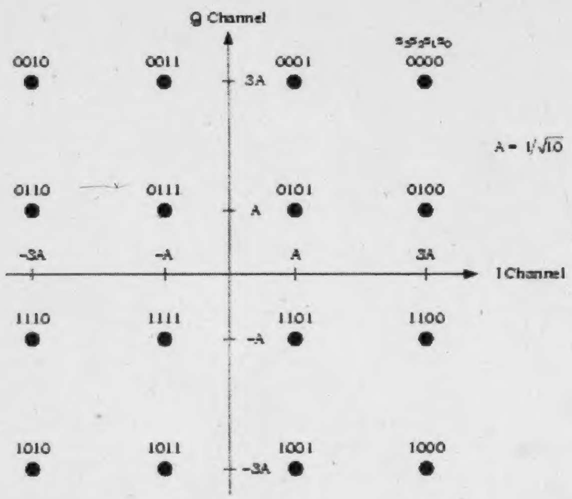
Q Channel
s3s2s1s0
0010
0011
0001
0000
3A
A = 1/√10
0110
0111
0101
0100
A
-3A
-A
A
3A
I Channel
1110
1111
1101
1100
-A
1010
1011
1001
1000
-3A

Figure 4.7. Signal constellation for 16QAM modulation.

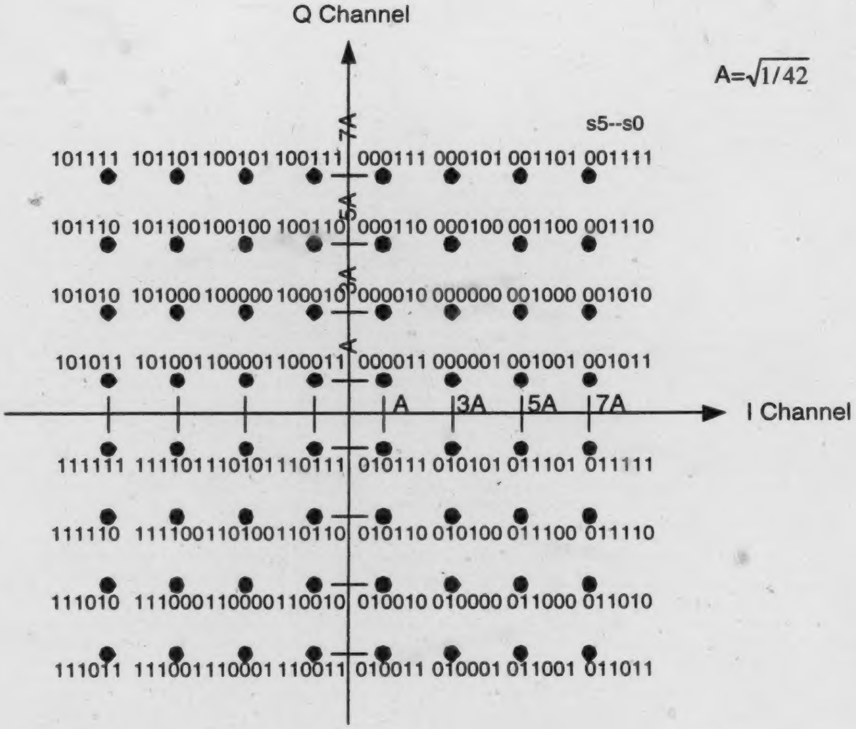
Q Channel
A=√1/42
s5--s0
7A
5A
3A
A
101111 101101 100101 100111 000111 000101 001101 001111
101110 101100 100100 100110 000110 000100 001100 001110
101010 101000 100000 100010 000010 000000 001000 001010
101011 101001 100001 100011 000011 000001 001001 001011
A
3A
5A
7A
I Channel
111111 111101 110101 110111 010111 010101 011101 011111
111110 111100 110100 110110 010110 010100 011100 011110
111010 111000 110000 110010 010010 010000 011000 011010
111011 111001 110001 110011 010011 010001 011001 011011

Figure 4.8. Signal constellation for 64QAM modulation.

4.3.1.4.1 HDR forward traffic channel spreading

In the HDR Forward Traffic Channel, the modulated symbols after channel interleaver are repeated or punctured as necessary. The resulting sequences of modulation symbols are de-multiplexed to form 16 pairs (in-phase and quadrature) of parallel streams. Each of the parallel streams is then spread with a distinct 16-ary Walsh function to yield Walsh symbols at rate 76.8ksp/s (or chip rate of 1228.8kcp/s). After that, the Walsh-coded symbols of all the streams are summed together at the chip level to form a single in-phase stream and a single quadrature stream at a chip rate of 1.2288 Mcp/s.

The resulting chips are time-division multiplexed (without changing the chip rate) with the preamble, Pilot Channel, and MAC Channel chips for the quadrature chip level scrambling operation. The scrambling sequence is a quadrature sequence of length 2^{15} (i.e., 32768 PN chips long). This sequence is called the *pilot PN sequence* and is generated by the following characteristic polynomials:

$P_I(x)=x^{15}+x^{10}+x^8+x^7+x^6+x^2+1$ (in-phase sequence I-PN)

$P_Q(x)=x^{15}+x^{12}+x^{11}+x^{10}+x^9+x^5+x^4+x^3+1$ (quadrature-phase sequence Q-PN)

4.3.1.4.2 1XTREME forward shared channel spreading

In the 1XTREME Forward Shared Channel, the modulated symbol sequences are serial-to-parallel converted to form up to 14 pairs (in-phase and quadrature) of parallel streams. Each of the parallel streams is later spread with one of fourteen 16-ary Walsh codes (W_2^{16} to W_{15}^{16}) to yield Walsh symbols at rate 76.8ksp/s (or chip rate of 1228.8 kcp/s); one Walsh symbol per modulation symbol is used. Following orthogonal spreading, the modulation sequence is quadrature scrambled by a quadrature pilot PN sequence of length 2^{15} (i.e., 32768 PN chips in length) generated by the following characteristic polynomials:

$P_I(x)=x^{15}+x^{13}+x^9+x^8+x^7+x^5+1$ (for the in-phase sequence IPN)

$P_Q(x)=x^{15}+x^{12}+x^{11}+x^{10}+x^6+x^5+x^4+x^3+1$ (for the quadrature-phase sequence QPN)

Each of up to 14 orthogonal Walsh code channels assigned to packet data traffic is assigned 1/14 of the power allocated to the traffic channels; 80% of the total sector transmit power is allocated to the traffic channels. Hence, effectively, the signal carrying the packet data traffic experiences processing gain of 16/14, or 0.58dB. In other words, spreading the modulation symbols by a factor of 16 in each of the 14 orthogonal code channels reduces the symbol energy required to achieve a given PER by a factor of 16/14 in comparison to a link without spreading using the same modulation/coding scheme and symbol rate. The spreading and scrambling operations are not explicitly implemented in the link level simulations. The processing gain is taken into account at the system level.

4.3.1.5 Slot and code channel structure

4.3.1.5.1 HDR forward channel structure and slot structure

The Forward Traffic Channel data modulation chips are time-division multiplexed with the Preamble, Pilot Channel, and MAC Channel chips as shown in Figure 4.9; the chip rate of 1228.8kcp/s is preserved in the TDM operation. All time-division-multiplexed channels are transmitted at the maximum power of the sector. Forward Traffic Channel Physical Layer packets are transmitted in 1 to 16 slots. The Forward Traffic Channel data symbols fill the slots as shown in Figure 4.10. Due to the 16-way parallelizing operation and subsequent 16-ary Walsh spreading and chip-wise addition of parallel streams, effectively each chip carries one QPSK, 8PSK or 16QAM symbol.

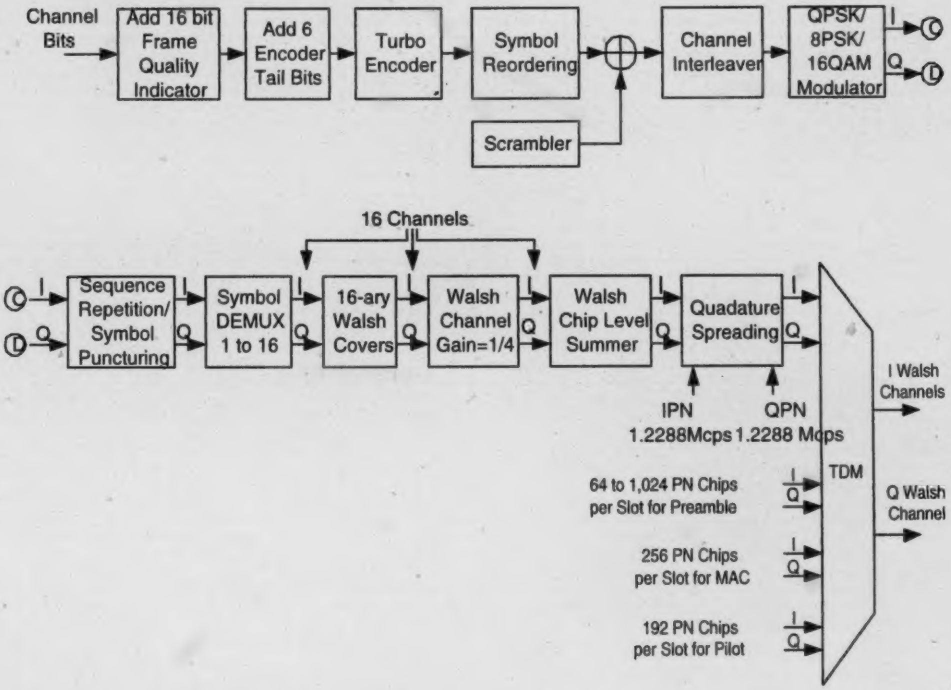
Channel Bits
Add 16 bit Frame Quality Indicator
Add 6 Encoder Tail Bits
Turbo Encoder
Symbol Reordering
Scrambler
Channel Interleaver
QPSK/ 8PSK/ 16QAM Modulator
I
Q
C
D
16 Channels
Sequence Repetition/ Symbol Puncturing
Symbol DEMUX 1 to 16
16-ary Walsh Covers
Walsh Channel Gain=1/4
Walsh Chip Level Summer
Quadature Spreading
IPN 1.2288Mcps
QPN 1.2288 Mcps
TDM
I Walsh Channels
Q Walsh Channel
64 to 1,024 PN Chips per Slot for Preamble
256 PN Chips per Slot for MAC
192 PN Chips per Slot for Pilot

Figure 4.9. HDR forward channel structure.

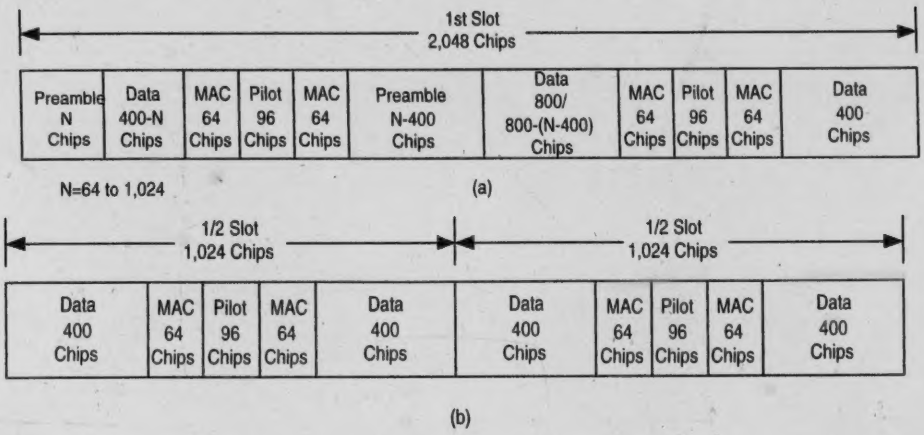
1st Slot
2,048 Chips
Preamble N Chips
Data 400-N Chips
MAC 64 Chips
Pilot 96 Chips
MAC 64 Chips
Preamble N-400 Chips
Data 800/ 800-(N-400) Chips
MAC 64 Chips
Pilot 96 Chips
MAC 64 Chips
Data 400 Chips
N=64 to 1,024
(a)
1/2 Slot
1,024 Chips
1/2 Slot
1,024 Chips
Data 400 Chips
MAC 64 Chips
Pilot 96 Chips
MAC 64 Chips
Data 400 Chips
Data 400 Chips
MAC 64 Chips
Pilot 96 Chips
MAC 64 Chips
Data 400 Chips
(b)

Figure 4.10. HDR forward channel active slot structure (a) the first slot (b) the non-first slot for multi-slot transmission.

A slot during which no traffic is transmitted is referred to as an idle slot. Idle slot structure is shown in Figure 4.11. During an idle slot, the sector transmits only the Pilot Channel and the MAC Channel.

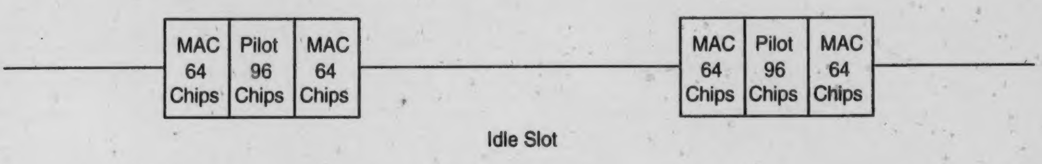
MAC 64 Chips
Pilot 96 Chips
MAC 64 Chips
MAC 64 Chips
Pilot 96 Chips
MAC 64 Chips
Idle Slot

Figure 4.11. HDR forward channel idle slot structure.

4.3.1.5.2 1XTREME code channel structure

The 1XTREME Forward Shared Channel structure is shown in Figure 4.12.

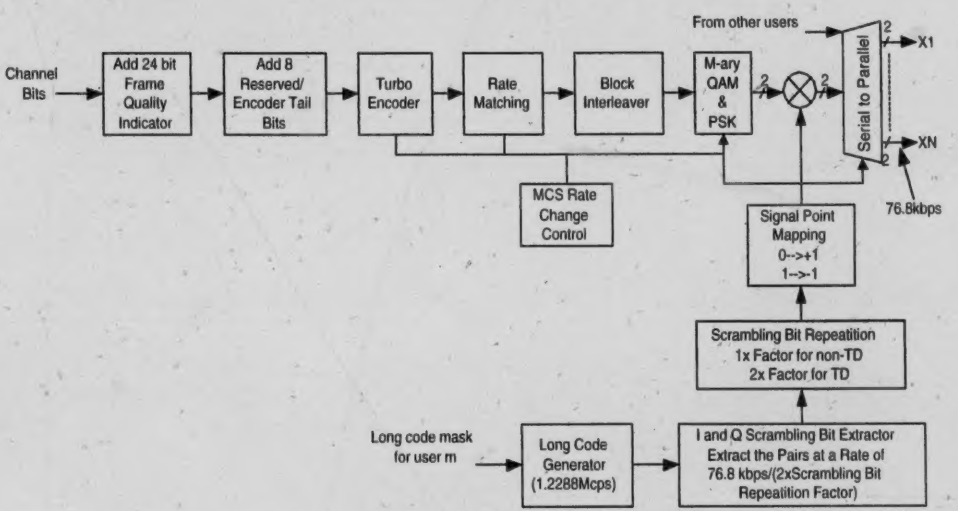
From other users
Channel Bits
Add 24 bit Frame Quality Indicator
Add 8 Reserved/ Encoder Tail Bits
Turbo Encoder
Rate Matching
Block Interleaver
M-ary QAM & PSK
2
2
Serial to Parallel
2
X1
XN
2
MCS Rate Change Control
76.8kbps
Signal Point Mapping 0-->+1 1-->-1
Scrambling Bit Repeatition 1x Factor for non-TD 2x Factor for TD
Long code mask for user m
Long Code Generator (1.2288Mcps)
I and Q Scrambling Bit Extractor Extract the Pairs at a Rate of 76.8 kbps/(2xScrambling Bit Repeatition Factor)

Figure 4.12. 1XTREME forward shared channel structure.

4.3.1.6 Hybrid ARQ for HDR

The HDR Forward Channel employs Type II Hybrid Automatic Repeat Request (ARQ) scheme. The hybrid ARQ scheme employs turbo codes as inner forward error correction (FEC) codes, and cyclic redundancy check (CRC) codes as outer error detection codes. It also takes advantage of incremental redundancy and soft packet combining. The application of type II hybrid ARQ allows for bit rate adaptation to the current radio channel conditions even after the specific transmission format (modulation & coding, and packet size) is selected. Due to the inclusion of incremental redundancy in the HDR hybrid ARQ scheme, it needs to be simulated at the link level, leading to the need for considering link level performance of 41 transmission formats as listed in Table 4.1.

The HDR Forward Channel uses multi-slot transmission with 4-slot interlacing. The consecutive slots allocated for transmission of a given packet are separated by 3 slots allocated to other transmissions. If a positive is received on the reverse link ACK Channel and the Physical Layer packet has been received before all of the allocated slots have been transmitted, the remaining reserved slots are made available to the next Physical Layer packet transmission. Figure 4.13 illustrates the multi-slot interlacing approach for the 153.6kbps data rate case where 4 slots per packet are used. In this case, up to 4 re-transmissions are allowed.

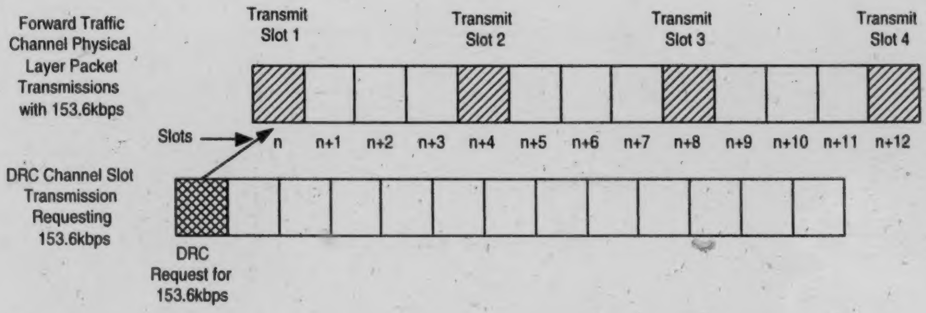
Forward Traffic Channel Physical Layer Packet Transmissions with 153.6kbps
Transmit Slot 1
Transmit Slot 2
Transmit Slot 3
Transmit Slot 4
Slots
n
n+1
n+2
n+3
n+4
n+5
n+6
n+7
n+8
n+9
n+10
n+11
n+12
DRC Channel Slot Transmission Requesting 153.6kbps
DRC Request for 153.6kbps

Figure 4.13. Example of slot interlacing for multi-slot packet transmission in HDR forward channel.

Hybrid ARQ scheme used in 1XTREME does not employ incremental redundancy, and therefore it is easy to account for its function at the system level. Hence, it is not simulated at the link level.

4.3.1.7 Soft packet combining and incremental redundancy

The HDR Forward Traffic Channel uses soft packet combining and incremental redundancy to achieve slot-by-slot data rate adaptation to the channel conditions. The Physical Layer packet is first encoded using a rate 1/3 or 1/5 turbo code. With the selected modulation and coding scheme (MCS), the initial slot transmission of the packet consists of only those encoded bits that fit in the slot (Figure 4.10-a). On receiving a negative acknowledgement (NACK) for the packet, incremental amounts of redundancy (i.e., the remaining parity bits of the encoded data) are transmitted. If all the encoded data have been transmitted, the cycle is repeated, starting again with the very first coded bit. On receiving a positive acknowledgement (ACK) for the packet before the maximum allowed number of re-transmissions (slots), the current Physical Layer packet transmission stops and the next Physical Layer packet transmission starts. This procedure effectively matches the code rate and bit rate to the channel SINR. In addition, the transmission of parity bits dispersed in time provides a diversity gain during decoding. Soft packet combining and incremental redundancy operations require the receiver to store soft information corresponding to the Physical Layer packets that have not yet been decoded successfully. Each time the receiver obtains a repetition of coded bits, it combines them with previously stored soft information corresponding to the same coded bits. This process is repeated until the receiver has acummulated sufficient SINR to allow correct decoding to be performed.

4.3.1.8 AWGN performance evaluation and its relevance

In our link level simulations PER vs. E_s / N_o curves in AWGN are determined for all HDR and 1XTREME transmission formats, as listed in Tables 4.1 and 4.2. Not all functions depicted in Figs. 4.9 to 4.12 are relevant to such performance evaluation. Figures. 4.14 and 4.15 show the functional modules of the HDR and 1XTREME forward channel transmitter relevant to the AWGN performance evaluation.

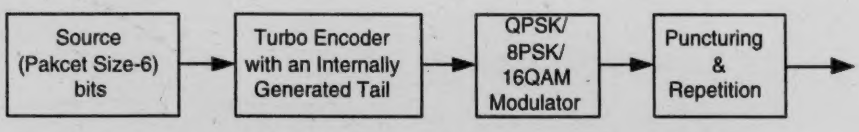
Source
(Pakcet Size-6)
bits
Turbo Encoder
with an Internally
Generated Tail
QPSK/
8PSK/
16QAM
Modulator
Puncturing
&
Repetition

Figure 4.14. HDR forward traffic channel structure in simulation.

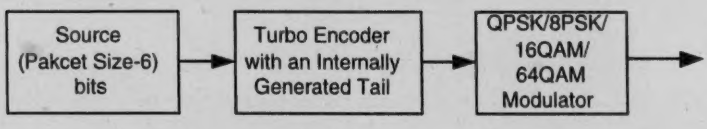
Source
(Pakcet Size-6)
bits
Turbo Encoder
with an Internally
Generated Tail
QPSK/8PSK/
16QAM/
64QAM
Modulator

Figure 4.15. 1XTREME forward shared channel structure in simulation.

The PER curves obtained from AWGN link level simulations will be used at the system level for transmission format selection and packet erasure determination. In spite of the fact that the HDR and 1XTREME systems operate over fading mobile radio channels, AWGN link level curves can be used to simplify system level simulations due to the fact that both HDR and 1XTREME use very short transmission bursts over which the SIR seen by the mobile receiver is either constant, or can be represented as constant for the purpose of transmission format selection or packet erasure determination.

4.3.2 PER vs. E_s/N_0 curves in AWGN

A packet error rate (PER) curve vs. E_s / N_o in an AWGN channel is created using the link level simulation for each data rate, modulation and coding scheme given in Tables 4.1 and 4.2.

4.3.2.1 HDR forward traffic channel PER curves

Figures A.1 to A.6 in Appendix A present PER AWGN curves obtained after 8 iterations of the turbo decoder for all transmission formats and bit rates specified in Table 4.1. In the figures, data rate in kb/s, physical layer packet size in bits, and maximum allowable number of transmission slots are denoted as *R*, M_p, and *S*, respectively. Figures A.7 to A.11 compare the HDR Forward Traffic Channel PER curves corresponding to the same bit rate transmissions in different formats.

4.3.2.2 1XTREME forward shared channel PER curves

The PER vs. E_s / N_o curves for the cases of N = 2,…,10 can be obtained from those in Figure A.7. Due to the absence of incremental redundancy in 1XTREME, these curves will be the same as those in Figure A.7, except the corresponding values of E_s / N_o will be reduced by a factor N (on a linear scale). The processing gain of 16/14 is notincluded in the link-level curves, and will be accounted for in system level simulations.

4.4 Summary

The general structure of the HDR and 1XTREME simulations was depicted in Figure 4.1. The link-level and system level simulations are performed separately. The link-level simulation involves the modeling of the most relevant functional block diagrams of the channel structure for HDR and 1XTREME, including Turbo encoder/decoder, modulator/demodulator, and repetition/puncturing operations. The AWGN channel is assumed for the link-level simulations due to the short-time duration of the packets. The fading channel is practically time-invariant in these short periods of time, and hence it behaves as an AWGN channel. In the following chapter the description of the system level simulator will be presented.

Chapter 5

System level simulation

5.1 Introduction

The system-level simulation of a cellular network implies the modeling of the radio environment and the specific operations involved in the transmission of information from multiple base stations to multiple mobile terminals. The main objective of this research work is to perform the system-level simulations of the HDR and 1XTREME systems in order to obtain system-level performance metrics for comparison purposes.

The system-level simulation as previously depicted in Figure 4.1 (Chapter 4), combines the results of the link-level simulator and the parameters and assumptions about the radio environment and radio transmission operations. The link-level simulations described in Chapter 4 provide the performance results of a single transmitter-receiver pair in the form of AWGN PER vs. E_s / N_o curves for each transmission format, and the different models described in Chapter 3 provide the basis for the modeling of the system-level radio environment.

System-level simulation is performed in two stages as shown in Figure 5.1. First, a signal-to-interference ratio (SIR) lookup table is generated with the estimated values of SIR for all the mobiles located in the given sector of the central cell. The SIR lookup table is used by the second stage of the system-level simulator, which performs the scheduling, frame-erasure determination, and computation of performance metrics operations.

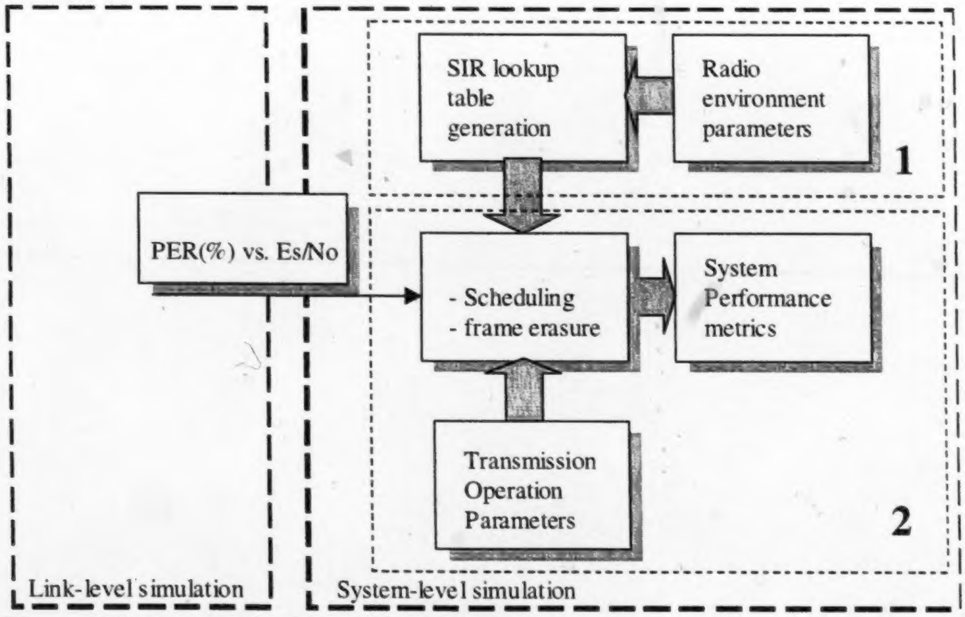
SIR lookup table generation
Radio environment parameters
1
PER(%) vs. Es/No
- Scheduling
- frame erasure
System Performance metrics
Transmission Operation Parameters
2
Link-level simulation
System-level simulation

Figure 5.1. System-level simulation structure.

In this chapter the description of the system-level simulation will be presented focusing on the HDR system. Section 5.2 describes the method for the generation of the SIR lookup table for the multiple mobile terminals present in the network. Section 5.3 addresses the modulation & coding scheme (MCS) selection procedures. Section 5.4 presents the two schedulers used: a proportionally fair (PF) scheduler and a modified round robin scheduler. Section 5.5 describes the algorithm used for packet erasure determination. In Section 5.6 the description of the entire system-level simulator is presented by combining the information of the previous sections. Finally a description of the unique assumptions of the 1XTREME system-level simulator is presented in Section 5.7.

5.2 SIR lookup table generation in HDR

The SIR lookup table contains the estimated SIR values of a set of users uniformly distributed in the sector 1 of cell 1 (see Figure 3.1). The SIR values are estimated for two different radio environments and a slow best sector selection method that result in two different SIR lookup tables.

The ITU pedestrian A, and ITU vehicular B radio channels are modeled following the definitions in [20]. The main characteristic of the ITU pedestrian A channel is that multi-path components are closer together in time as a consequence of the denser distribution of scatterers around the mobile receiver, also the Doppler shift is usually quite low (e.g 5Hz) due to low speed of the mobile terminal. Table 5.1 shows the relative delays and powers among the different multi-paths for a ITU pedestrian A channel.

Multi-path	**Excess delay (nano-seconds)**	**Average power (dB)**
1	0	0
2	110	-9.7
3	190	-19.2
4	410	-22.8

Table 5.1. Power and delay profile of the ITU Pedestrian A channel [20].

The ITU vehicular B channel is characterized by more multi-paths distributed over a larger delay spread due to the presence of several scatterers separated by larger distances than in the pedestrian environment. Doppler shifts are higher due to higher speeds of the mobile. Table 5.2 shows relative delays and powers of resolvable multi-paths as defined in [20].

Multi-path	Excess delay (nano-seconds)	Average power (dB)
1	0	-2.5
2	300	0.0
3	8,900	-12.8
4	12,900	-10.0
5	17,100	-25.2
6	20,000	-16.0

Table 5.2. Power and delay profile of the ITU vehicular B channel [20].

We assume the Rake finger synchronization with the resolvable paths is perfect. For a chip period of $T_c = 814$ ns, pedestrian A results in a flat fading channel whereas vehicular B is frequency selective. Pedestrian A and vehicular B environments have basically one and three resolvable paths respectively. Paths 1 and 2 together comprise the only resolvable significant path in pedestrian A. In vehicular B environment, paths 1 and 2 together, path 3, and path 4 comprise the three significant resolvable paths. Contributions of the other paths to the desired signal, are neglected but they contribute to interference.

The evaluation of SIR is accomplished with the techniques described in Chapter 3. The parameters and models used are summarized in Table 5.3.

The simulation plan consists of 100 drops of 16, 8, and 4 mobiles in the embedded sector. Each drop lasts for 30 seconds during which SIR values for the set of uniformly distributed mobiles are computed and stored in an array. These

Parameter	**Value**	**Comments**
General:		
Carrier Frequency	1960MHz	
BS Antenna height	21 m	
AT Antenna height	1.5 m	
BS Bore-sight antenna gain ($Gant_{BS}$)	17.54dBi	EMS WIRELESS RR 65-18-00DP (section 3.3)
AT Antenna gain	0 dBi	
Cable loss	3 dB	
Tx power per sector (Pt_{max})	17 Watts (42.3dBm)	
Effective Data Tx Power	13.28 Watts (41.2dBm)	0.8*17Watts
System Bandwidth (W)	1.25 MHz	
Chip rate (Rc)	1.2288 Chips/sec	
Thermal noise density	0 Watts/Hz	Neglected
Number of cells in cluster	19	
Number of sectors per BS	3	
Cell Layout		UMTS 30.03 v3.2.0
Site-to-Site separation	709m	Computed in section 3.3
Implementation imperfections	13 dB	See section 5.2 for explanation
Shadowing & fading:		
BS correlation for shadow fading	0.5	Among different BS's
Sector correlation for shadow fading	1	Among different sectors of the same BS
Std deviation for shadow fading	6.5dB	
Spatial auto-correlation function	Exponential, [20]	Rec.ITU-R M.1225 section 1.2.1.4
De-correlation Length	5m for ITU pedestrian A. 20 m for ITU vehicular B	
Rayleigh fading simulation	Modified Smith method Based on IDFFT [50]	
ITU veh. B and ITU ped. A channels	Specified in [20]	Speed for ITU ped.A = 3 km/h Speed for ITU veh. B = 60 km/h
Path-Loss:		
Path-loss model		COST231-Walfish-Ikegami
Building separation	40m	
Street width	20m	
Average Building height	18m	6x3m
City	Medium city and sub-urban	Influence on the K_f term in the path loss model
L_{ori}	0 dB	In Path-loss model

Table 5.3. Parameters and assumptions of the system level simulation.

values will later be used for throughput and delay performance evaluation. The 30-seconds simulation is considered enough for the purposes of our study, longer simulation time was tried at 100 seconds and no substantial difference was observed. The uniform number generator was verified by plotting the probability density function of the uniform numbers generated, and by plotting the positions that the users will take in a hexagon area (x and y coordinates). This revealed no clusters or a tendency of users to be positioned in a particular area, but on the contrary users were spread uniformly. SIR determination and cell site selection methods are described in the following.

We assume that all the users experience the same type of channel during the whole duration of the simulation. The simulations are run for pedestrian A and vehicular B radio environments.

The SIR values are computed following a mechanism of best sector selection called *slow best sector selection* (SBSS). In SBSS, the mobile chooses the sector with the highest desired signal received power at the beginning of the drop (time = 0s). Taking into account path-loss and shadow fading only, the SBSS tries to select the best average sector. The SBSS method was chosen for its simplicity of implementation and relatively good results for 30s drop-time simulation. A *fast* BSS not only implies the selection of a best sector more frequently (e.g., every few slots), but also the added complexity of not allowing the switching to a different sector while a packet re-transmission process is in progress.

5.2.1 Power captured by the rake receiver.

The path power gains α are normalized such that

$$\sum_{i=1}^{\text{number of paths}} \alpha_i^{\,2} = 1 \tag{5.1}$$

The path power gains represent the fraction of the total signal power in a path. However, the fractional power recovered by a finger of the Rake receiver depends on the number of paths separated in time by less than one chip-time which form a set of non-resolvable paths. It also depends on the auto-correlation of the spreading waveform $R_x(\tau)$. The auto-correlation function is approximately triangular, such that

$$R_X(\tau) \cong \begin{cases} 1 - \dfrac{|\tau|}{T_c} & -T_c \le \tau \le T_c, \\ 0 & \text{otherwise.} \end{cases} \tag{5.2}$$

We assume that the Rake finger is locked to the strongest path within a set of non-resolvable paths. Therefore, if τ is the path delay with respect to the strongest path in a set of non-resolvable paths, $R_x(\tau)$ is the fraction of the power gain of a path in the set of non-resolvable path that is recovered by the Rake finger.

For the ITU pedestrian A channel all paths are non-resolvable with a chip period of $T_c = 814\,\text{ns}$, therefore they result in a single Rayleigh fading path (i.e., flat fading). The Rake receiver synchronizes on the strongest path (first path shown in Table 5.1). The second path is attenuated through $R_x(\tau)$. Substituting the 110ns of relative delay into (5.2), a 0.63 dB attenuation is found for the second path, and hence the relative power of the second path is –10.33 dB, and it is combined with the power of the first path. The third path's relative power is attenuated by 1.15 dB to become –20.35 dB, and the fourth path becomes –25.8 dB; the third and fourth contributions to the captured power are neglected due to their small relative values. The fraction of the total received power that is captured by the Rake receiver is then

$$\frac{\text{Power captured}}{\text{Total received power}} = \frac{10^{0/10} + 10^{(-9.7-0.63)/10}}{10^{0/10} + 10^{-9.7/10} + 10^{-19.2/10} + 10^{-22.8/10}} \approx 0.97 \qquad (5.3)$$

The ITU vehicular B channel has three resolvable paths (neglecting the 5th and 6th paths due to their small relative powers). The first resolvable path is the combined 1st and 2nd paths at 0 and 300 ns respectively (see Table 5.2); the second path is the one at 8,900 ns, and the third path at 12,900 ns. The Rake consists of three fingers perfectly locked to the paths at 300, 8,900, and 12,900 ns. The path at 0 ns contributes to the output power of the first finger with a reduced contribution according to (5.2). The fraction of the total power received captured by the first, second and third fingers are

$$\frac{\mathrm{P}_{\mathrm{F1}}}{\mathrm{p}_{\mathrm{R}}}=\frac{10^{0/10}+10^{(-2-2.5)/10}}{10^{0/10}+10^{-2.5/10}+10^{-12.8/10}+10^{-10/10}+10^{-25.2/10}+10^{-16/10}}\approx 0.78$$

$$\frac{\mathrm{P}_{\mathrm{F2}}}{\mathrm{P}_{\mathrm{R}}}=\frac{10^{-12.8/10}}{10^{0/10}+10^{-2.5/10}+10^{-12.8/10}+10^{-10/10}+10^{-25.2/10}+10^{-16/10}}\approx 0.03 \qquad (5.4)$$

$$\frac{\mathrm{P}_{\mathrm{F3}}}{\mathrm{P}_{\mathrm{R}}}=\frac{10^{-10/10}}{10^{0/10}+10^{-2.5/10}+10^{-12.8/10}+10^{-10/10}+10^{-25.2/10}+10^{-16/10}}\approx 0.057$$

Where P_{Fi} is the power captured by finger i, and P_R is the Total received power.

5.2.2 Evaluation of SIR values in the ITU pedestrian A radio channel.

In the ITU pedestrian A channel individual paths in the multi-path profile are not resolvable at 1.2288Mc/s, and hence the signals experience flat fading. To account for the desired signal and interference powers received by a mobile, 57 independent Rayleigh fading processes of 30s duration, and time resolution of 1.667ms are generated per dropped mobile to represent the received signal and interference from 56 interfering sectors. Fading rate determined by Doppler shift of 5.28Hz corresponds to the assumed 3km/h speed of the mobile. 97% power capture factor is used for the signal as computed in (5.3).

The effective signal power received by the i^{th} mobile from its serving sector accounting for path-loss, shadow fading, Rayleigh fading, and excluding the overhead bits is given by

$$P_i = 0.97\overline{P}_i(R_i)^2 \text{ W} \qquad (5.5)$$

where $\overline{P_i}$ is the small-scale average power received by the i^{th} mobile from the serving sector, accounting for path loss and shadow fading; R_i is a Rayleigh variable representing small scale fading of the signal channel to the i^{th} mobile.

$\overline{P_i}$ is computed as follows

$$\overline{P_i} = P_{t\max}(dBm) - L^i(dB) + G_{ant\,BS}(dBi) - G(\theta)(dB) - L_c(dB) - X^i(dB) \qquad (5.6)$$

where $P_{t\max}$ and $G_{ant\,BS}$ are transmitted power and bore-sight antenna gain (Table 5.3); L^i is the path-loss between the serving sector and the i^{th} mobile terminal; $G(\theta)$ is the horizontal directivity loss of the antenna that depends on the angle between the mobile and the serving sector; L_c is the cable loss, and X^i is the contribution of shadow fading.

Interference is computed as

$$I_i = \sum_{\substack{i=1 \\ i \neq serving \\ sector}}^{57} \overline{P_i}(R_i)^2 \text{ Watts} \qquad (5.7)$$

The signal-to-interference ratio SIR_i for the i^{th} mobile is the ratio of P_i in (5.5) and I_i in (5.7).

As an intermediate verification of the SIR evaluation procedure, cumulative distribution functions (CDF) of the SIR values obtained with SBSS have been determined and they are plotted in Figure 5.2.

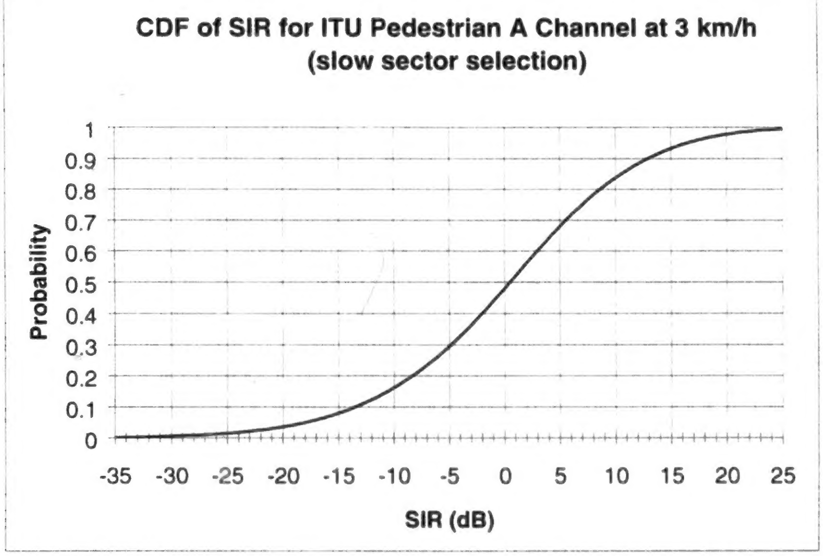

Figure 5.2. cdf's of SIR values in ITU ped. A radio environment with SBSS at 3km/h.

5.2.3 Evaluation of SIR values in the ITU vehicular B radio channel.

In the ITU vehicular B channel there are effectively three paths which are resolvable at 1.2288 Mc/s, and contribute non-negligible power to the output of the Rake combiner. We assume the first finger of the Rake locks on to the path at 300 ns, and the non-resolvable path at 0 ns contributes to the output power of the same finger, but is reduced proportionally to its time offset. Second finger of the Rake locks on to the path at 8,900 ns, and third finger on to the path at 12,900 ns. The other paths in the profile are ignored since they contribute negligibly to the output of the Rake. However their contribution to interference is taken into account.

To account for the desired signal and interference powers received by a mobile, 59 independent Rayleigh fading processes of 30s duration, and time resolution of 1.667 ms are generated per dropped mobile to represent 3 Rayleigh fading signals from the serving sector captured by the three fingers of the Rake, and interference from 56 interfering sectors. Fading rate determined by Doppler shift of 105.5 Hz corresponds to the assumed 60 km/h speed of the mobile. 78%, 3%, and 5.75% signal power capture factors by the three Rake fingers are used, as computed in (5.4).

The effective received signal powers for the three fingers of the Rake in the i^{th} mobile are given by

$$\begin{aligned}
Ps_1 &= 0.78\overline{P}_i(R_0{}^1)^2 && \text{combined 1}^{\text{st}}\text{ and 2}^{\text{nd}}\text{ path of the profile} \\
Ps_2 &= 0.03\overline{P}_i(R_0{}^2)^2 && \text{path at 8,900 ns} \\
Ps_3 &= 0.057\overline{P}_i(R_0{}^3)^2 && \text{path at 12,900 ns}
\end{aligned} \tag{5.8}$$

Where $\overline{P}_i$ is the small-scale average power received by the i^{th} mobile as computed in (5.6); $R_0{}^\gamma$ is the Rayleigh fading signal contribution coming from the serving sector and the γ^{th} resolvable path.

Interference per finger is computed as follows

$$\begin{aligned}
I_1 &= \sum_{\substack{i=1 \\ i \neq \text{serving} \\ \text{sector}}}^{57} P_i(R_i)^2 + (Ps_2 + Ps_3) \\
I_2 &= \sum_{\substack{i=1 \\ i \neq \text{serving} \\ \text{sector}}}^{57} P_i(R_i)^2 + (1.15Ps_1 + Ps_3)
\end{aligned} \tag{5.9}$$

$$I_3 = \sum_{\substack{i=1 \\ i \neq serving \\ sector}}^{57} P_i (R_i)^2 + (1.15 Ps_1 + Ps_2)$$

The factor 1.15 is the result of the interference caused by paths at 0 ns and 300 ns in the second and third fingers (this is 90% of total power received from all the multi-paths from the serving sector, therefore 0.78x1.15 = 0.9)

Maximal ratio combining is assumed, therefore SIR at the output of the Rake receiver is given by

$$SIR = 10\log_{10}\left(\frac{Ps_1}{I_1} + \frac{Ps_2}{I_2} + \frac{Ps_3}{I_3}\right) \tag{5.10}$$

Similarly to the pedestrian A channel case, as an intermediate verification of the SIR evaluation procedure, CDFs of the SIR values obtained with SBSS have been determined for the vehicular B channel, and they are plotted in Figure 5-3.

The SIR values computed in (5.5)-(5.9) are further modified by the implementation imperfections encountered in non-ideal systems. The imperfections taken into account are

- Inter-chip interference (ICI)
- Loss of channel orthogonality due to transmitter non-linearity
- Non-ideal waveform quality

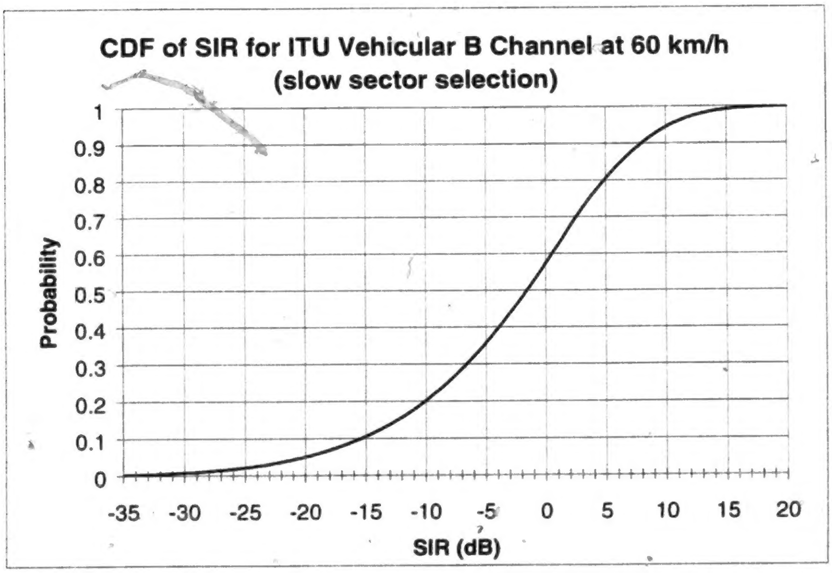

Figure 5.3. cdf of SIR values in ITU veh. B radio environment with SBSS at 60km/h.

- ADC quantization noise
- Adjacent channel interference

Measurements of the effects of these imperfections have been performed by different research groups. The effects of the different imperfections on the signal level are given as ratios of signal power to imperfection-interference power, and are denoted as SIR_I in Table 5.4, which includes measurement results obtained by Ericsson Wireless [52]

For the ITU pedestrian A channel the SIR estimated using (5.5)-(5.7) is modified as follows to account for imperfections

$$\mathrm{SIR}_M = \frac{\mathrm{SIR}}{1+\dfrac{\mathrm{SIR}}{\alpha}} \qquad (5.11)$$

where $\alpha = 10^{\mathrm{SIR}_I^T/10}$, and SIR is the original SIR value as computed using (5.5)-(5.7).

For the ITU vehicular B channel the original SIR estimated using (5.8)-(5.10) is also modified as in (5.11) to account for imperfections. Figures 5.4 and 5.5 show the cumulative distribution functions of the modified SIR values for pedestrian A and vehicular B channels respectively.

Imperfection	SIR_I **(dB)**
Inter-chip interference	16.5
Loss of channel orthogonality	29.0
Non-ideal waveform quality	18.1
ADC quantization noise	20.0
Adjacent channel interference	27.0
Total: (SIR_I^T)	12.95

Table 5.4. SIR_I due to imperfections, source [52].

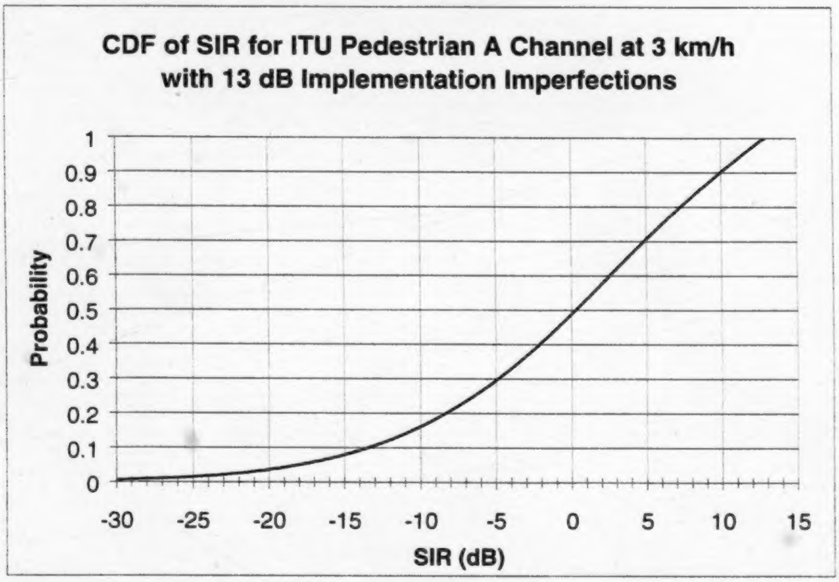

Figure 5.4. cdf's of estimated SIRs in pedestrian A channel with $\mathrm{SIR}_I^T = 13\mathrm{dB}$

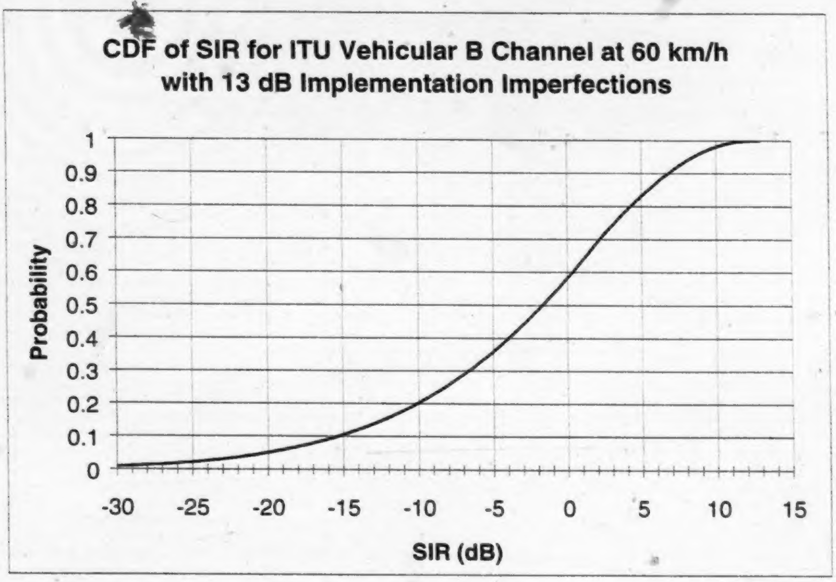

Figure 5.5. cdf's of estimated SIRs in vehicular B channel with $SIR_I^T = 13dB$

5.3 MCS format determination

The delay between the MCS request made by the DRC channel and the actual transmission of the packet in HDR is approximately 3 slots, therefore the SIR value three slots ahead $SIR(n+3)$ needs to be predicted from the actual value $SIR(n)$ if a proper format determination scheme is desired. An effective prediction algorithm for the wireless channel is a complicated task out of the scope of this work. For a good review of research in this area refer to [53]. In this work, out-of-date channel information reduced by a margin is used to select a suitable transmission format.

A 1dB margin (to account for estimation and prediction inaccuracies) is used to find an estimate at SIR(n+3)

$$\hat{\mathrm{SIR}}(n+3) = SIR(n) - 1dB \qquad (5.12)$$

We call this $\hat{SIR}$ predicted SIR.

The MCS format determination is achieved by choosing at all times the highest possible transmission format. The MCS format determination procedure makes use of the AWGN PER vs. SIR curves generated in the link-level simulation.

The MCS format determination procedure compares the SIR value computed in (5.12) with the SIR value needed to achieve PER = 1% for the maximum number of re-transmissions allowed for each format (ie., $SIR_{1\%}$). The $SIR_{1\%}$ values for all transmission formats are presented in Table 5.5. If $\hat{SIR}$ is higher than more than one value of $SIR_{1\%}$ in Table 5.5, the highest format is chosen. With this latter criterion it is very unlikely that formats 4, 5, and 8 will be chosen because of their close proximity to the higher formats 6, 7, and 11 respectively. The procedure selects the DRC with smaller maximum number of slots in Pedestrian A,and the DRC with larger maximum number of slots in Vehicular B due to higher uncertanty in SIR prediction with higher mobility.

5.4 Scheduling of transmissions

In a time-division multiplex system like HDR and 1XTREME forward links, scheduling determines which one of the requesting users is served by the system. Scheduler design is of vital importance to quality of service and overall performance of packet data services. The scheduling algorithm depends on the optimization criterion for system resource allocation.

Format Number	**Max. Allowed Slots**	**Packet Size (bits)**	**Turbo Code Rate**	**Modulation**	$SIR_{1\%}$
1	16	1,024	1/5	QPSK	-13.5
2	8	1,024	1/5	QPSK	-10.4
3	4	1,024	1/5	QPSK	-7.4
4	2	1,024	1/5	QPSK	-4.3
5	1	1,024	1/5	QPSK	-1.0
6	4	2,048	1/3	QPSK	-4.2
7	2	2,048	1/3	QPSK	-1.2
8	1	2,048	1/3	QPSK	3.7
9	2	3,072	1/3	8PSK	1.6
10	1	3,072	1/3	8PSK	7.1
11	2	4,096	1/3	16QAM	3.4
12	1	4,096	1/3	16QAM	9.2

Table 5.5. SIR required to achieve PER = 1% for the maximum number of re-transmissions allowed for each format ($SIR_{1\%}$).

A scheduler tries to maximize some performance metrics (e.g. average sector throughput), while trying to maintain some degree of fairness, and subject to packet error rate not exceeding 1%. Performance of Round-Robin, and Proportionally Fair schedulers is investigated by simulations. This work assumes full packet-queues for each user, which means that there is always data to transmit to a given user.

5.4.1 Round robin scheduler

When this scheduler is used, data packets are transmitted to users in a round-robin fashion. However, since the channel conditions change from one packet transmission to the next, users must qualify for transmission before they are granted transmission permission. To qualify for transmission a user must have a predicted SIR greater than the minimum SIR to ensure 1% PER at the lowest bit rate. According to the results of the link-level simulation of HDR, this threshold is approximately –13.5 dB.

At all times the round-robin scheduler must verify if a given slot is available. A slot is available if no user claims the slot for the re-transmission of a packet; users that are in the process of re-transmitting a packet have priority every 4 slots until the maximum number of allowed re-transmissions have been reached, or early termination occurred.

The round-robin scheduler works in a three-cycle scheme as follows:

1. If a slot is available, the round-robin scheduler goes around the circle of users and tries to assign the slot to a user whose predicted SIR is above the minimum threshold, and who is not in the process of transmitting another packet.
2. If the round-robin scheduler makes full circle, and no user is assigned to the slot, it starts another round around the circle, trying to assign the slot to the first user whose predicted SIR is above threshold, and who is in the process of transmitting another packet.
3. If the round-robin scheduler makes second full circle, and both 1 and 2 slot assignment attempts fail, the round-robin scheduler picks the user whose predicted SIR is below threshold, and is the highest of all users at the time.

The round-robin scheduler's main purpose is to ensure the maximum degree of fairness in the allocation of radio resources.

5.4.2 Proportionally fair (PF) scheduler

One of the most commonly used criteria for scheduler design is to maximize the overall system throughput under certain fairness constraints on each user's utilization of system resources. The scheduler described in the following maximizes the system overall throughput while ensuring fair utilization of resources.

A scheduler that is based only on the SIR received by a mobile will maximize the average throughput per sector, but at the expense of giving priority to the users close to the base station. Hence it is unfair to the users far from the base station. The PF scheduler [23] will schedule the user with highest ratio $Rreq/\overline{R}$. $Rreq$ is the rate requested by the mobile according to the SIR predicted; $\overline{R}$ is the average rate received by the mobile in a window of time in the past. In this approach users are scheduled in such a way as to maximize a performance criterion that offers maximum possible average throughput per sector (by scheduling users with higher rates), while maintaining a reasonable level of fairness (by scheduling users with lower $\overline{R}$). The PF scheduler schedules the transmission of a user packet when the user sees the best relative channel conditions.

As in the round-robin scheduler, the PF scheduler must give priority to a user in re-transmission. A slot is available if no user in re-transmission claims the use of the given slot.

Specifically, the PF scheduler works as follows:

1. If a slot is available, the user with ratio $\max_{1 \le i \le N} \{Rreq / \overline{R}^i\}$ out of N users is scheduled for transmission. Ties are broken randomly.
2. The average rate of the i^{th} user is updated with the following first-order recursion

   $$\overline{R}^i_{n+1} = \left(1 - \frac{1}{t_c}\right)\overline{R}^i_n + \frac{1}{t_c} R^i_n \tag{5.13}$$

   where R^i_n is the current transmission rate of i^{th} user, computed as

   $$R^i_n = \frac{\text{Packet size}_{\text{slot } n}\,(symbols)}{\text{slot - time}} \tag{5.14}$$

   $R^i_n = 0$, when user i is not receiving service in slot n

   t_c is the duration of the averaging window; a higher value of t_c makes the update of $\overline{R}^i$ slower. A slower update of $\overline{R}^i$ can effectively increase overall throughput because the algorithm waits longer for the channel to improve, but at the same time delay per user increases. We have chosen a value for t_c that works best in terms of delays per user and overall throughput achieved.

Users that are in the process of receiving a re-transmitted packet are allowed to receive another packet in parallel.

5.5 Packet erasure determination

The purpose of the packet erasure determination procedure is to determine if a packet has been successfully delivered over the allowed maximum number of re-transmissions for a given selected transmission format. The SIR values used for erasure determination are the actual average SIR values that include Rayleigh fading, shadowing and path-loss (read from a look-up table as computed in Section 5.2). An actual average SIR value is obtained through averaging of actual SIR values obtained from the look-up table for the slots used for the successive transmissions of the packet (multi-slot transmission). Arithmetic averaging of SIR values expressed on a linear scale is performed.

All 41 AWGN PER curves determined for HDR explicit and implicit transmission formats and bit rates (listed in Table 4.1) are used in the packet erasure determination procedure as follows:

1. If the actual average SIR is equal or larger than SIR (@PER = 1%) on the curve corresponding to the current number of packet transmissions (or number of slots used up to the present moment) in the selected transmission format, then the transmission is successful, and the achieved bit rate corresponds to the AWGN PER vs E_s / N_o curve used;
2. If the actual average SIR is smaller than SIR (@PER = 1%) on the curve corresponding to the current number of packet transmissions (or number of slots used up to the present moment) in the selected transmission format, then the transmission is unsuccessful, and another transmission is requested. If the unsuccessful transmission was the last allowed transmission, the packet is discarded.

Only successfully received packets are counted towards throughput; PER = 1% is implicit (packets received successfully in the manner described above contain 1% of packets with errors).

5.6 HDR system level simulator

The SIR look-up table generation, MCS format determination, scheduling and packet erasure determination procedures described in previous sections are combined to create the system-level simulator for HDR.

The current SIR values of *n* users and 18,000 slots are used by equation (5.12) to roughly predict the SIR values three slots ahead for each user. The predicted SIR is used by the format determination, scheduling, and frame erasure determination procedures according to the descriptions in Sections 5.3, 5.4 and 5.5 respectively. The performance metrics are finally computed in the last step of the system level simulation. The procedure runs with a time resolution of one slot (1.67ms) for 18,000 slots per drop (30s), and is re-initialized for every drop for a total of 100 drops of 16, 8, and 4 users each.

The results of the system-level simulation will be presented in Chapter 6.

5.7 1XTREME system level simulator

The system-level simulation in 1XTREME has a similar structure to the HDR system-level simulation in its basic components, with the exception of two differences.

In order to capture all the variations of a Rayleigh fading channel, the time resolution of the simulation must be smaller than the coherence time of the channel at the maximum speed simulated. The coherence time of a fading channel is a time interval over which a fading channel does not change substantially. In order to quantify the coherence time some authors define it as the interval in time during which the auto-correlation of the desired signal reaches 50% of its maximum, this time is given as [2]

$$T_{coh} \approx \frac{9}{16\pi f_m} \qquad (5.15)$$

where f_m is the maximum Doppler frequency. At 60 km/h the maximum Doppler frequency is 105.5Hz and T_{coh}= 1.7 ms. Hence, if T_{coh}= 1.7 ms and slot duration is 1.67 ms like in HDR, then the channel and hence the SIR in principle does not change during a slot.

In HDR system-level simulation the resolution used is 1.67 ms, therefore a value of SIR corresponds to the value of the SIR in one slot. The slots in 1XTREME on the other hand are 5 ms long, therefore the channel changes considerably during a 1-slot duration, and as a consequence there is more than one SIR value per slot. The simulation time-resolution used in 1XTREME is 1.25 ms, hence four SIR values are computed per slot describing well the changes in the channel. This issue is only present at 60 km/h, at 3 km/h T_{coh}= 33 ms, and hence one SIR is sufficient per 5 ms slot to model the channel variation in 1XTREME. We need only one SIR value per 5ms slot to be able to:

- Choose the modulation and coding scheme (MCS).
- Determine packet erasure for that MCS from the AWGN PER.

Hence, a mapping from four SIR values to one is needed in 1XTREME. There are various methods to map these SIR values to an equivalent SIR in AWGN channel [54]. For each MCS, the equivalent SIR value in AWGN channel should result in the same PER as the sequence of four SIR values in the fading channel.

The mapping used in vehicular B channel is geometric averaging, in which the arithmetic average of SIR values in dB is used as the equivalent SIR value

$$\frac{C^j}{I} = \frac{1}{4}\sum_{i=1}^{4}\left(\frac{C^j{}_i}{I_i}\right)_{\mathrm{dB}} \tag{5.16}$$

In 1XTREME the Hybrid-ARQ procedure is implemented in the system level simulation, whereas in HDR it is included in the link-level simulations. Hybrid ARQ is implemented by soft combining of repeated packets over multiple slots based on the approach of Chase in [28]. Once a packet is given transmission permission, an either even or odd channel is assigned to the packet. If the base station does not receive an ACK after the time out, the packet is retransmitted on the subsequent even or odd time slot. In this scheme, it is assumed that the maximum processing and propagation delay is no longer than 2 slots. Each subsequent noisy-packet accumulates the SIR value of its predecessors to simulate the soft-packet combining procedure.

5.8 Summary

The system level simulation of HDR and 1XTREME involves not only the estimation of SIR values of users in a cellular network for different types of environments, but also the simulation of procedures such as: Prediction, Format of transmission determination, Scheduling, and Frame erasure determination. All these procedures have to be performed in coordination with one another, and within the desired range of PER per user (usually around 1%).

In this chapter, the different functional-blocks and procedures used to perform the system level simulation of HDR and 1XTREME were presented. One mechanism of sector selection called slow BSS, and two scheduling procedures, the Round robin, and the PF schedulers were introduced. A simple mechanism is also proposed for prediction with desired PER, given by (5.12).

The results of the system level simulations are presented in Chapter 6, along with the analysis and future recommendations.

Chapter 6

Performance of HDR and 1XTREME

6.1 Introduction

The performance metrics presented in this chapter are obtained for users located in one of the sectors of the central cell of the network depicted in Figure 3.1 (Chapter 3). The performance metrics obtained for HDR and 1XTREME are

- Distribution of peak bit rates over the set of users
- Distribution of the throughput over the set of users
- Average throughput per sector
- Distribution of delay over the set of user
- Average delay per sector
- Distribution of the number of slots allocated per user

These performance metrics are evaluated within the following scenarios

- Radio environment: ITU pedestrian A and ITU vehicular B channels
- Sector selection: slow best sector selection (SBSS)
- Scheduling method: Round Robin (RR) scheduler, and Proportionally Fair (PF) scheduler.

This chapter is divided into 6 main sections, each of which presents the values of every performance metric for HDR and 1XTREME. Last Chapter presents the discussion, conclusion, and guidelines for future research in this area.

6.2 Distribution of peak bit rates over the set of users

Figures 6.1 to 6.8 depict the distribution of peak bit rates over a set of 16 users. These are the rates requested by the mobiles over the DRC channel to the base station. The rates requested are such that a PER=1% can be achieved in the decoder given the predicted SIR (Table 5.5 in Chapter 5 shows the mapping of SIR predicted to format of transmission on the forward link). A total of 16 users are present in the embedded sector, and the simulation is run for 30 seconds of real time.

6.2.1 Pedestrian A channel

Figures 6.1to 6.4 show the distributions of peak bit rates over the set of users for pedestrian A channel with slow sector selection for the Round-robin and PF schedulers. Note that the PF scheduler in all cases for both systems, schedules higher data rates than the RR scheduler; this is due to the proportionally fair scheduling algorithm which always schedules users during relatively best channel conditions.

6.2.1.1 1XTREME

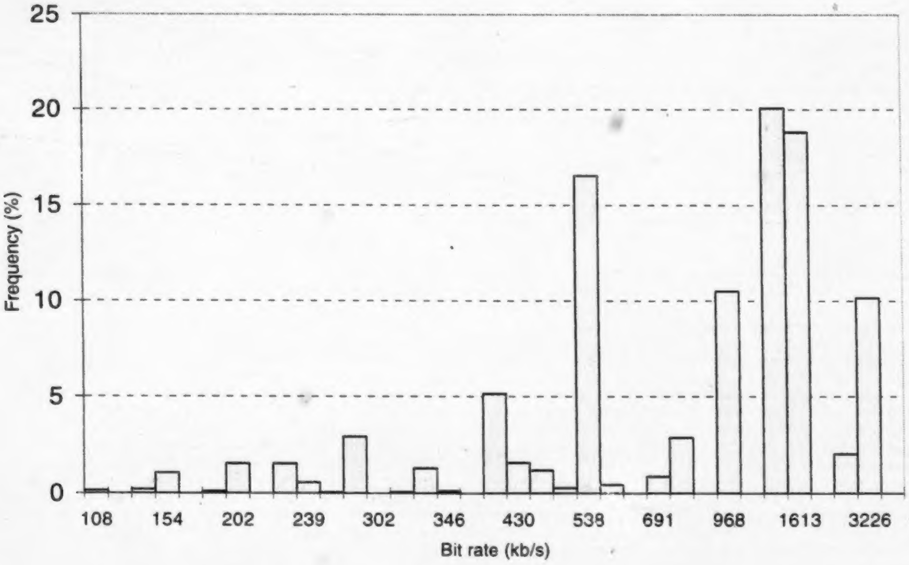

Figure 6.1. Distribution of peak bit rates in an embedded sector for 100 drops of 16 users each for the ITU pedestrian A channel with RR scheduler.

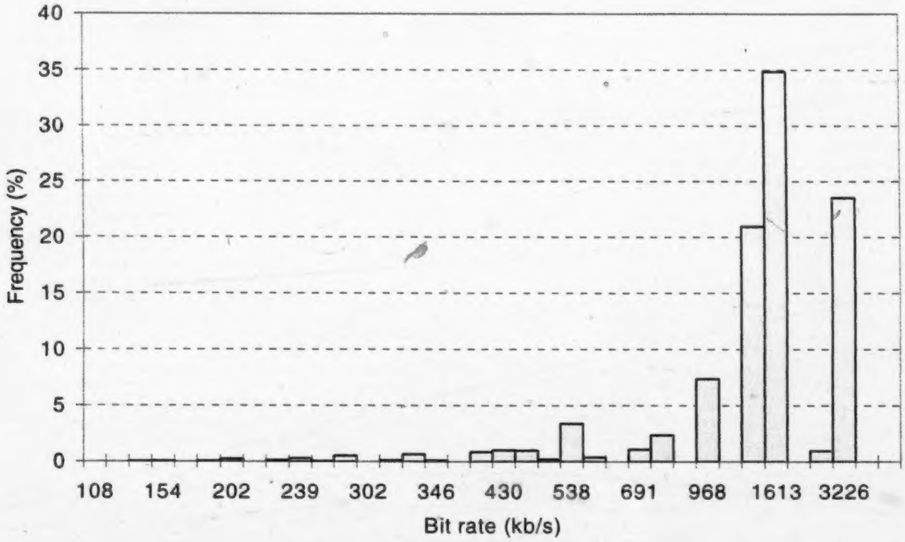

Figure 6.2. Distribution of peak bit rates in an embedded sector for 100 drops of 16 users each for the ITU pedestrian A channel with PF scheduler.

6.2.1.2 HDR

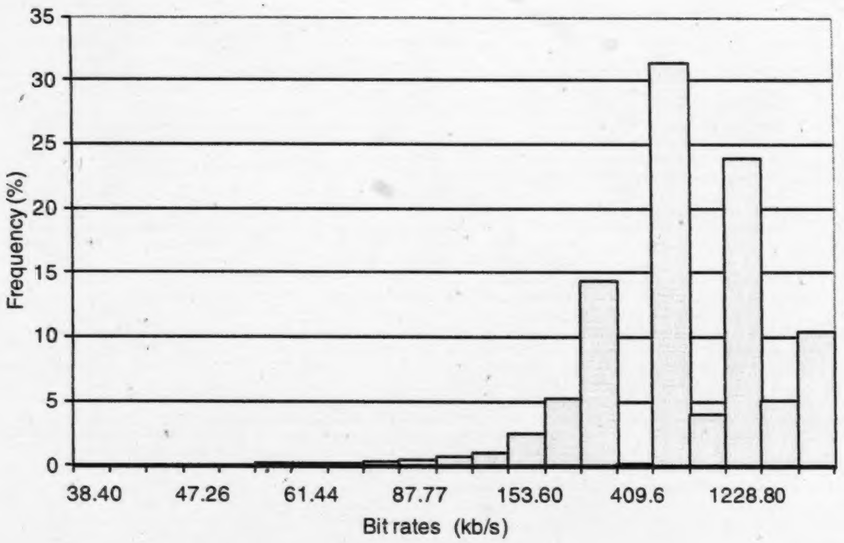

Figure 6.3. Distribution of peak bit rates in an embedded sector for 100 drops of 16 users each for the ITU pedestrian A channel with RR scheduler.

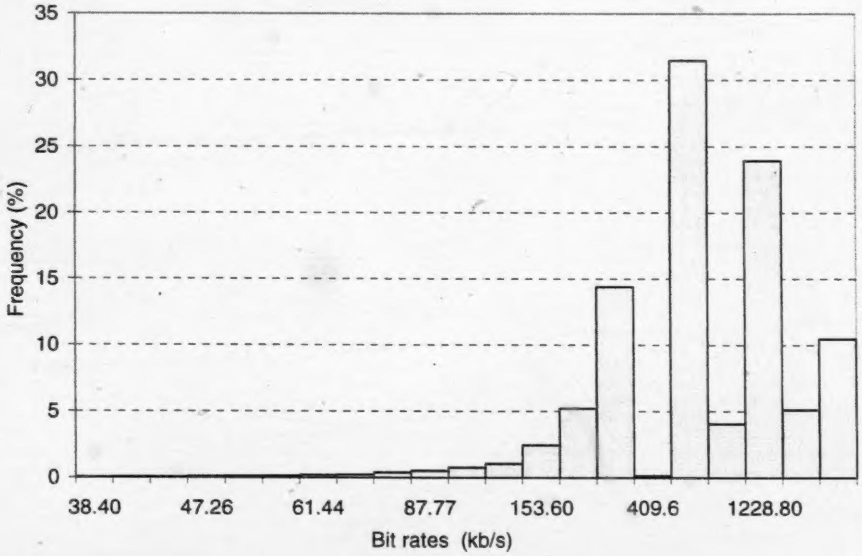

Figure 6.4. Distribution of peak bit rates in an embedded sector for 100 drops of 16 users each for the ITU pedestrian A channel with PF scheduler.

6.2.2 Vehicular B channel

6.2.2.1 1XTREME

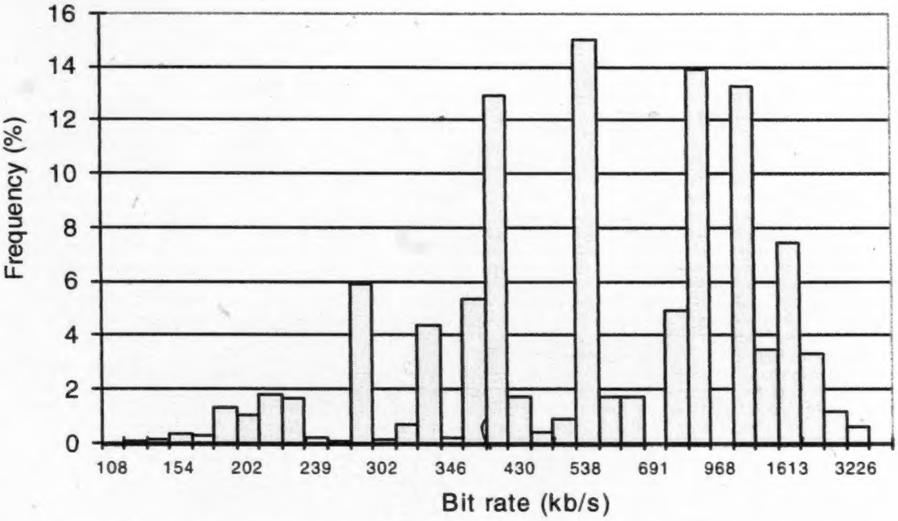

Figure 6.5. Distribution of peak bit rates in an embedded sector for 100 drops of 16 users each for the ITU vehicular B channel with RR scheduler.

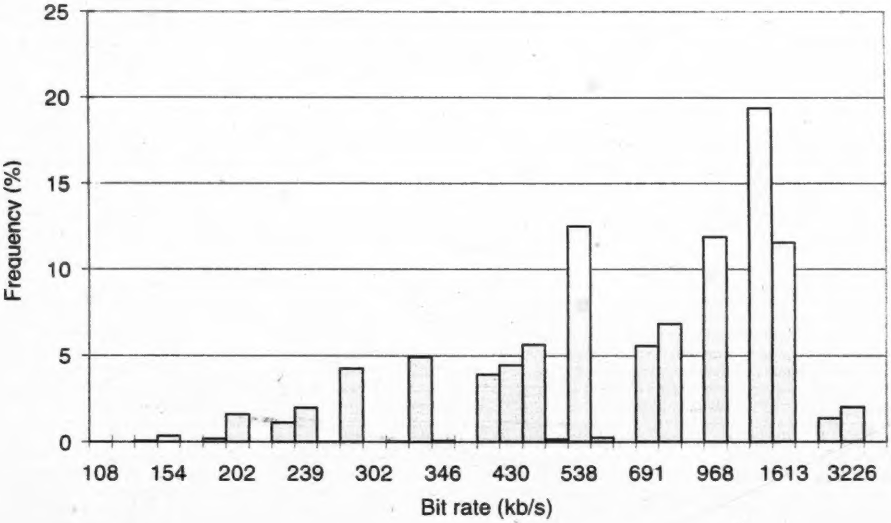

Figure 6.6. Distribution of peak bit rates in an embedded sector for 100 drops of 16 users each for the ITU vehicular B channel with PF scheduler.

6.2.2.2 HDR

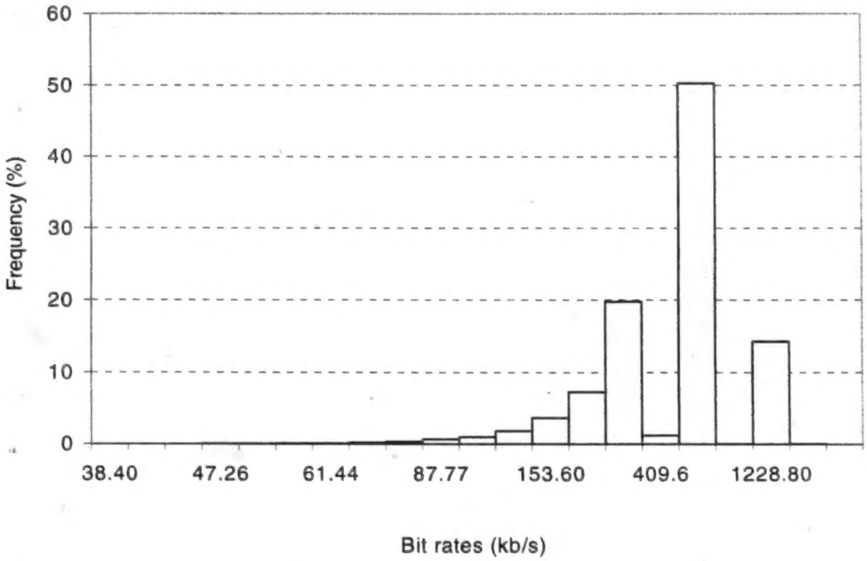

Figure 6.7. Distribution of peak bit rates in an embedded sector for 100 drops of 16 users each for the ITU vehicular B channel with RR scheduler.

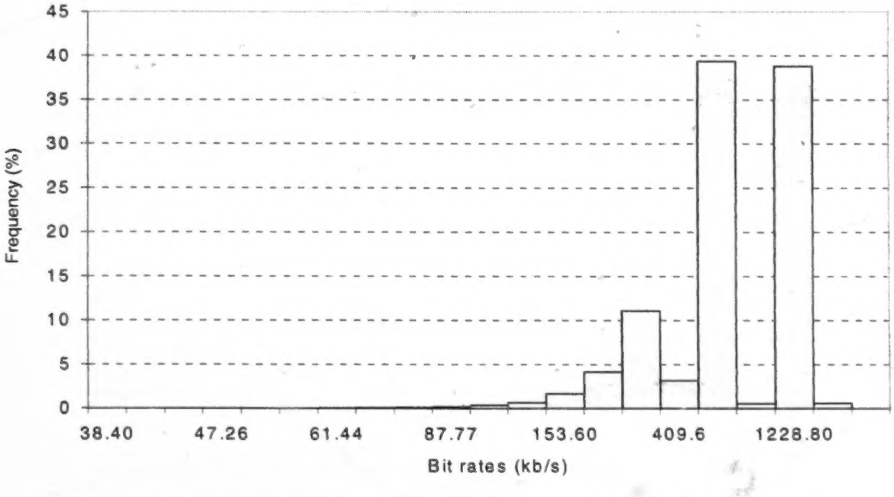

Figure 6.8. Distribution of peak bit rates in an embedded sector for 100 drops of 16 users each for the ITU vehicular B channel with PF scheduler.

It is observed that in all cases the tendency is to request higher bit rates; this is more pronounced for the pedestrian channel at 3km/h with PF scheduler due to the better performance of the predictor in this slowly changing channel. The 1XTREME system requests higher bit rates than HDR, but it will be shown later that the average sector throughput is lower for 1XTREME, which tells us that prediction is more accurate in the HDR system due to the shorter time-slot.

6.3 Distribution of throughput over the set of users

Figures 6.9 to 6.16 show the probability and cumulative distributions of throughput achieved per user in a 30 seconds simulation run with 16 users in the embedded sector. Results for the two systems are presented in pedestrian and vehicular channel, with PF and Round-robin schedulers.

6.3.1 Pedestrian A channel

6.3.1.1 1XTREME

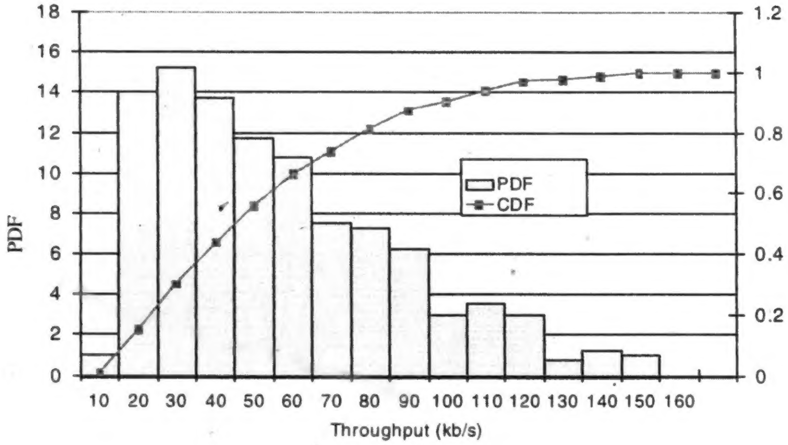

Figure 6.9. Distribution of throughput per user over the set of users (100 drops of 16 users each) in an embedded sector for ITU pedestrian A channel with RR scheduler.

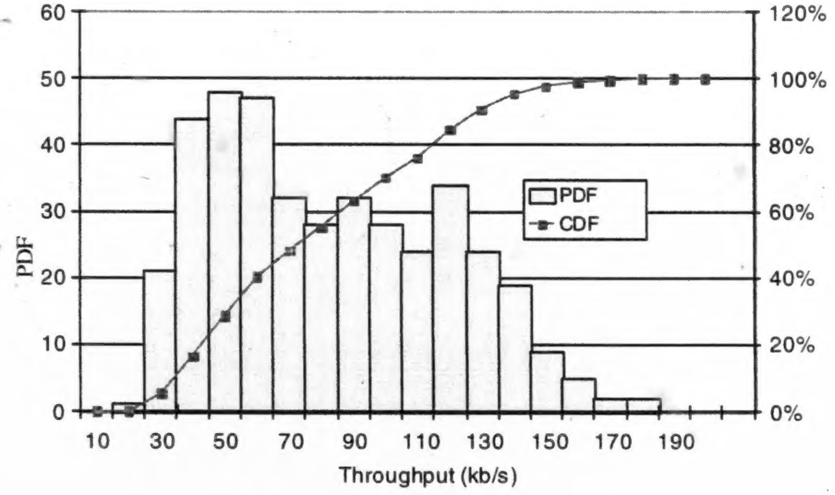

Figure 6.10. Distribution of throughput per user over the set of users (100 drops of 16 users each) in an embedded sector for ITU pedestrian A channel with PF scheduler.

6.3.1.2 HDR

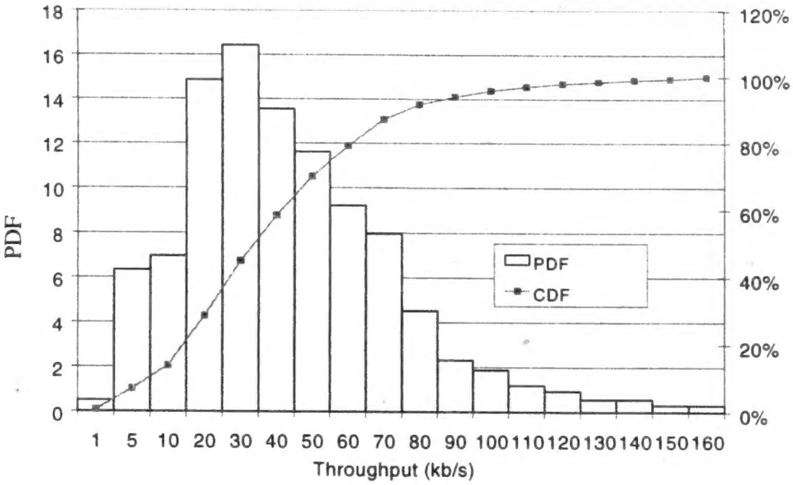

Figure 6.11. Distribution of throughput per user over the set of users (100 drops of 16 users each) in an embedded sector for ITU pedestrian A channel with RR scheduler.

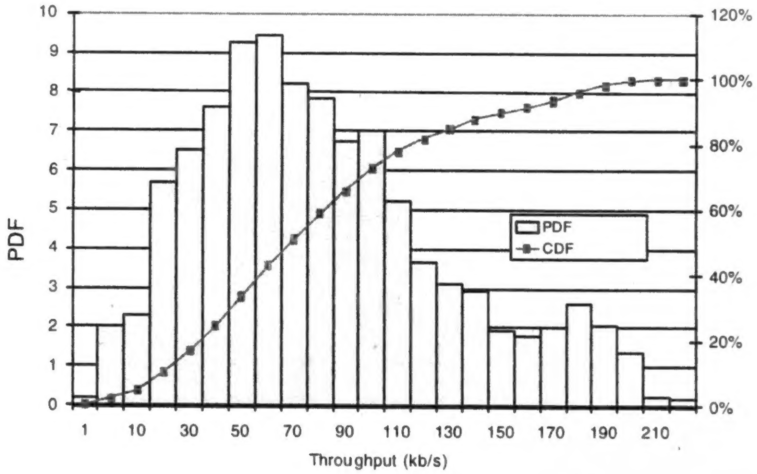

Figure 6.12. Distribution of throughput per user over the set of users (100 drops of 16 users each) in an embedded sector for ITU pedestrian A channel with PF scheduler.

6.3.2 Vehicular B channel

6.3.2.1 1XTREME

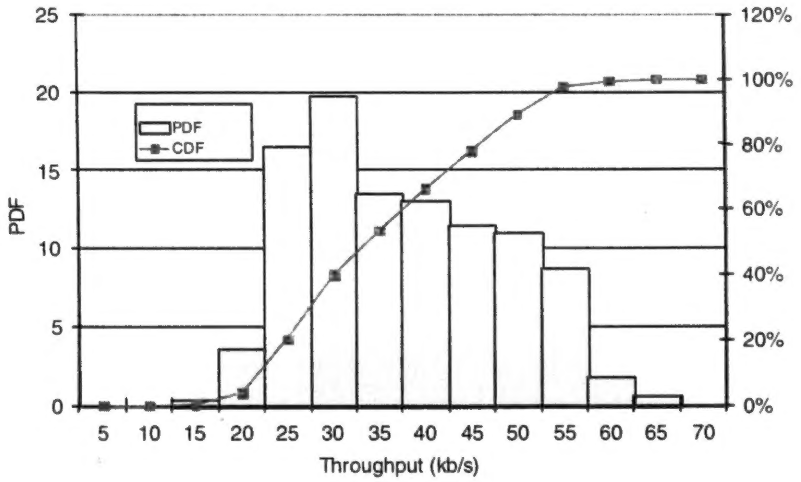

Figure 6.13. Distribution of throughput per user over the set of users (100 drops of 16 users each) in an embedded sector for ITU vehicular B channel with RR scheduler.

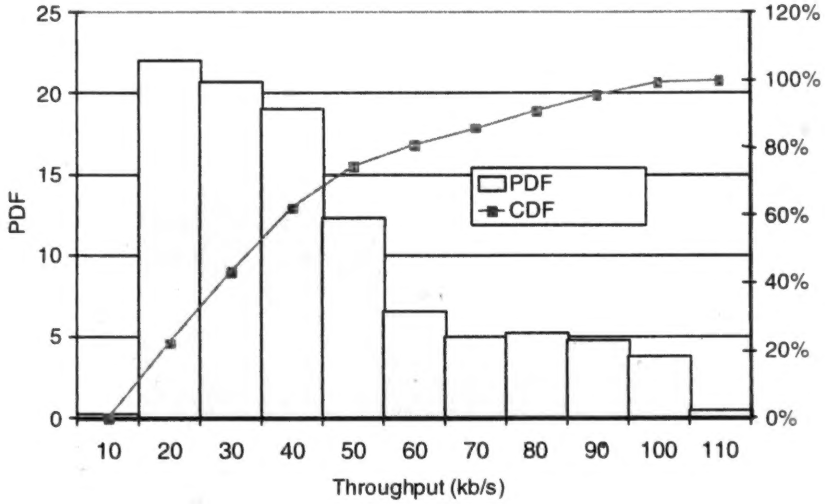

Figure 6.14. Distribution of throughput per user over the set of users (100 drops of 16 users each) in an embedded sector for ITU vehicular B channel with PF scheduler.

6.3.2.2 HDR

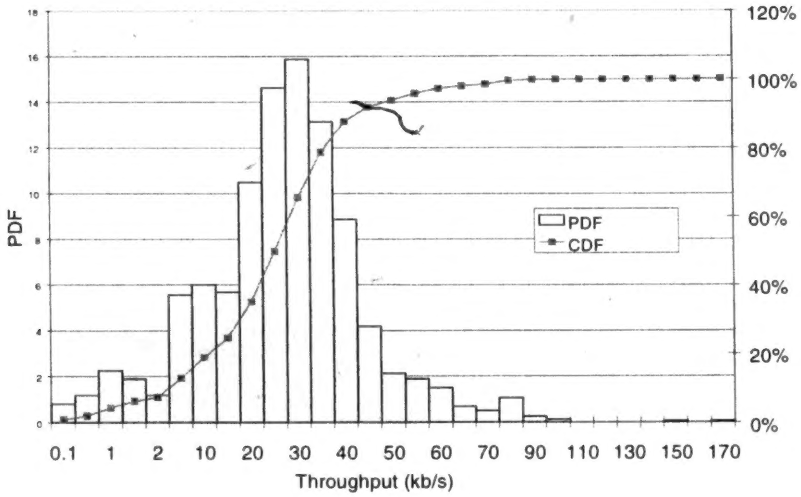

Figure 6.15. Distribution of throughput per user over the set of users (100 drops of 16 users each) in an embedded sector for ITU vehicular B channel with RR scheduler.

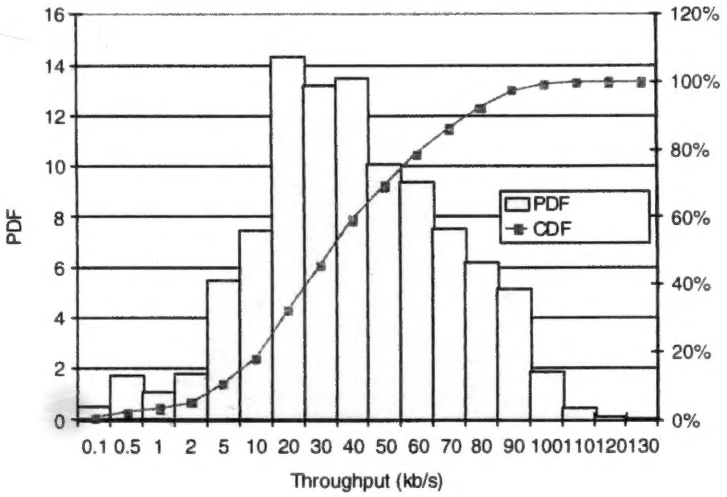

Figure 6.16. Distribution of throughput per user over the set of users (100 drops of 16 users each) in an embedded sector for ITU vehicular B channel with PF scheduler.

In the pedestrian channel the median throughput for HDR is approximately 50 kb/s, and 95 kb/s for round-robin and PF schedulers respectively. 1XTREME results are 45 kb/s and 73 kb/s. In the vehicular channel the throughput achieved per user is lower across all systems and scheduling algorithms. This is due to the higher uncertainty of the channel at higher speeds, and as a consequence more re-transmissions per given packet. The throughput gain of the PF scheduler with respect to the RR scheduler is lower in the high-speed vehicular channel due to the marginal multi-user diversity gain. The marginal PF scheduler gain due to significant channel uncertainty in high-speed vehicular environments has also been observed by other authors [55].

It is realized then, that throughput per user increases in these systems when the scheduler takes the channel conditions into account, highlighting the importance of an intelligent scheduling algorithm. Better performance results are also obtained for those systems that implement as short as possible time-slots. In shorter time-slot systems, the range of speeds for which the coherence time of the channel is less than or equal to the prediction time-interval is wider, which translates into more accurate prediction for a given speed, and therefore higher throughput. There are practical limitations as to how short the slots can be, including minimum packet sizes needed for optimum turbo-decoding performance. Lower speeds also tend to show higher throughput due to greater multi-user diversity gain.

The standard deviation of the throughput per user is also of interest, since it is an indication of the scheduler fairness. For the case of the pedestrian channel, PF scheduler, the standard deviation of throughput per user is 55.6 kb/s for HDR and 36.1 kb/s for 1XTREME. A higher standard deviation suggests a fairer scheduler.

6.4 Average sector throughput

Figures 6.17 to 6.20 show the average sector throughput within the embedded sector for pedestrian A and vehicular B channels in 1XTREME and HDR with slow sector selection, and the RR and PF schedulers. As expected, higher predictability of SIR in pedestrian A channel results in higher throughput. In every case we drop *N* users (*N* = 4, 8, 16) 100 times; after each drop, 30 seconds of transmission follow. Average throughput per sector is computed as the number of free-error bits delivered successfully per drop for all *N* users and averaged over the 100 drops.

6.4.1 1XTREME

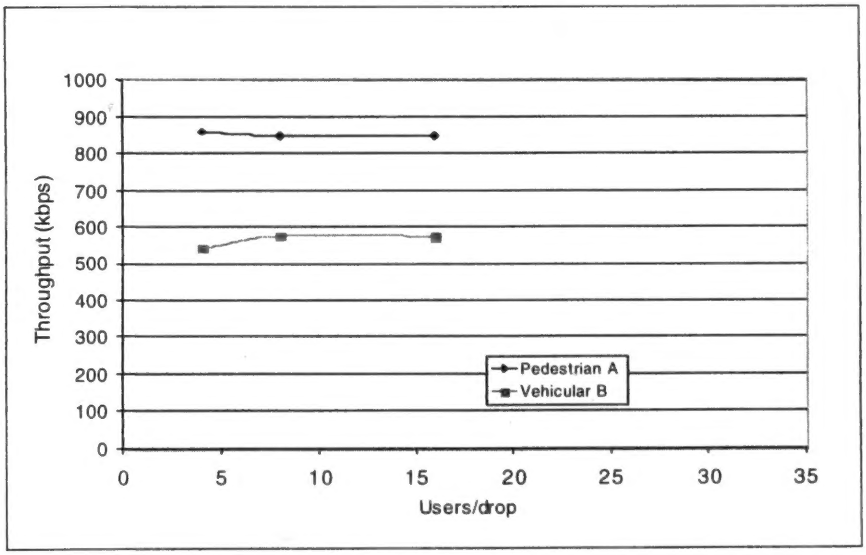

Figure 6.17. Total average throughput per embedded sector as a function of the number of users per drop for 100 drops, RR scheduler.

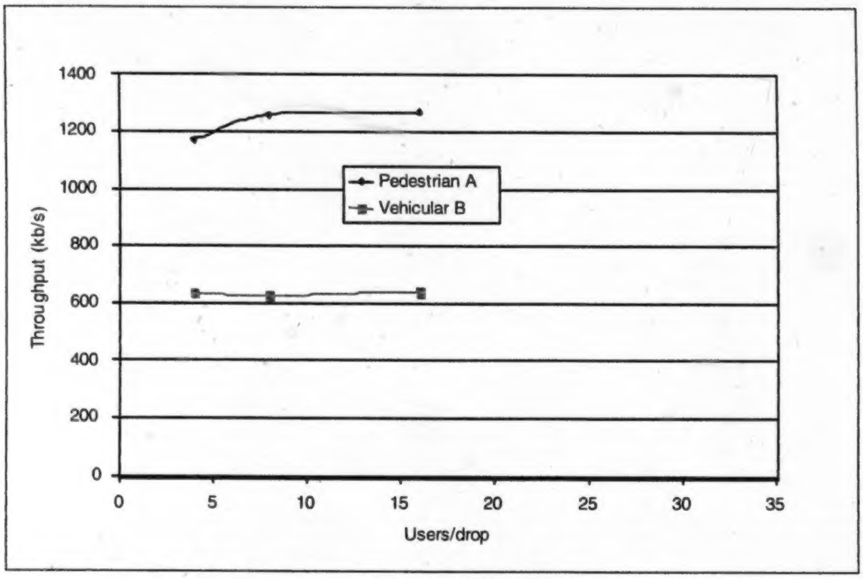

Figure 6.18. Total average throughput per embedded sector as a function of the number of users per drop for 100 drops, PF scheduler.

6.4.2 HDR

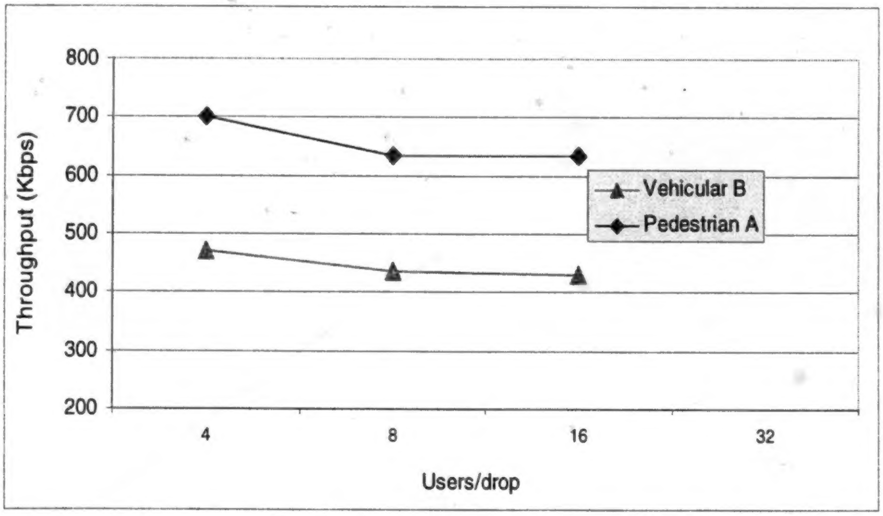

Figure 6.19. Total average throughput per embedded sector as a function of the number of users per drop for 100 drops, RR scheduler.

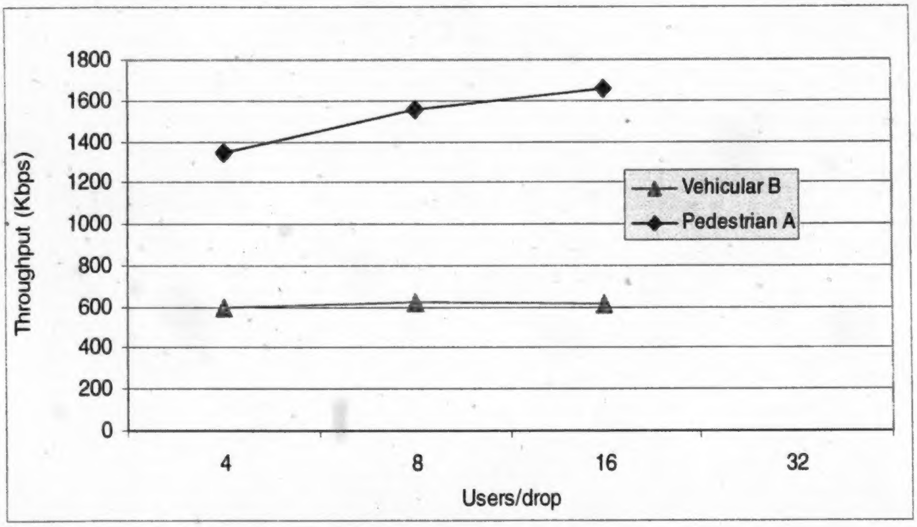

Figure 6.20. Total average throughput per embedded sector as a function of the number of users per drop for 100 drops, PF scheduler.

As expected, the PF scheduler offers more throughput gain than RR scheduler in all scenarios and for both systems. In the pedestrian channel with PF scheduler, HDR's throughput increases from around 1,200 kb/s to 1,600 kb/s, with the number of users increasing from 4 to 16. This is the consequence of multi-user diversity. A similar effect can be observed in 1XTREME, although to a lesser extent than for HDR (an increase from around 1,200 to 1,300 kb/s). Clearly, the multi-user diversity gain decreases with increasing duration of the slot. In the vehicular channel, the multi-user diversity gain is marginal for both systems and the channel uncertainty not only almost obliterates scheduler gain, but also lowers the average sector throughput to about 600 kb/s.

It can be noted that due to shorter time slots, HDR takes greater advantage of multi-user diversity than 1XTREME. Scheduling gain due to multi-user diversity is significant in the pedestrian channel, but negligible in the vehicular one.

6.5 Distribution of delays

Figures 6.21 to 6.28 show the probability density and cumulative distributions of the packet delays per individual users. Packet delays are given in seconds and are defined as the time interval between the moment the mobile requests the packet, to the instant in time the packet is successfully received at the mobile. Note that this times includes the time it takes the scheduler to deliver the given packet, and the possible re-transmissions needed for the packet to get through successfully.

6.5.1 Pedestrian A channel

6.5.1.1 1XTREME

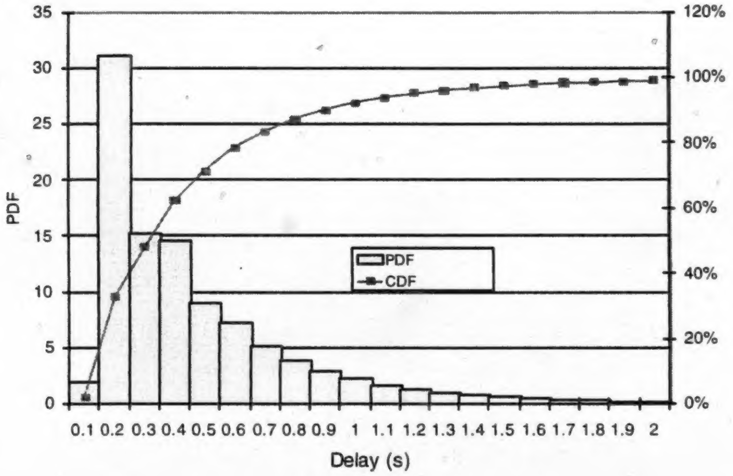

Figure 6.21. Distribution of delays per delivered packet over the set of users (100 drops of 16 users each) in an embedded sector for ITU pedestrian A channel with RR scheduler.

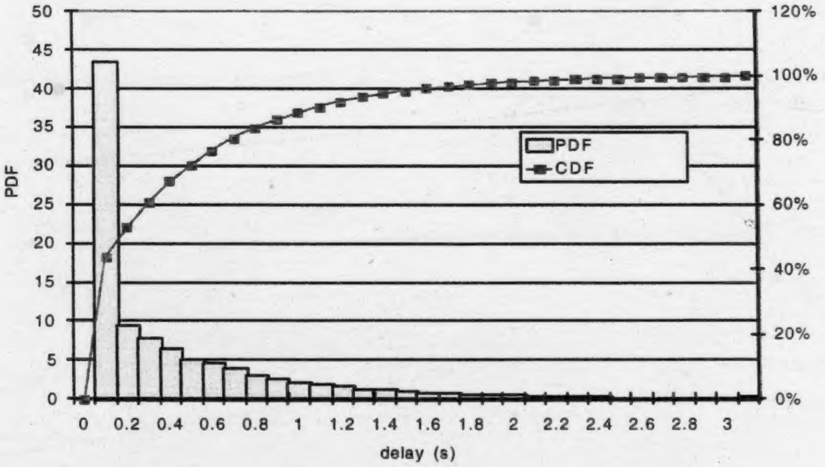

Figure 6.22. Distribution of delays per delivered packet over the set of users (100 drops of 16 users each) in an embedded sector for ITU pedestrian A channel with PF scheduler

6.5.1.2 HDR

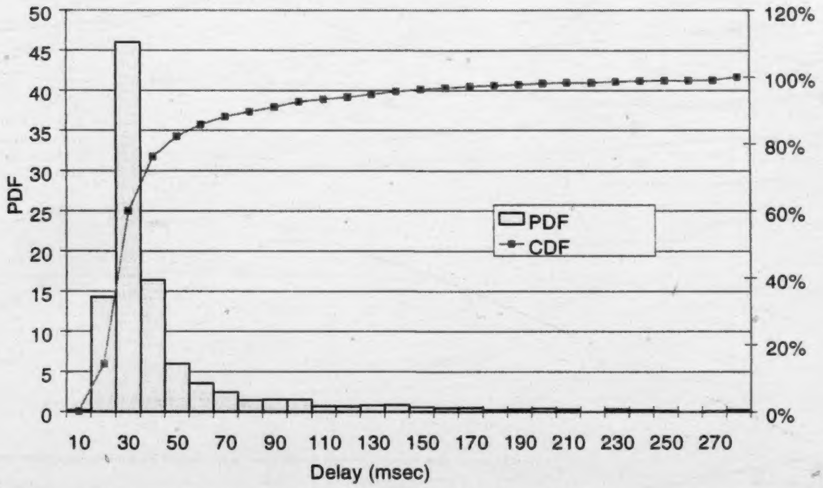

Figure 6.23. Distribution of delays per delivered packet over the set of users (100 drops of 16 users each) in an embedded sector for ITU pedestrian A channel with RR scheduler.

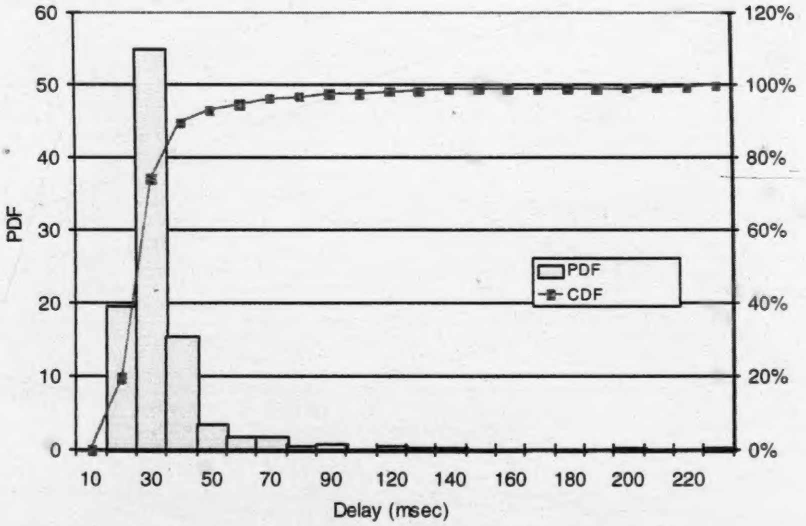

Figure 6.24. Distribution of delays per delivered packet over the set of users (100 drops of 16 users each) in an embedded sector for ITU pedestrian A channel with PF scheduler.

6.5.2 Vehicular B channel

6.5.2.1 1XTREME

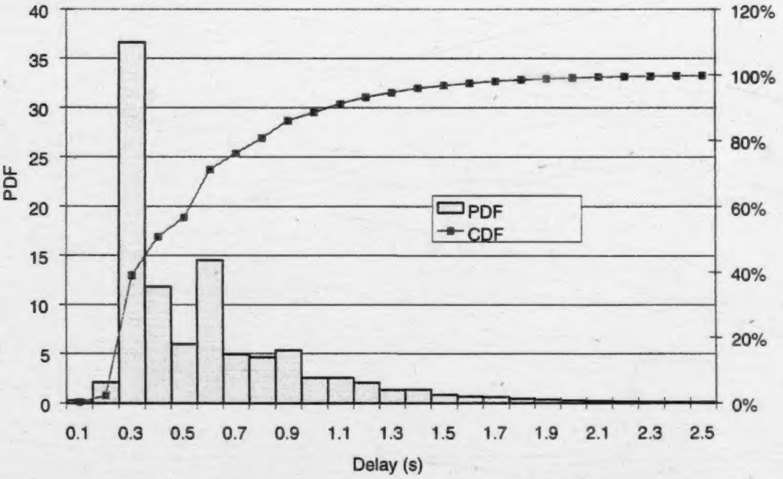

Figure 6.25. Distribution of delays per delivered packet over the set of users (100 drops of 16 users each) in an embedded sector for ITU vehicular B channel with RR scheduler.

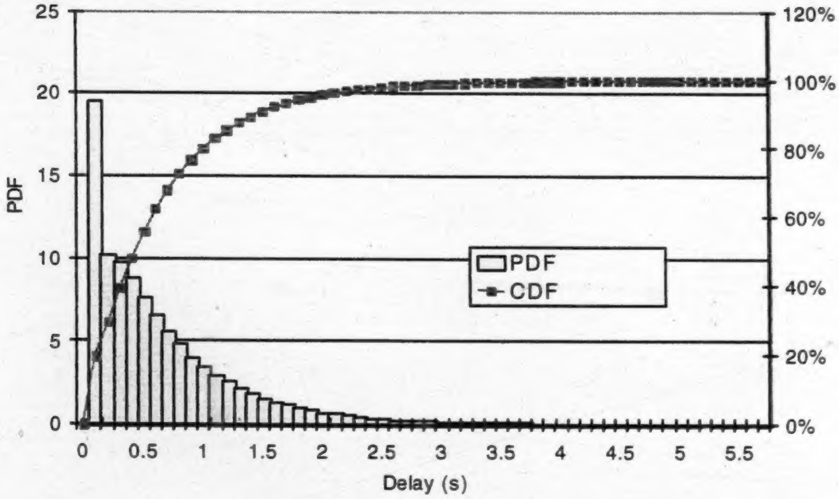

Figure 6.26. Distribution of delays per delivered packet over the set of users (100 drops of 16 users each) in an embedded sector for ITU vehicular B channel with PF scheduler.

6.5.2.2 HDR

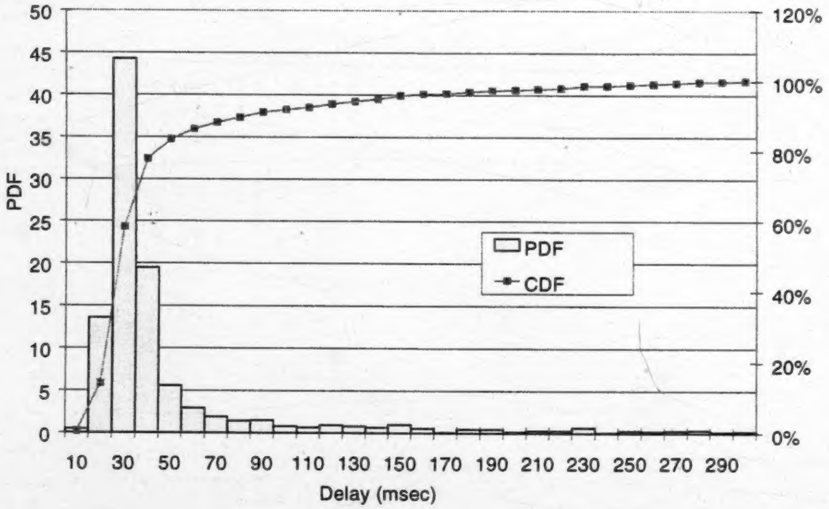

Figure 6.27. Distribution of delays per delivered packet over the set of users (100 drops of 16 users each) in an embedded sector for ITU vehicular B channel with RR scheduler.

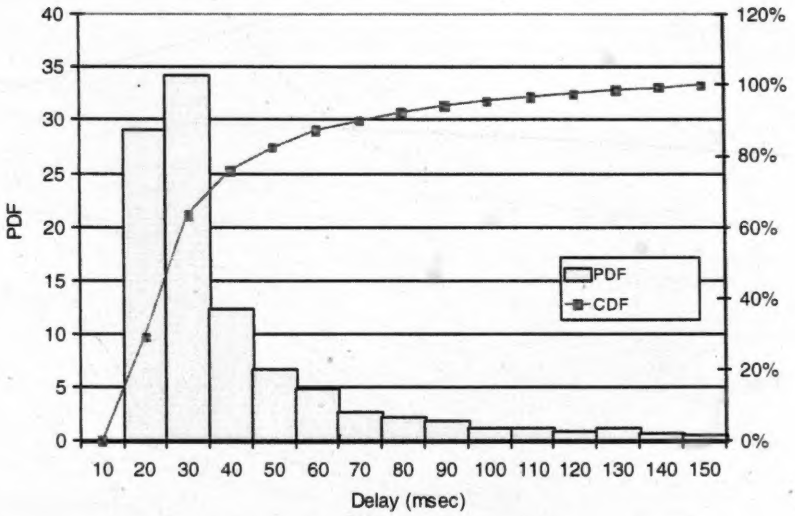

Figure 6.28. Distribution of delays per delivered packet over the set of users (100 drops of 16 users each) in an embedded sector for ITU vehicular B channel with PF scheduler.

The previous figures mainly show that the PF scheduler delivers packets to users roughly as fast as the RR scheduler, which suggests that the PF scheduling algorithm achieves a good level of fairness. There is slight increased in delay for the vehicular channel in both systems and all cases due to the uncertainty of the channel at the higher speed, which increases the number of re-transmissions and therefore the packet delay.

6.6 Average delay per sector

Figures 6.29 to 6.32 depict the average delay per delivered packet within the embedded sector for pedestrian A and vehicular B channels in 1XTREME and HDR. These are the averages of Section 6.5, but adding the cases for 4, and 8 users located in the embedded sector (Section 6.5 shows the distribution of delays for 16 users located in the embedded sector).

6.6.1 1XTREME

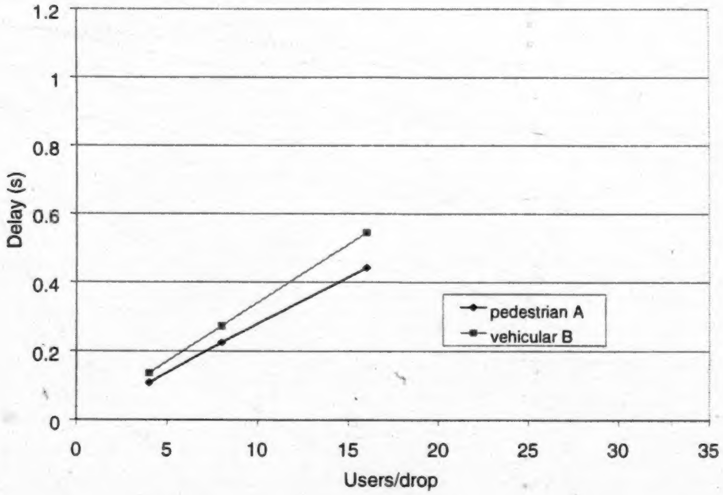

Figure 6.29. Average delay per delivered packet in an embedded sector as a function of the number of users per drop for 100 drops, RR scheduler.

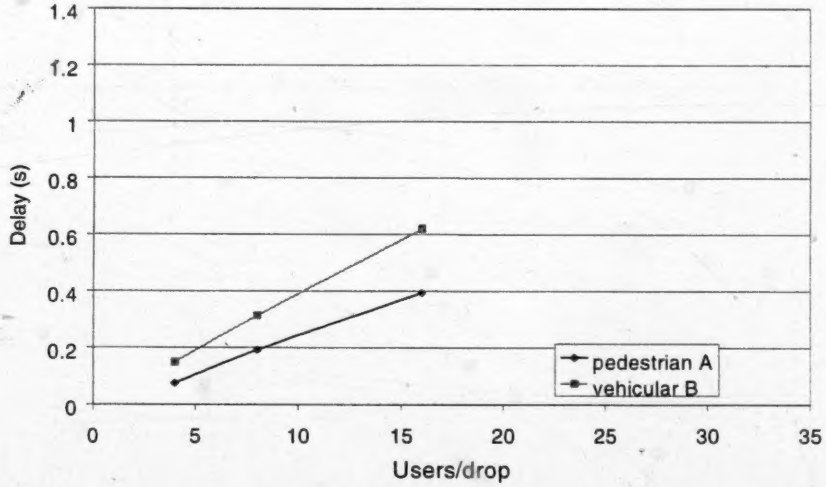

Figure 6.30. Average delay per delivered packet in an embedded sector as a function of the number of users per drop for 100 drops, PF scheduler

6.6.2 HDR

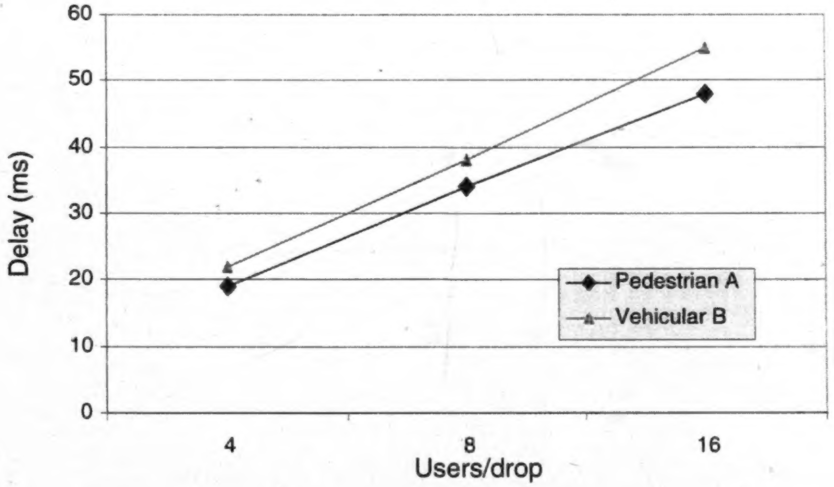

Figure 6.31. Average delay per delivered packet in an embedded sector as a function of the number of users per drop for 100 drops, RR scheduler.

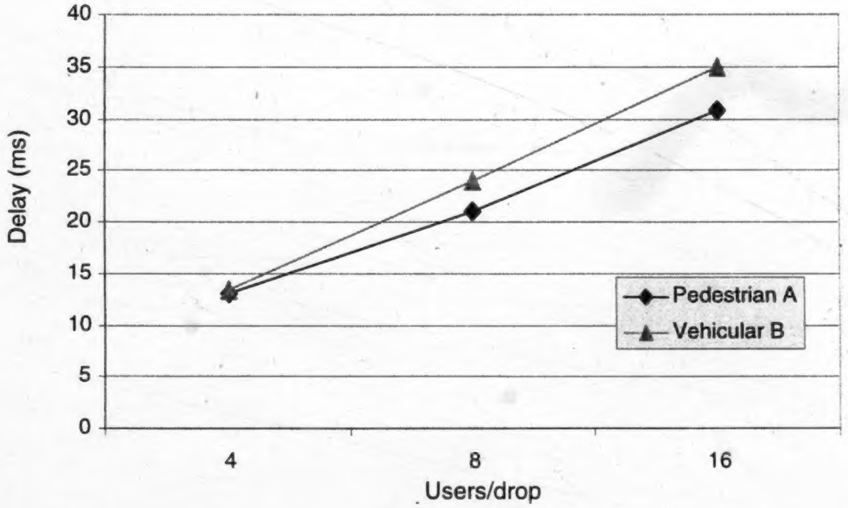

Figure 6.32. Average delay per delivered packet in an embedded sector as a function of the number of users per drop for 100 drops, PF scheduler.

The average packet delay increases as the number of users increases due to greater scheduling delays. The vehicular channel shows greater delays due to the greater uncertainty of this channel with respect to the pedestrian channel.

6.7 Number of slots allocated per user

Figures 6.33 to 6.40 show the distributions of slots allocated per user when 16 users are dropped 100 times in the embedded sector. Note that the number of slots allocated should be around 375 slots for 1XTREME and 1120 slots for HDR in this particular case of 16 users in the embedded sector.

6.7.1 Pedestrian A channel

6.7.1.1 1XTREME

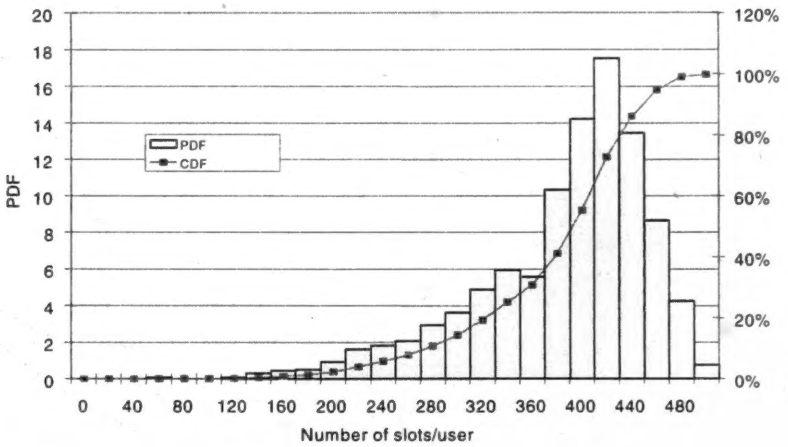

Figure 6.33. Distribution of the number of slots allocated per user over the set of users (100 drops of 16 users each) in an embedded sector for ITU pedestrian A channel with RR scheduler.

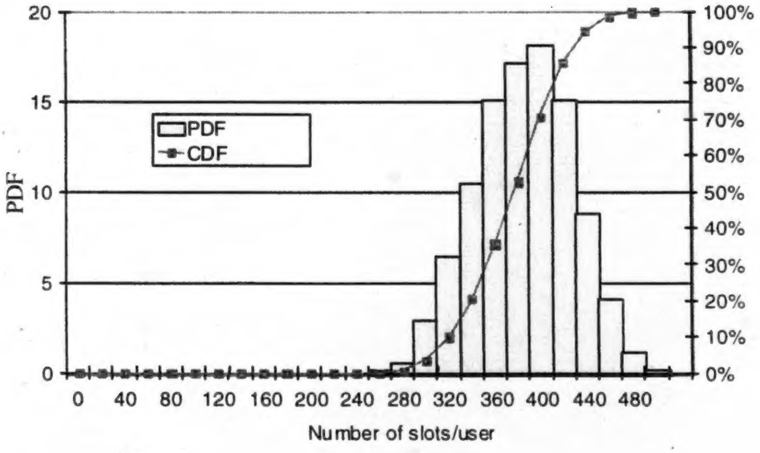

Figure 6.34. Distribution of the number of slots allocated per user over the set of users (100 drops of 16 users each) in an embedded sector for ITU pedestrian A channel with PF scheduler.

6.7.1.2 HDR

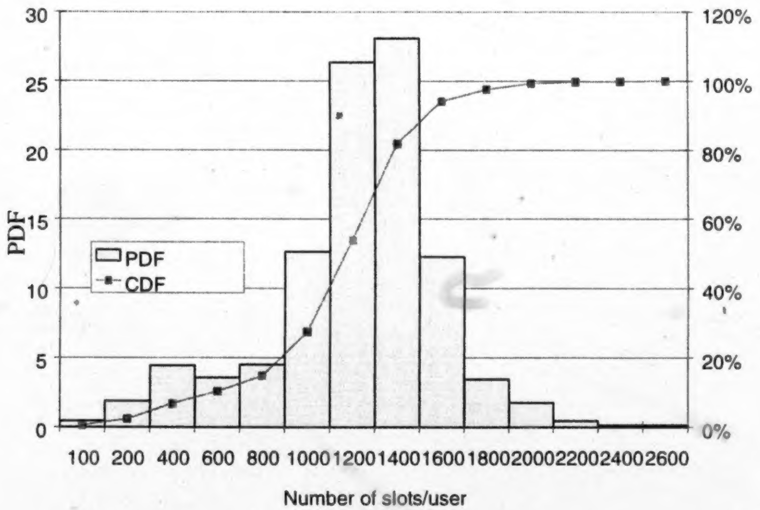

Figure 6.35. Distribution of the number of slots allocated per user over the set of users (100 drops of 16 users each) in an embedded sector for ITU pedestrian A channel with RR scheduler.

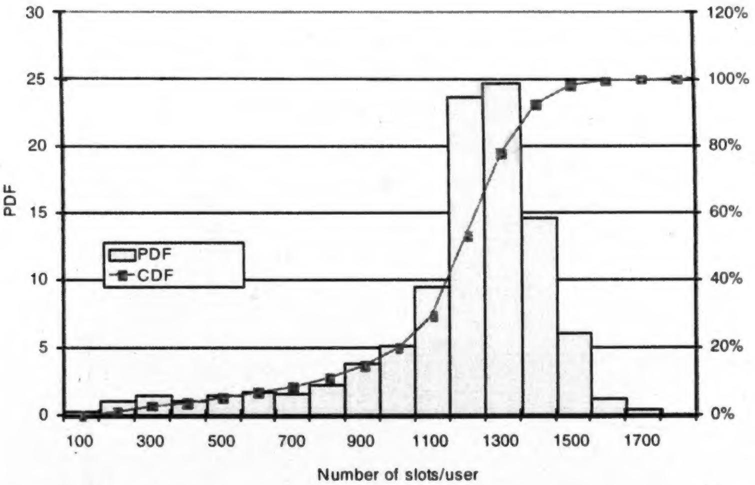

Figure 6.36. Distribution of the number of slots allocated per user over the set of users (100 drops of 16 users each) in an embedded sector for ITU pedestrian A channel with PF scheduler.

6.7.2 Vehicular B channel

6.7.2.1 1XTREME

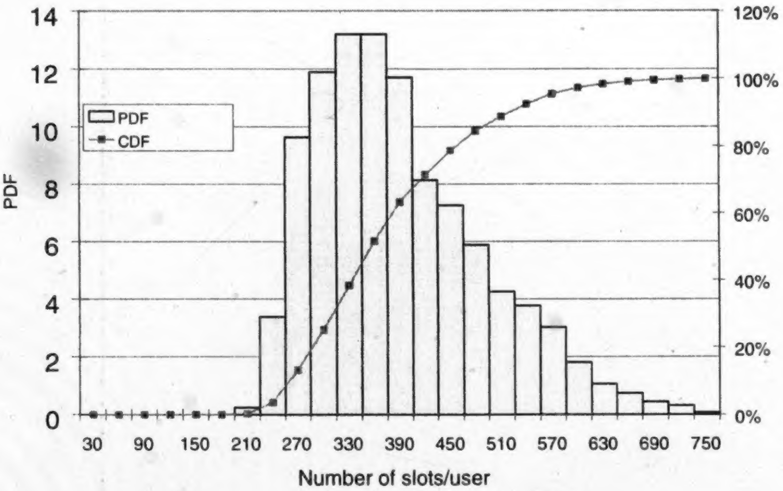

Figure 6.37. Distribution of the number of slots allocated per user over the set of users (100 drops of 16 users each) in an embedded sector for ITU vehicular B channel with RR scheduler.

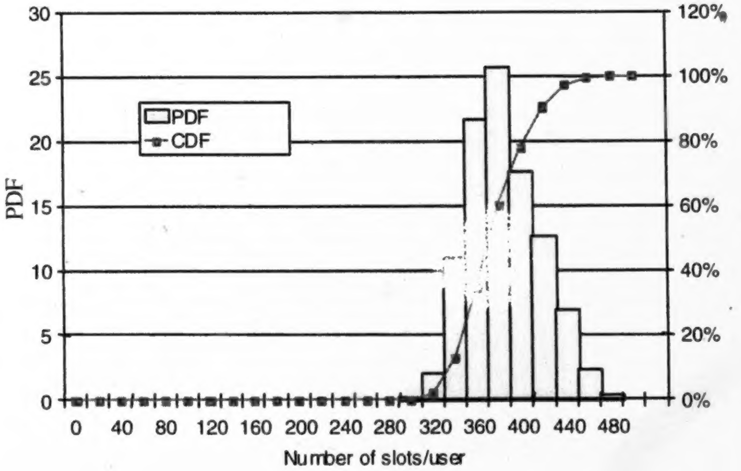

Figure 6.38. Distribution of the number of slots allocated per user over the set of users (100 drops of 16 users each) in an embedded sector for ITU vehicular B channel with PF scheduler.

6.7.2.2 HDR

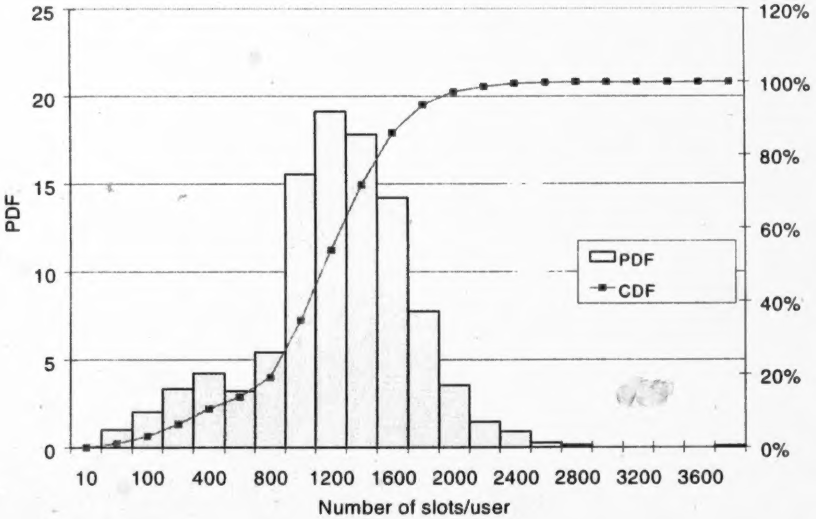

Figure 6.39. Distribution of the number of slots allocated per user over the set of users (100 drops of 16 users each) in an embedded sector for ITU vehicular B channel with RR scheduler.

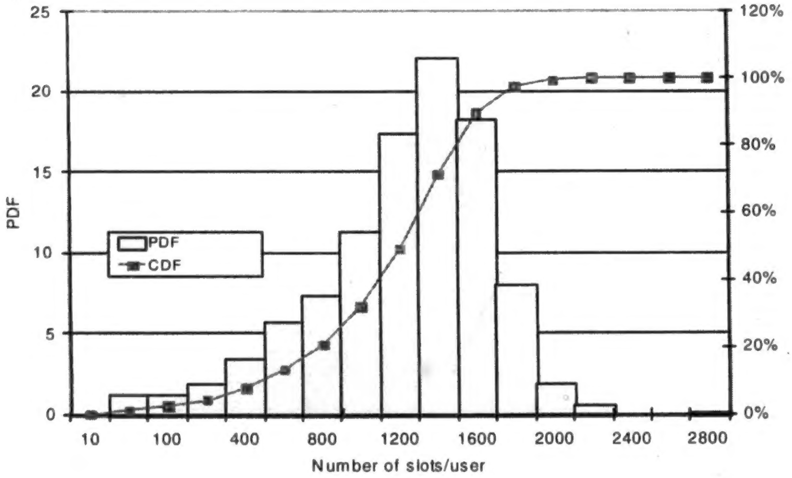

Figure 6.40. Distribution of the number of slots allocated per user over the set of users (100 drops of 16 users each) in an embedded sector for ITU vehicular B channel with PF scheduler.

The number of allocated slots can serve as a measure of fairness of the scheduling algorithms. Let us define the fairness metric F as follows

$$F = \frac{\textit{Max.}\text{ number of slots allocated to the worst 10\% users in the sector}}{\textit{Min.}\text{ number of slots allocated to the best 10\% users in the sector}} \qquad (6.1)$$

A small value of F is an indication of un-fairness, whereas a value of F close to unity is an indication of a fairer scheduler. The values of F in the various scenarios considered for RR and PF schedulers are given in Table 6.1.

Scenario	RR	PF
Pedestrian A-1XTREME	0.59	0.79
Vehicular B-1XTREME	0.48	0.74
Pedestrian A-HDR	0.34	0.48
Vehicular B-HDR	0.14	0.21

Table 6.1. Fairness metric F for the number of slots allocated per user over 16 users per sector.

6.8 Summary

We have presented performance results for 1XTREME and HDR obtained using the system level simulator developed in this research work. Due to shorter time slots, HDR takes greater advantage of multi-user diversity than 1XTREME. Average sector throughput with 16 users per sector in the pedestrian A channel is much higher for HDR (over 1.6 Mb/s) than in 1XTREME (less than 1.3 Mb/s). Both systems achieve similar throughput in relatively fast fading (110 Hz) vehicular B channel. Fairness has also been quantified and discussed throughout this chapter.

Chapter 7

Conclusion and future research

1XTREME and HDR average sector throughput results for pedestrian A and vehicular B channels with slow sector selection are summarized in Table 7.1 for a representative number of users.

These results indicate that HDR yields higher throughput than 1XTREME particularly in the low-speed pedestrian A channel with the PF scheduler. Key to the better performance of HDR is the greater advantage it takes of multi-user diversity through the use of the PF scheduler and shorter time-slot duration. Interesting to note is that for RR scheduler the 1XTREME system shows higher throughput performance than HDR, highlighting the great importance of a *good* scheduling algorithm for this system. The greater overall gain is achieved when PF scheduler and HDR are used. Note that going from RR to PF scheduling scheme, the 1XTREME shows a throughput improvement of 52%, and 7% in pedestrian A, and vehicular B respectively, whereas HDR shows 150%, and 47%.

The smaller throughput improvement of 1XTREME vs. HDR in PF scheduler could be attributed to the higher scheduling frequency in HDR (shorter time-slot duration). The higher scheduling frequency, the higher multi-user diversity gain.

kb/s	RR (kb/s)	PF (kb/s)
Pedestrian A-1XTREME	841	1280
Vehicular B-1XTREME	585	625
Pedestrian A-HDR	640	1620
Vehicular B-HDR	420	620

Table 7.1. Average throughput per sector for pedestrian A and vehicular B channels with 16 users per sector and slow sector selection.

The difference in gain between the pedestrian and vehicular channels when the PF scheduler is used can be attributed to the fact that in the systems with users that have higher Doppler shift, there is already a time diversity gain. In other words the gain offered by a PF scheduler due to multi-user diversity is more significant in pedestrian A channel at lower speeds.

Note that simulation results suggest that the forward link transmission using 64 QAM with code rate ¾, which is admissible by the 1XTREME numerology, is unfeasible in the case of pedestrian A channel. That is because of the 13dB upper bound on the maximum achievable SIR due to receiver imperfections. In the vehicular B channel the maximum achievable SIR, limited by the multi-path and other cells interference makes 64 QAM with code rate ¾, unfeasible even without accounting for implementation losses.

Values of the fairness metric *F* as defined in Chapter 6 were given in Table 6.1. One can note that the PF and RR schedulers are fairer in pedestrian A channel with respect to vehicular B channel in both systems, although the absolute values of *F* in HDR are smaller. It is observed that the PF scheduler is fairer both in pedestrian A and vehicular

B channels in 1XTREME and HDR. The increase in fairness is 34% (54%) in 1XTREME in pedestrian A (vehicular B) channel and 41% (50%) in HDR pedestrian A (vehicular B) channel. Therefore, the gain is slightly higher in vehicular B when going from the RR scheduler to PF scheduler. If fairness is defined based on equal access to the system resources, the parameter *F* is a *good* measure of fairness in resource allocation.

In terms of average packet delay (Figures 6.29 to 6.32) it is observed a clear longer latency in the vehicular channel with respect to the pedestrian channel due to the more frequent number of re-transmissions needed to successfully transmit a packet as a consequence of inaccurate channel prediction. Due to the different structure in terms of packet size and time-slot format of HDR and 1XTREME it is difficult to draw accurate conclusions regarding which system offers more or less latency. HDR delays are in the order of 35msec in pedestrian A, and 60msec in Vehicular B. 1XTREME experiences 400msec delays in pedestrian A, and 600msec in vehicular B. All these delays are at the physical layer level.

HDR has been standardized as IS-856, on the other hand 1XTREME is still a proposed system under development. Both systems are still in their infancy and therefore require optimization and improvement in theoretical and practical fields. This research work has demonstrated the capabilities of these two systems to offer wireless internet access at the speed of present wireline-DSL connections. The effects of different channels on the scheduling algorithms and on the capacity and performance of these systems has also been addressed.

This research work has served three general purposes. Firstly, the main goal has been to provide performance comparison at the system level of two important high-bit-rate packet data wireless transmission systems. Secondly, it has been in our interest to provide a platform for a system level simulation of packetized data wireless systems using cellular infrastructure based on a TDM forward link with adaptive modulation and coding. Finally, the system level simulator developed has helped us identify important parameters and features affecting the performance of these systems.

Future research activities should include the study of improved scheduling algorithms for vehicular environments, and a comprehensive study of the effects on the system performance of different parameters such as, antenna pattern, sectorization, and other.

Bibliography

[1] V.H Mac Donald, "The Cellular Concept," *The Bell System Technical Journal*, vol. 58, no. 1, 1979, pp. 15-25.

[2] T. S Rappaport, *Wireless Communications Principles & Practice*, Upper Saddle River, New Jersey: Prentice Hall PTR, 1996.

[3] E. Dinan and B. Jabbari, "Spreading Codes for Direct Sequence CDMA and Wideband CDMA cellular Networks," *IEEE Comm. Magazine*, vol. 36, no. 9, Sept. 1998, pp. 48-52.

[4] Y. Lin and I. Chlamtac, *Wireless and Mobile Network Architectures*, New York: Published by John Wiley & Sons, Inc, 2001.

[5] W. C. Y. Lee, *Mobile Communications Engineering*, 2nd Edition, New York: Published by McGraw Hill, 1998.

[6] V. K. Garg and J. E Wilkes, *Wireless and Personal Communications Systems*, Upper Saddle River, New Jersey: Prentice Hall PTR, 1996.

[7] R. Peterson, R. Ziemer, and D. Borth, *Introduction to Spread Spectrum Communications*, Englewood Cliffs, New Jersey: Prentice Hall, 1995.

[8] J. S. Lee and L. E. Miller, *CDMA Systems Engineering Handbook*, Boston-London: Artech House, 1998.

[9] T. Ojamperä and R Prasad, "An Overview of CDMA Evolution Toward Wideband CDMA," *IEEE Comm. Surveys*, vol. 1, no. 1, 4th Quarter 1998, pp. 2-8.

[10] T. Ojamperä and R Prasad Editors, *Wideband CDMA for Third Generation Mobile Communications*, Boston-London: Artech House, 1998.

[11] Q. Bi, G. Zysman, and H. Menkes, "Wireless Mobile Communications at the Start of the 21st Century," *IEEE Comm. Magazine*, vol. 39, no. 1, January 2001, pp. 110-116.

[12] P. Bender et al., "CDMA/HDR: A Bandwidth-Efficient High-Speed Wireless Data Service for Nomadic Users," *IEEE Comm. Magazine*, vol. 38, no. 7, July 2000, pp. 70-77.

[13] Y. Jou, "Developments in Third Generation (3G) CDMA Technology," in *Proc. IEEE International Symposium on Spread-Spectrum Techniques and Applications* (ISSSTA), New Jersey, 2000, pp.460-466.

[14] G. Fry and G. Mandyam, "Evolving the capabilities of IS-2000: an overview of 1XTREME," in *Proc. IEEE Radio and Wireless Conference* (RAWCON). Denver, 2000, pp. 1-4.

[15] H. Holma and A. Toskala Editors, *WCDMA for UMTS: Radio Access for Third Generation Mobile Communications*, Chichester: Published by John Wiley & Sons, Inc, 2000.

[16] M. Haardt and W. Mohr, "The Complete Solution for Third-Generation Wireless Communications: Two Modes on Air, One Winning Strategy," *IEEE Personal Comm. Magazine*, vol. 7, no. 6, December 2000, pp. 18-22.

[17] P. Lehne and M. Pettersen, "An Overview of Smart Antenna Technology for Mobile Communications Systems," *IEEE Comm. Surveys*, vol. 2, no. 4, 4th Quarter 1999, pp. 2-6.

[18] W. Mohr and W. Konhäuser, "Access Network Evolution Beyond Third Generation Mobile Communications," *IEEE Comm. Magazine*, vol. 38, no. 12, Dec. 2000, pp. 122-126.

[19] S. Ohmori, Y. Yamao, and N. Nakajima, "The Future Generations of Mobile Communications Based on Broadband Access Technologies," *IEEE Comm. Magazine*, vol. 38, no. 12, Dec. 2000, pp. 134-137.

[20] Recommendation ITU-R M.1225, "Guidelines for Evaluation of Radio Transmission Technologies for IMT-2000," 1997.

[21] S. Hämäläinen, H. Holma and K. Sipilä, "Advanced WCDMA Radio Network Simulator," in *Proc. Personal Indoor and Radio Communications Conf.* (PIMRC), Osaka, 1999.

[22] "Universal Mobile Telecommunications Systems (UMTS); Selection procedures for the choice of radio transmission technologies of UMTS," TR 101 112 V3.1.0 (1997-11), UMTS 30.03.

[23] A. Jalali, R. Padovani and R. Pankaj, "Data Throughput of CDMA-HDR a High Efficiency-High Data Rate Personal Communication Wireless System," in *Proc. IEEE Vehicular Technology Conf.* (VTC2000-Spring), Tokyo, 2000, pp. 1854-1860.

[24] A. Ghosh, L. Jalloul, M. Cudak, and B. Classon, " Performance of Coded Higher Order Modulation and Hybrid ARQ for Next Generation Cellular CDMA Systems," in *Proc. IEEE Vehicular Technology Conf.* (VTC2000-Fall), Boston, 2000, pp 7-14.

[25] L. Kleinrock, "On Some Principles of Nomadic Computing and Multi-Access Communications," *IEEE Comm. Magazine*, vol. 38, no. 7, July 2000, pp. 46-51.

[26] B. Sklar, "Rayleigh Fading Channels in Mobile Digital Communication Systems Part 1: Characterization," *IEEE Comm. Magazine*, vol. 35, no. 7, July 1997, pp. 90-95.

[27] A.J. Goldsmith and S.G. Chua, "Adaptive coded modulation for fading channels," *IEEE. Trans. on Communications*, vol. 46, no. 5, Oct.1998, pp. 595-600

[28] D. Chase, "Code Combining- A Maximum-Likelihood Decoding Approach for Combining an Arbitrary Number of Noisy Packets," *IEEE Trans. on Communications*, vol. 33, no. 5, May 1985, pp. 385-390.

[29] Q. Zhang and S. A. Kassan, "Hybrid ARQ with Selective Combining for Fading Channels," *IEEE. Trans. on Communications*, vol. 17, no. 5, May 1999, pp. 867-873.

[30] S.N. Nanda, K. Balachandran, and S. Kumar, "Adaptation Techniques in Wireless Packet Data Services," *IEEE Comm. Magazine*, vol. 38, no. 1, January 2000, pp. 54-60.

[31] cdma2000 High Rate Packet Data Air Interface Specification (IS-856). 3GPP2 C.S0024. August 23rd, 2001.

[32] D.M. Mandelbaum, "An Adaptive Feedback Coding Scheme Using Incremental Redundancy," *IEEE. Trans. on Information Theory*, pp. 388-389,May 1974.

[33] E. Esteves, P. Black, "HDR forward link throughput with H-ARQ," 3GPP2 C30-20000710-007 QCOM ARQ Performance.

[34] T. Eyceoz, A. D. Hallen and H. Hallen, "Deterministic channel modeling and long range prediction of fast fading mobile radio channels," *IEEE Communications Letters*, vol. 2, Sept. 1998, pp. 159-166.

[35] J.B. Andersen, J. Jensen, S.H. Jensen and F. Frederiksen, "Prediction of future fading based on past measurements," in *Proc. IEEE Vehicular Technology Conf.* VTC'99-Fall, Sept.1999, pp. 151-157.

[36] J.K. Hwang and J.H. Winters, "Sinusoidal modeling and prediction of fast fading porcesses," in *Proc. IEEE GLOBECOM Conf.* GLOBECOM'98, pp. 892-895.

[37] W. Stallings, *High-Speed Networks TCP/IP and ATM design principles*, Upper Saddle River, New Jersey: Prentice Hall PTR, 1998.

[38] W. Sipmson, "The Point-to-point protocol (PPP)," RFC 1661 (STD 51), July 1994.

[39] B. Vucetic and J. Yuan, *Turbo Codes: Principles and Applications,* Published by Kluwer Academic, 2000.

[40] J. G. Proakis, *Digital Communications*, 3rd Edition, Published by McGraw Hill, 1995.

[41] L. W. Couch II, *Digital and Analog Communication Systems*, 3rd Edition, New York: Published by Macmillan, 1990.

[42] G. Fry and G. Mandyam, "Evolving the capabilities of IS-2000: an overview of 1XTREME," in *Proc. IEEE Radio and Wireless Conference* (RAWCON). 2000, pp. 1-4.

[43] T. Okumura, E. Ohmori, K. Fukuda, "Field Strength and Its Variability in VHF and UHF Land Mobile Service," *Review Electrical Communication Laboratory*, vol. 43, no. 9-10, Sept-Oct. 1968, pp. 825.

[44] M. Hata, "Empirical Formula for Propagation Loss in Land Mobile Radio Services," *IEEE. Trans. Vehicular Technology*, vol. VT-29, no. 3, August 1980, pp. 317.

[45] "Propagation Prediction Models," COST 231 Final Rep., chapter 4, pp.17.

[46] D. Parsons, *The Mobile Radio Propagation Channel*, New York-Toronto: Published by John Wiley & Sons, Inc, 1992

[47] G. L. Stüber, *Principles of Mobile Communication,* Published by Kluwer Academic, 1996.

[48] M. Gudmundson, "Correlation Model for Shadow Fading in Mobile Radio Systems," *IEE. Electronic Letters*, vol. 27, no. 23, November 1991, pp. 2145.

[49] R. H. Clarke, "A Statistical Theory of Mobile-radio Reception," *Bell System Technical Journal*, vol. 47, 1968, pp. 957.

[50] D. Young and N.C. Beaulieu, "The Generation of Correlated Rayleigh Random Variates by IDFT," *IEEE. Trans. on Communications*, vol. 48, no. 7, July 2000, pp. 1114.

[51] S. B Wicker, *Error Control Systems for Digital Communication and Storage*, Upper Saddle River, New Jersey: Prentice Hall PTR, 1995.

[52] V. Vanhgi, Ericsson Wireless Communications, San Diego CA, Private communication, Oct 2000.

[53] A.D. Hallen, S. Hu, and H. Hallen, "Long-Range Prediction of Fading Signals," *IEEE Signal Processing Magazine*, vol. 38, no. 1, May 2000, pp. 62.

[54] 1xEV-DV Evaluation Methodology-Strawman (Rev.15). WG5 Evaluation Ad hoc. Seattle, WA. March 27th 2001.

[55] E. Esteves, M. Gurelli, "HDR Forward Link Throughput with H-ARQ", 3GPP2 C30-20000710-007,July 10th 2000.

Appendix

Link level simulation results

A.1 HDR forward traffic channel PER curves

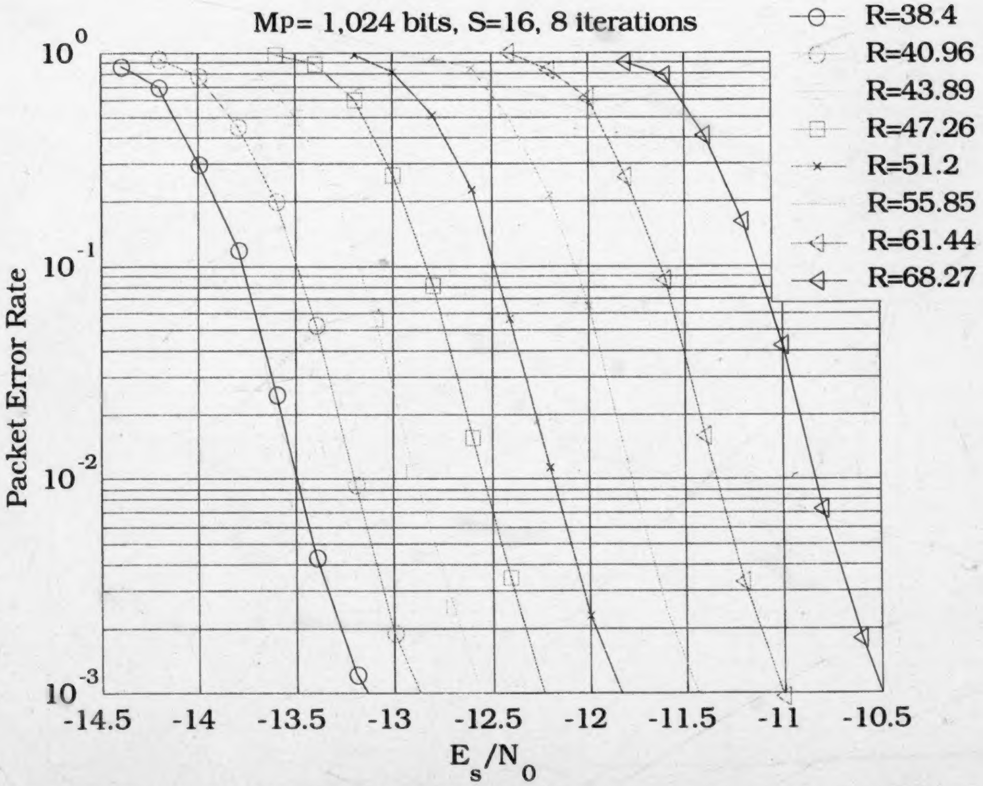

Figure A.1. PER vs. E_s / N_o curves in AWGN for transmission formats 1 – 8 in Table 2-1after 8 iterations of the logMAP turbo decoder. Bit rates R in kb/s, packet size M_p = 1024 bits, max no. of slots S_{max} = 16.

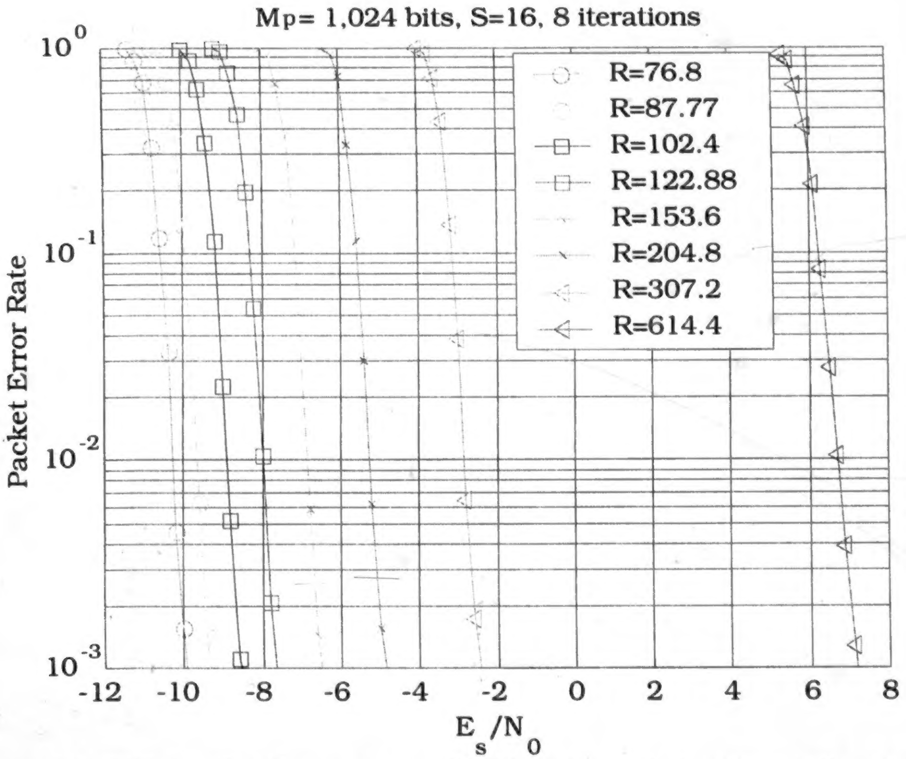

Figure A.2. PER vs. E_s / N_o curves in AWGN for transmission formats 9 – 16 in Table 2-1after 8 iterations of the logMAP turbo decoder. Bit rates R in kb/s, packet size M_p = 1024 bits, max no. of slots S_{max} = 16.

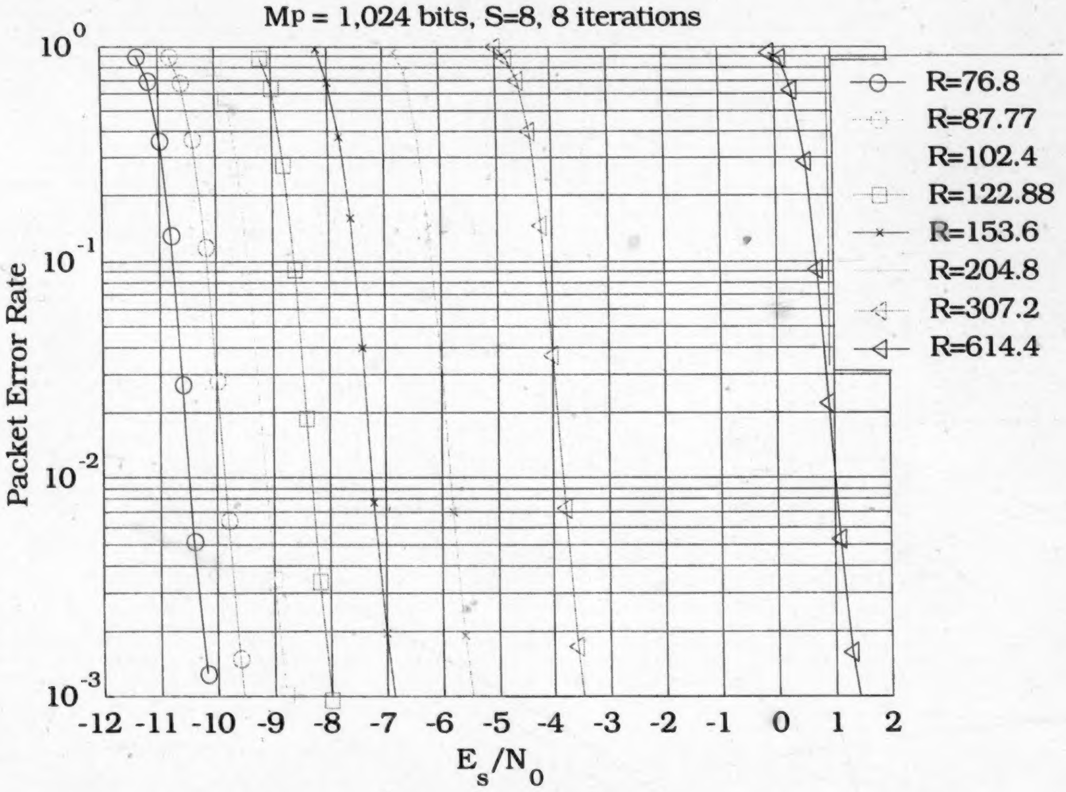

Figure A.3. PER vs. E_s / N_o curves in AWGN for transmission formats 17 – 24 in Table 2-1after 8 iterations of the logMAP turbo decoder. Bit rates *R* in kb/s, packet size M_p = 1024 bits, max no. of slots S_{max} = 8.

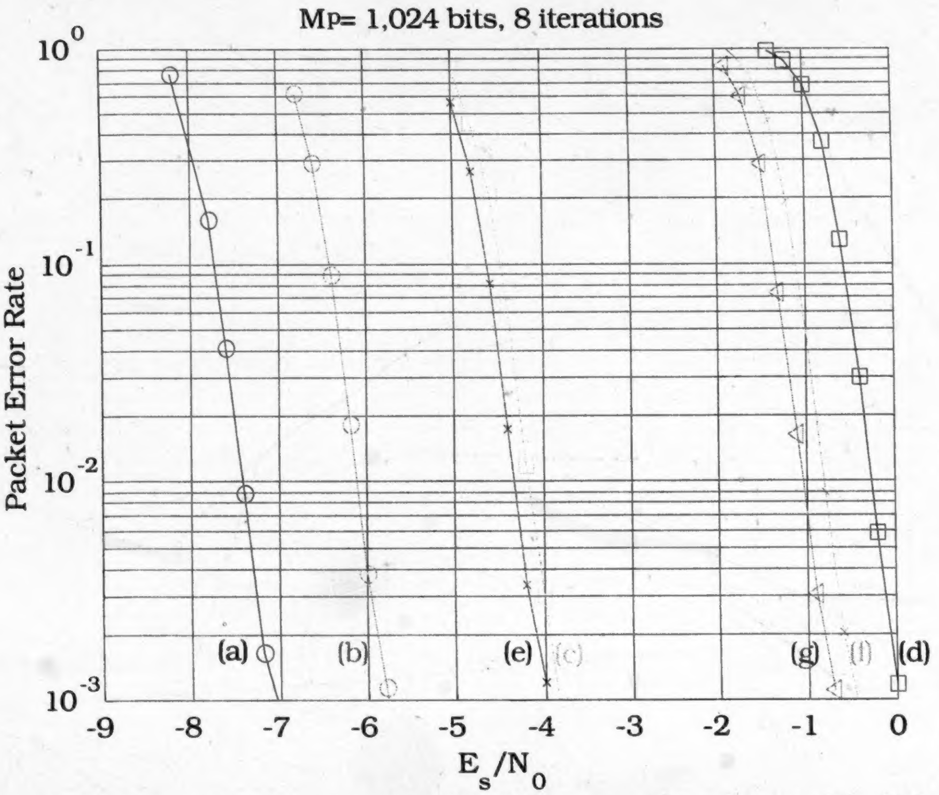

Figure A.4. PER vs. E_s / N_o curves in AWGN for transmission formats 25 - 31 in Table 2-1after 8 iterations of the logMAP turbo decoder. Packet size M_p = 1024 bits, bit rates R in kb/s, max no. of slots S_{max}: (a) R=153.6, S_{max} =4; (b) R=204.8, S_{max} =4; (c) R=307.2, S_{max} =4; (d) R=614.4, S_{max} =4; (e) R=307.2, S_{max} =2; (f) R=614.4, S_{max} =2; (g) R=614.4, S_{max} =1.

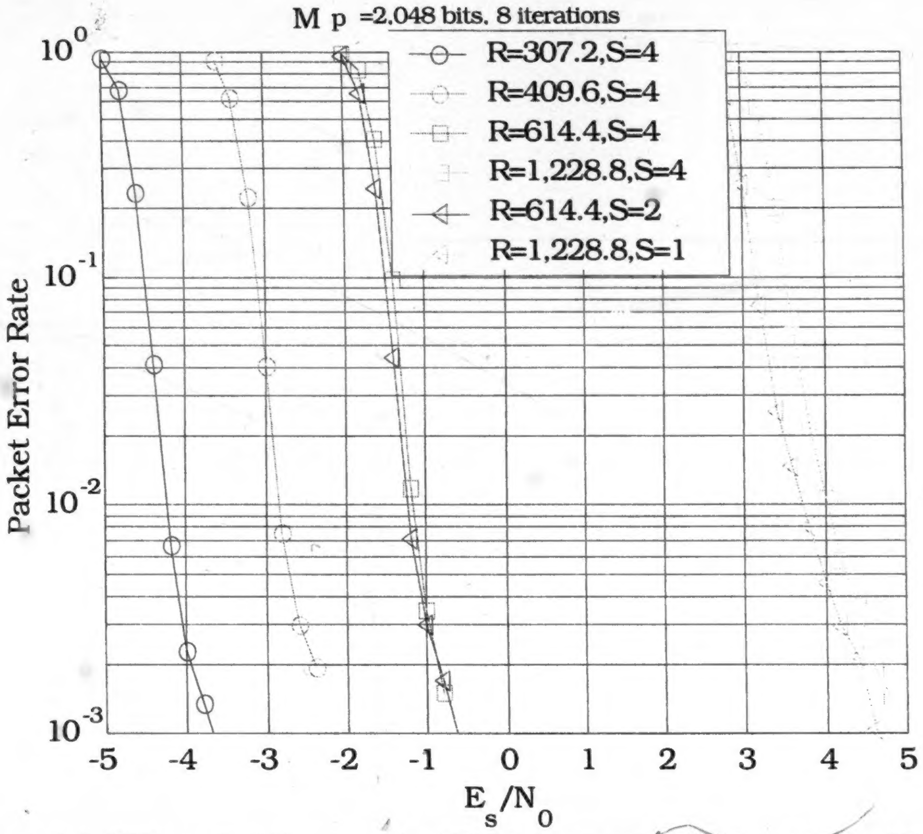

Figure A.5. PER vs. E_s / N_o curves in AWGN for transmission formats 32 - 37 in Table 2-1after 8 iterations of the logMAP turbo decoder. Packet size M_p = 2048 bits, bit rates *R* in kb/s, max no. of slots S_{max}..

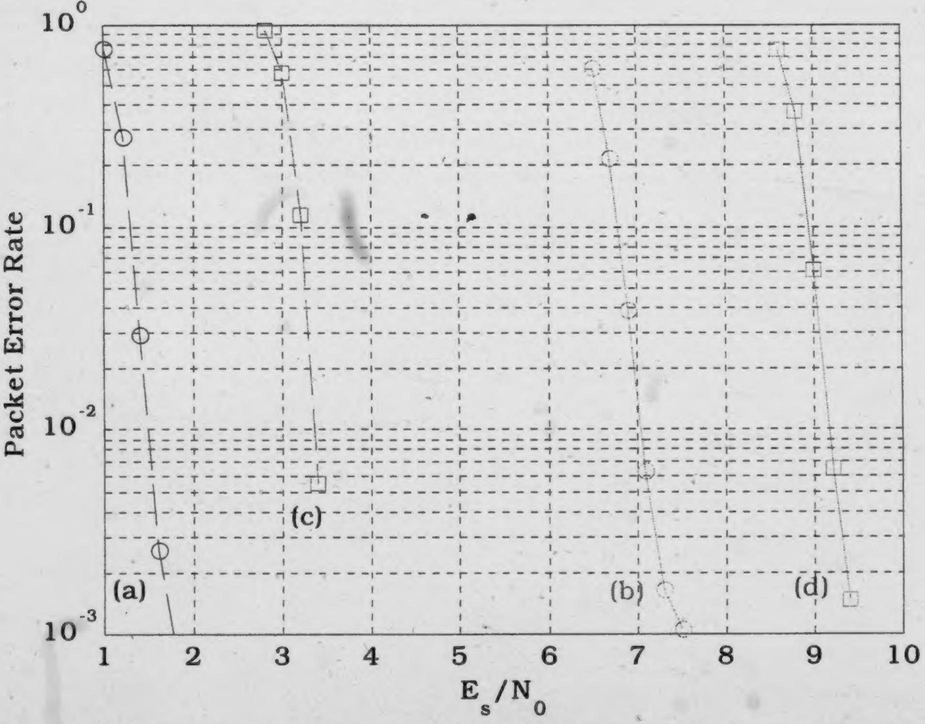

Figure A.6. PER vs. E_s / N_o curves in AWGN for transmission formats 38 - 41 in Table 2-1after 8 iterations of the logMAP turbo decoder. Packet size M_p, bit rate R in kb/s, max no. of slots S_{max}: (a) R=921.6, M_p=3,072, S_{max} =2; (b) R=1,843.2, M_p=3,072, S_{max} =1; (c) R=1,228.8, M_p=4,096, S_{max} =2; (d) R=2,457.6, M_p=4,096, S_{max} =1.

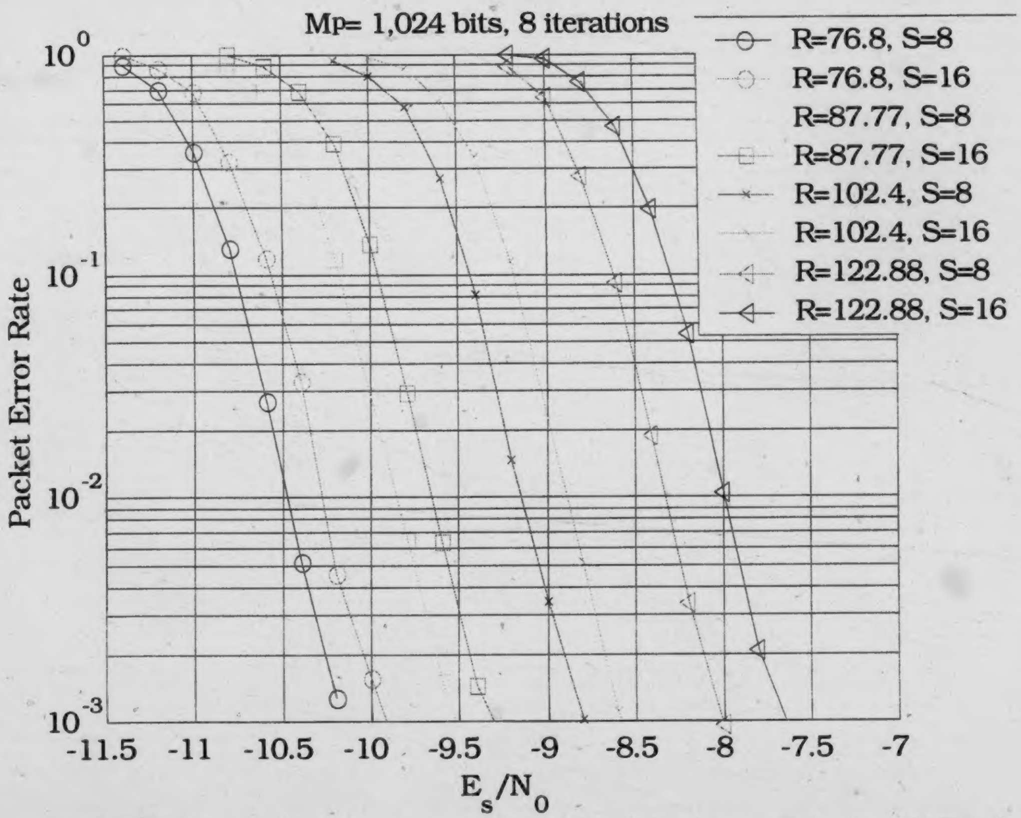

Figure A.7. PER vs. E_s / N_o curves in AWGN after 8 iterations of the logMAP turbo decoder. Packet size M_p = 1024 bits, bit rates R in kb/s, max no. of slots S_{max}.

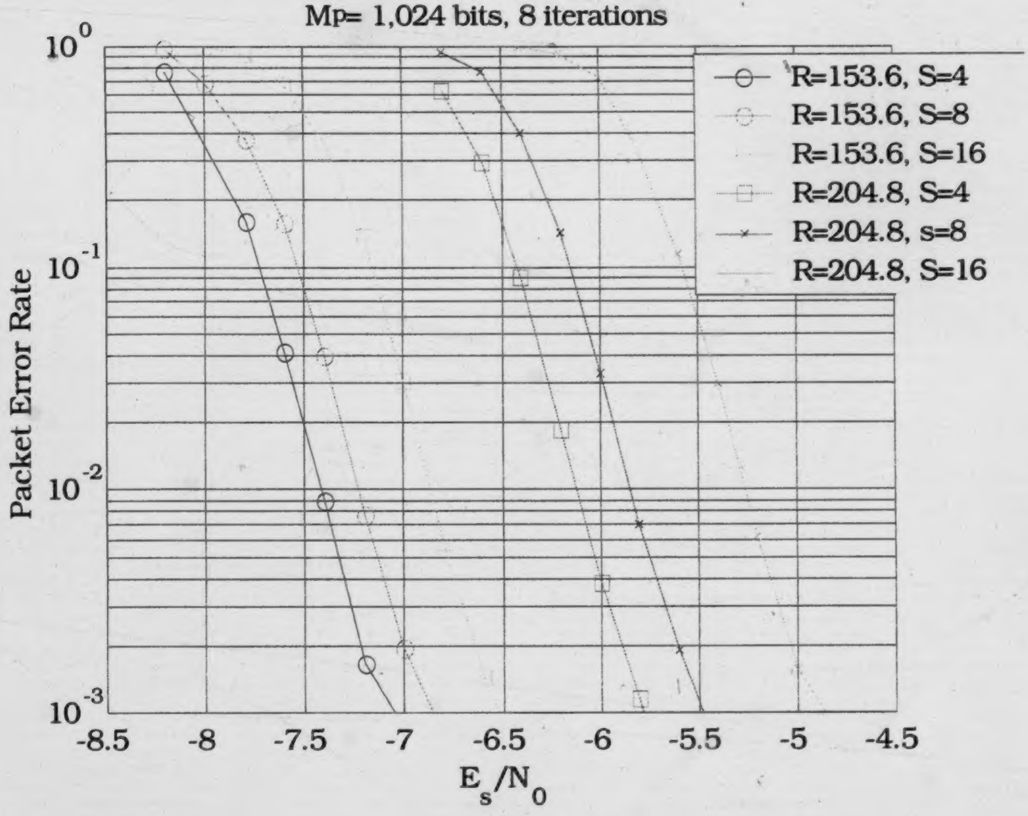

Figure A.8. PER vs. E_s / N_o curves in AWGN after 8 iterations of the logMAP turbo decoder. Packet size M_p = 1024 bits, bit rates R in kb/s, max no. of slots S_{max}.

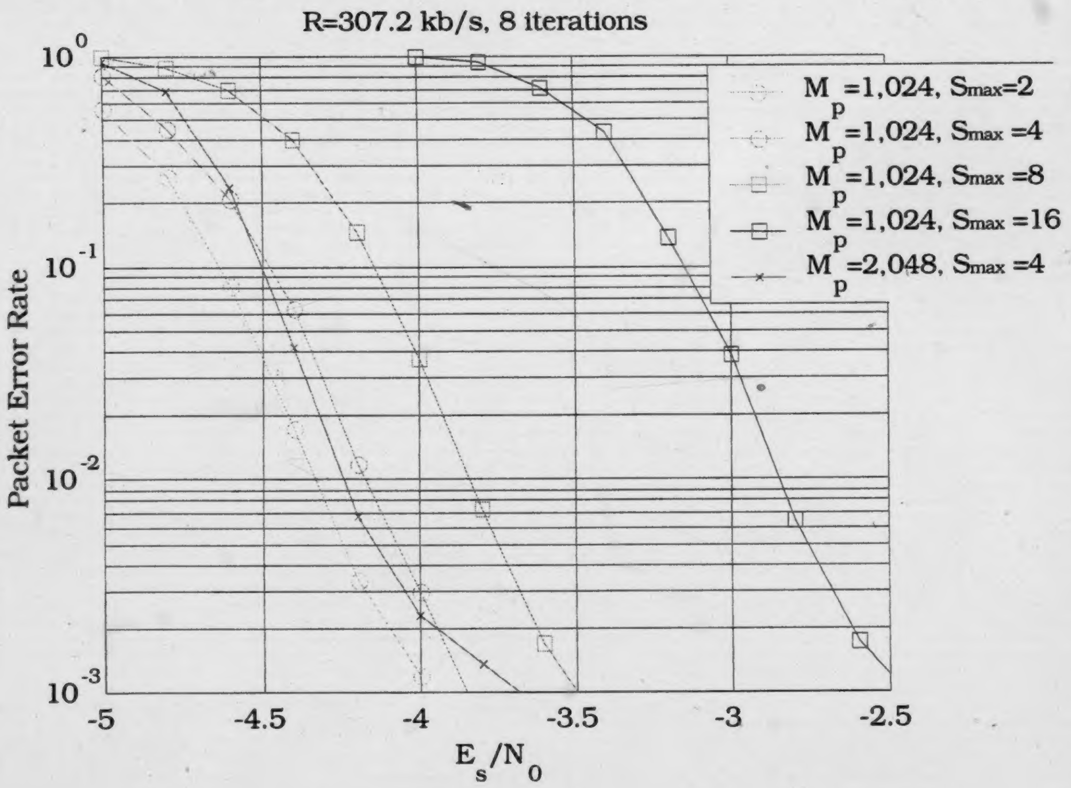

Figure A.9. PER vs. E_s / N_o curves in AWGN after 8 iterations of the logMAP turbo decoder. Packet size M_p bits, bit rate R =307.2 kb/s, max no. of slots S_{max}.

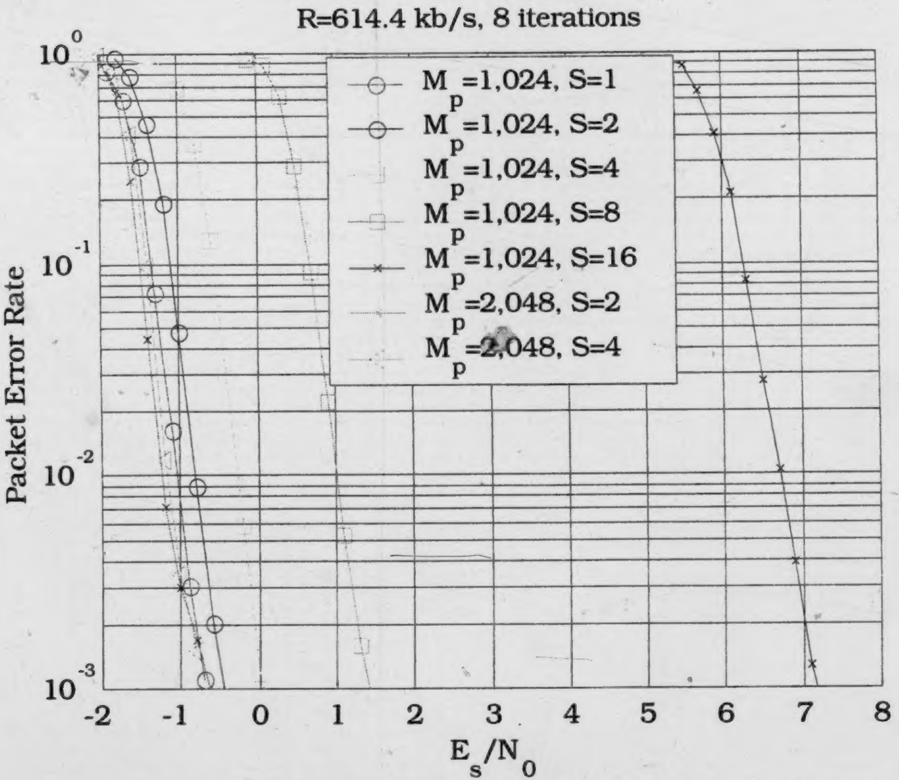

Figure A.10. PER vs. E_s / N_o curves in AWGN after 8 iterations of the logMAP turbo decoder. Packet size M_p bits, bit rate R = 614.4 kb/s, max no. of slots S_{max}.

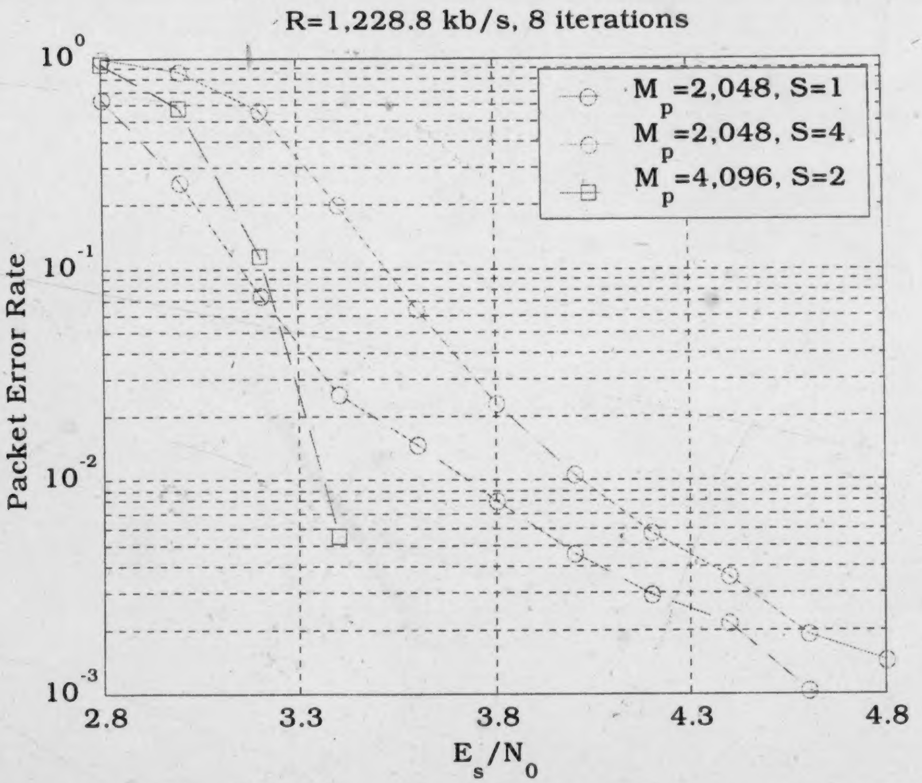

Figure A.11. PER vs. E_s / N_o curves in AWGN after 8 iterations of the logMAP turbo decoder. Packet size M_p bits, bit rate R = 1 228.8 kb/s, max no. of slots S_{max}.

A.2 1XTREME forward shared channel PER curves

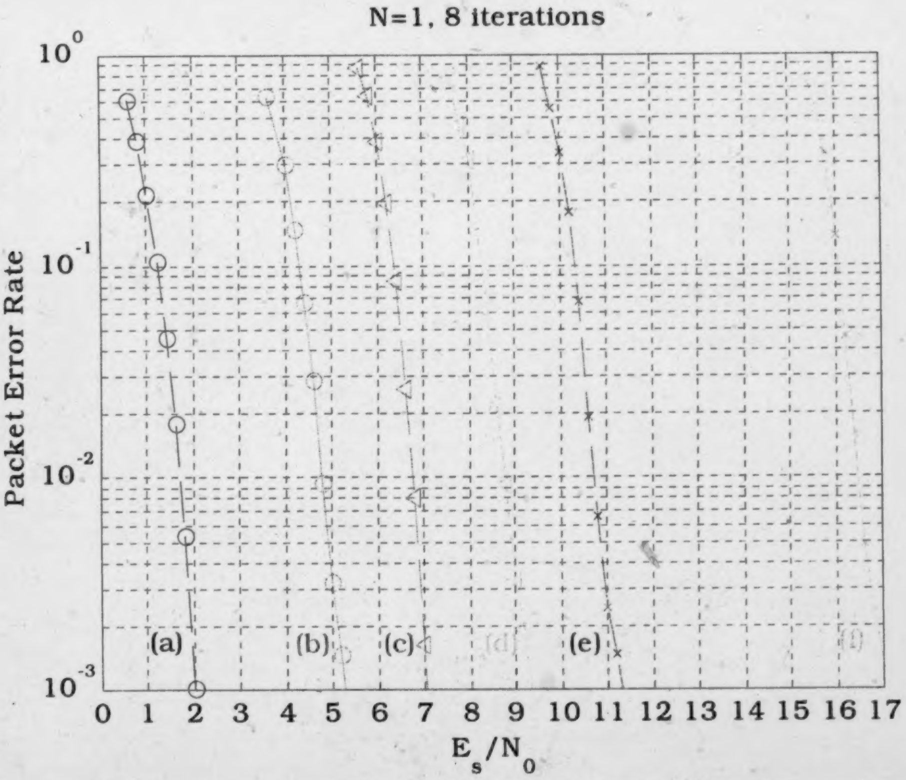

Figure A.12. PER vs. E_s / N_o curves for 1XTREME Forward Shared Channel in AWGN after 8 iterations of the logMAP turbo decoder. Bit rate R kb/s, packet size M_p bits: (a) R=76.8, M_p=384; (b) R=115.4, M_p=576; (c) R=153.6, M_p=768; (d) R=172.8, M_p=864; (e) R=230.4, M_p=1,152; (f) R=345.6, M_p=1,728.